UNIVERSITY OF CALIFORNIA, SAN DIEGO

Arctic sea ice retreat and mixed-layer processes

A dissertation submitted in partial satisfaction of the requirements for the degree
Doctor of Philosophy

in

Oceanography

by

Erica Rosenblum

Committee in charge:

Ian Eisenman, Chair
Sarah Gille, Co-Chair
David Saintillan
Lynne Talley
Maria Vernet
Shang-Ping Xie

2018

The Dissertation of Erica Rosenblum is approved, and it is acceptable in quality and form for publication on microfilm and electronically:

Co-Chair

Chair

University of California, San Diego

2018

Table of Contents

Signature Page . . . . . **iii**

Table of Contents . . . . . **iv**

List of Figures . . . . . **vii**

List of Tables . . . . . **xii**

Acknowledgements . . . . . **xiii**

Vita . . . . . **xv**

Abstract of the Dissertation . . . . . **xvi**

Chapter 1 Introduction **1**
1.1 Simulated sea ice trends in climate models 2
1.2 Arctic Mixed Layer Evolution 4

Chapter 2 Sea ice trends in climate models only accurate in runs with biased global warming **8**
2.1 Abstract 8
2.2 Introduction 9
2.3 Observed and simulated sea ice trends 12
2.4 Sea ice scales with global temperature 14
2.5 Effective sea ice trend 16
2.6 Pseudo-ensemble from longer time period 20
2.7 Discussion 24
2.8 Conclusion 31
2.A Methods 32
2.B Robustness to changes in methods 34
2.B.1 Using ice area instead of ice extent 34
2.B.2 Paired Trends Tests 34
2.B.3 Using scaled histograms in pseudo-ensemble analysis 35
2.B.4 Using total least squares to compute sea ice sensitivity 36
2.B.5 Using HadCRUT4 instead of GISTEMP 37
Acknowledgements 37

Chapter 3 Faster Arctic sea ice retreat in CMIP5 than in CMIP3 due to volcanoes . . . 39
3.1 Abstract . . . 39
3.2 Introduction . . . 40
3.3 Results . . . 42
3.4 Discussion . . . 46
3.4.1 Do volcanoes influence sea ice sensitivity? . . . 46
3.4.2 Comparing CMIP3 and CMIP5 sea ice sensitivities . . . 48
3.5 Additional Points . . . 51
3.6 Summary . . . 54
3.A Method . . . 55
Acknowledgements . . . 57

Chapter 4 Factors controlling seasonal mixed layer freshening in the Canada Basin during 1975, 2006, and 2007 . . . 58
4.1 Introduction . . . 58
4.2 Observations . . . 60
4.2.1 Oceanographic data . . . 60
4.2.2 Sea ice concentration data . . . 62
4.2.3 Sea ice and mixed-layer evolution . . . 64
4.3 Idealized Framework . . . 65
4.3.1 Heat Fluxes . . . 66
4.3.2 Salt Budget . . . 68
4.4 Results . . . 69
4.4.1 Validation . . . 69
4.4.2 Heat Flux . . . 71
4.4.3 Sea Ice Thickness . . . 73
4.4.4 Freshwater content from ice melt . . . 74
4.4.5 Mixed-Layer Salinity . . . 76
4.5 Discussion . . . 78
4.5.1 Observed Salinity Profiles . . . 78
4.5.2 Comparisons with other studies . . . 79
4.5.3 Sensitivity to Methods . . . 81
4.5.4 Additional points . . . 83
4.6 Summary . . . 84
4.A Method for data selection . . . 85
4.B Standard Error . . . 85
Acknowledgements . . . 86

Chapter 5 Factors controlling seasonal halocline stratification in the Canada Basin during 1975, 2006, and 2007 . . . 87
5.1 Introduction . . . 87
5.2 Methods . . . 89
5.3 Observations . . . 91

5.4 Influence of Seasonal Halocline Stratification 93
5.4.1 Influence of surface processes on ΔPE 96
5.5 Idealized Framework 98
5.5.1 1D model of seasonal mixed-layer evolution 98
5.5.2 Influence of mixed-layer evolution on the seasonal halocline . . 99
5.5.3 Simplified Equations 103
5.6 Comparison with observations 104
5.6.1 Parameters 104
5.6.2 Model Estimates 107
5.7 The role of freshwater vs wind energy 108
5.7.1 The influence of freshwater flux 108
5.7.2 The influence of kinetic energy 111
5.8 Discussion 112
5.9 Summary 115
Acknowledgements 116

Appendix A Chapter 2 Supporting Figures 117

Appendix B Chapter 3 Supporting Figures 124

Appendix C Chapter 4 Supporting Figures 129

Appendix D Chapter 5 Supporting Figures 139

Bibliography 143

List of Figures

Figure 2.1 Observed and CMIP5 modeled linear trends in annual-mean (a,d) global-mean surface temperature, (b,e) Arctic sea ice extent, and (c,f) Antarctic sea ice extent. 13

Figure 2.2 CESM-LE annual-mean sea ice trends (a) in the Arctic and (b) in the Antarctic plotted versus the global-mean surface temperature trend for each ensemble member (red points), with the observations indicated by green lines. 17

Figure 2.3 As in Figure 2.2, but using CMIP5 simulations instead of CESM-LE. 21

Figure 2.4 Scatter of observed and simulated annual-mean (a) Arctic sea ice trends and (b) Antarctic sea ice trends versus the global-mean surface temperature trends from all overlapping 35-year periods in 73 CMIP5 simulations of 1900-2100. 25

Figure 2.5 Simulated annual-mean Antarctic sea ice trend versus Arctic sea ice trend in each run in the (a) CESM-LE and (b) CMIP5 ensembles. 26

Figure 3.1 Observed as well as CMIP3 and CMIP5 modeled trends in (a,c) annual-mean global-mean surface temperature, (b,e) annual-mean Arctic sea ice extent, and (c,f) September Arctic sea ice extent. 43

Figure 3.2 Observed and modeled (a) annual-mean global-mean surface temperature, (b) annual-mean Arctic sea ice area, and (c) September Arctic sea ice area. 44

Figure 3.3 As in Figure 3.1d-f, but neglecting the CMIP3 simulations that do not include volcanic forcing. 45

Figure 3.4 Simulated 35-year annual-mean global-mean temperature trends plotted versus the corresponding Arctic sea ice trends. 49

Figure 3.5 Observed and modeled annual-mean global-mean temperature trends plotted versus the corresponding Arctic (a) annual-mean sea ice trends and (b) September sea ice trends. 50

Figure 4.1 Position of ocean observations taken in the Canada Basin during May-August in (a) 1975, (b) 2006, and (c) 2007, overlaid on the average summer (May-August) sea ice concentration for each year. 60

Figure 4.2 Seasonal evolution of the (a) sea ice concentration, (b) mixed-layer temperature anomaly from freezing, (c) mixed-layer salinity, and (d) mixed-layer depth in 1975 (blue), 2006 (yellow), and 2007 (red). 63
Figure 4.3 Schematic of the one-dimensional framework. Red arrows indicate heat flux to sea ice and blue arrows indicate resulting freshwater flux into the mixed layer from sea ice melt (see Section 5.5 for details). 65
Figure 4.4 Observed (green) and estimated (black) seasonal mixed-layer freshening ($\mathfrak{F}$, eq. 4.9) in (a) 1975, (b) 2006, and (c) 2007. Thick lines indicate the 10-day mean, and the shading indicates the standard error. 69
Figure 4.5 The estimated change in heat flux towards (a) the top of the sea ice (F_{atm}, eq. 4.1) and the bottom of the sea ice (F_{ocean}, eq. 4.2), and (b) their sum (F_{est}, eq. 4.4) is show during 1975 (blue), 2006 (yellow), and 2007 (red). 71
Figure 4.6 The estimated change in sea ice thickness due to (a) top melt (h_{top}, eq. 4.12), (b) bottom melt (h_{bot}, eq. 4.12), and (c) their sum (h_{est}, eq. 4.5) is shown during 1975 (blue), 2006 (yellow), and 2007 (red). 72
Figure 4.7 The estimated change in freshwater content from sea ice melt during the melt season due to (a) top melt (ϕ_{top}, eq. 4.14), (b) bottom melt (ϕ_{bot}, eq. 4.14), and (c) their sum (ϕ_{est}, eq. 4.6) during 1975 (blue), 2006 (yellow), and 2007 (red). 74
Figure 4.8 The estimated change in mixed layer salinity during the melt season due to (a) top melt (S_{top}, eq. 4.16), (b) bottom melt (S_{bot}, eq. 4.16), and (c) their sum (S_{est}, eq. 4.7) during 1975 (blue), 2006 (yellow), and 2007 (red). 76
Figure 4.9 10-day mean salinity profile during the melt season in (a) 1975, (b) 2006, and (c) 2007. Thick colored lines indicate first profile of the melt season, and thick black lines indicate the last profile of the melt season (see Section 5a for details). 78
Figure 4.10 1975, 2006, 2007, and 2004-2012 estimated heat flux, estimated sea ice thickness, estimated freshwater content, and estimated seasonal mixed-layer freshening as well as the observed 2004-2012 mixed-layer freshening. 81

Figure 5.1 Location of ocean observations during (a) 1975, (b) 2006, and (c) 2007 in the Canada Basin. The average summer (July-September) sea ice concentration for each year is also shown. 90
Figure 5.2 Seasonal evolution of the (a) sea ice concentration, (b) mixed layer temperature anomaly from freezing, (c) mixed layer salinity, and (d) mixed layer depth in 1975 (blue), 2006 (yellow), and 2007 (red). 91

Figure 5.3 Observed 10-day mean salinity and temperature profiles for (a,d) June, (b,e) July, and (c,f) August during 1975 (blue), 2006 (yellow), and 2007 (red). 92
Figure 5.4 Observed change in potential energy to deepen the mixed layer to 25 meters (ΔPE) and associated haloclines in 1975 (blue), 2006 (yellow), and 2007 (red). 93
Figure 5.5 As in Figure 5.4, where thin black lines represent the observations and colored lines represent the constructed halocline and associated available potential energy. 96
Figure 5.6 (a) Estimated freshwater flux, (b) observed mixed layer depth, (c) observed mixed layer salinity, and (d-f) observed salinity profiles in 1975, 2006, and 2007. 100
Figure 5.7 Observed (colored lines) and model estimated (black lines) mixed layer evolution. 104
Figure 5.8 (a) Observed and modeled ΔPE evolution during the melt season and (b-d) corresponding modeled halocline profiles. . 106
Figure 5.9 (a) The theoretical relationship between the mixed-layer depth and the freshwater flux and (b) the theoretical relationship between the mixed-layer depth and kinetic energy input. . . 108
Figure 5.10 Observed and modeled (a) freshwater flux, (b) mixed-layer depth, (c) mixed-layer salinity, and (d) ΔPE evolution in 2006. 110
Figure 5.11 As in Figure 5.10, but for 2007. 113

Figure A.1 Annual (a) Arctic and (b) Antarctic sea ice extent versus global-mean surface air temperature using 30 CESM-LE simulations of 1920-2100. 118
Figure A.2 As in Figs. 4a,b but for the 30 CESM-LE simulations of 1920-2100 (4 410 points in total). 119
Figure A.3 (a-b) As in Figs. 4a,b, but here the red highlighted region indicates all 35-year global-mean surface air temperature trends that are within one standard deviation of the 1979-2013 CMIP5 ensemble mean (Fig. 1d). 119
Figure A.4 Time series of annual-mean (a) global-mean surface air temperature, (b) Arctic sea ice extent, and (c) Antarctic sea ice extent from two CESM-LE simulations. 120
Figure A.5 Distributions of annual (a,c,e) Arctic and (b,d,f) Antarctic sea ice trends divided by the annual global-mean surface temperature trends, which gives an estimate of the sea ice sensitivity, using 30 CESM-LE simulations of 2006-2080. 121
Figure A.6 Histograms of the correlations between (a,c) Arctic sea ice extent and (b,d) Antarctic sea ice extent with the global-mean surface air temperature from each (a,b) CESM-LE simulation and (c,d) CMIP5 simulation of 1979-2013. 122

Figure A.7 Distribution of 118 CMIP5 simulated 1979-2013 (a,c) Arctic and (b,d) Antarctic (a,b) sea ice trends and (c,d) effective sea ice trends, as in Figs. 1e,f and 3c,d. 123

Figure B.1 As in Figure 2, but showing the simulations only and looking at an extended time period that includes the additional volcanic eruptions of Santa Maria (1901) and Agung (1963). 124
Figure B.2 As in (a) Figure 2b and (b) Figure 3a, but for annual-mean Antarctic sea ice trends. 125
Figure B.3 As in Figure 4 but using initial Arctic sea ice extent on the horizontal axis rather than global surface temperature trends. 125
Figure B.4 As in Figure 1, but using sea ice area rather than extent. . . 126
Figure B.5 As in Figure 2, but using sea ice area rather than extent. . . 126
Figure B.6 As in Figure 3, but using sea ice area rather than extent. . . 126
Figure B.7 As in Figure 4, but using sea ice area rather than extent. . . 127
Figure B.8 As in Figure 5, but using sea ice area rather than extent. . . 128

Figure C.1 Location of observations in 1975, 2006, 2007, 2008, 2011, and 2004-2012. Different colors indicate that the observations come from different ITPs or AIDJEX ice camps. 130
Figure C.2 Temporal evolution of (a) the number of observations, (b) the average distance between points, and (c) the average drift of the observations from the beginning of the year for all available ITP data in 1975, 2006, 2007, 2008, and 2011. 130
Figure C.3 As in Figure S2, but using only observations from ITPs that collect data throughout the melt season. 131
Figure C.4 Observed sea ice concentration using two different methods in 1975/1979, 2006, and 2007. The blue line indicates the average over the Canada Basin in 1979, 2006, and 2007. . . . 131
Figure C.5 As in Figure 4, but using a different method to compute the observed sea ice concentration (red lines in Figure S12). . . . 131
Figure C.6 As in Figure 5c, 6c, 7c, and 8c, but using a different method to compute the observed sea ice concentration (red lines in Figure S12). 132
Figure C.7 As in Figure 4, but using a different method to compute the observed mixed layer depth. 132
Figure C.8 As in Figure S5, but using a different method to compute the observed mixed layer depth. 133
Figure C.9 As in Figure 10, but for 2008 instead of 2004-2012. 134
Figure C.10 As in Figure 10, but for 2011 instead of 2004-2012. 135
Figure C.11 Observed sea ice concentration, mixed layer temperature anomaly from freezing, mixed layer salinity, and mixed layer depth for all available, level 3 processed ITP data between 2004-2012 (black dots). 136

Figure C.12 As in Figure S11, but with colored solid lines indicating the mean of observations taken from different ITPs in 2006. . . . 136
Figure C.13 As in Figure S12, but for 2007. 137
Figure C.14 As in Figure S12, but for 2008. 137
Figure C.15 As in Figure S12, but for 2011. 138

Figure D.1 Observed change in potential energy required to deepen the mixed layer to 25 meters (ΔPE) in 1975 (blue), 2006 (yellow), and 2007 (red). 140
Figure D.2 The 1975 observed evolution of (top) the mixed layer depth and (center) mixed layer salinity. 141
Figure D.3 As in Figure S2, but for 2006 instead of 1975. 141
Figure D.4 As in Figure S2, but for 2007 instead of 1975. 142

List of Tables

Table 2.1 Fraction of runs with simulated sea ice trends that are at least as extreme as the observations using the distribution of CMIP5 simulated trends, effective trends, and a pseudo-ensemble of 35-year periods. 31

Table 3.1 For each CMIP3 model, the number of runs, 1979-2013 annual-mean global-mean surface temperature trend (K/decade) averaged over the runs, and 1979-2013 annual-mean and September Arctic sea ice trends (10^6 km^2/decade) averaged over the runs. 47

Table 3.2 Observed as well as CMIP3 and CMIP5 ensemble-mean effective sea ice trends (10^6 km^2/decade) and ice sensitivity (10^6 km^2/K), as shown in Figure 3.5. 52

Table C.1 Average and standard deviation of the number of observations, the average distance between observations, and the average drift from initial location during the 1975, 2006-2008, and 2011 melt season. 133

ACKNOWLEDGEMENTS

I wouldn't have much of a thesis without my advisors, Ian Eisenman and Sarah Gille. They are warmly thanked for the enormous amount of time, patience, energy, and guidance they have given me while carrying out this work. My committee members, David Saintillan, Lynne Talley, Maria Vernet, and Shang-Ping Xie are also acknowledged for their time, helpful comments, and feedback.

I wouldn't have gotten past my first year at Scripps without my cohort. Thank you, Greg, Kasia, Marion, Veronica, Travis, Kevin, Chris and the entire 2012 cohort for teaching me so much about math, physics, and the ocean.

I wouldn't have gotten past the next few years without my amazing groupmates: Shantong, Till, Rebecca, and Skipper. Thank you for teaching me so much about sea ice and the polar oceans. And thank you double for getting Ian to treat us to so many beers and meals.

I wouldn't have gotten past my qualifying exam without my hallmates, who suffered alongside me with their own qualifying exams and defenses. Thank you, Janin, Rachel, and Caitlin for keeping me sane while working nights and weekends and somehow making that whole process fun.

I wouldn't have made it through the cold winters in Canada or a very wet year in Brest without my adopted advisors and groupmates. Thank you, Robert, Verena, Heather, and Ben for keeping a smile on my face and somehow making me forget that I could be on a beach in San Diego. And thank you, Paul Kushner and Camille Lique for your scientific guidance and for welcoming me into your research groups.

Lastly, I wouldn't have gotten past the last few weeks without my friends and family. Thank you, Gayathri, Roxanne, Thiago, Babacar, René, Michèle, Mom, Dad, and Nico, for support, perspective, food, and hugs.

Chapter Two, in full, is a reprint as it appears in the Journal of Climate, 2017. Rosenblum, E. and Eisenman, I. (2017) Sea ice trends in climate models only accurate in runs with biased global warming. *J. Climate*, 30, 6265-6278. ©American Meteorological Society. Used with permission. The dissertation author was the primary investigator and author of this paper.

Chapter Three, in full, is a reprint as it appears in the Journal of Climate, 2016. Rosenblum, E. and Eisenman, I. (2016) Faster Arctic sea ice retreat in CMIP5 than in CMIP3 due to volcanoes. *J. Climate*, 29, 9179-9188. ©American Meteorological Society. Used with permission. The dissertation author was the primary investigator and author of this paper.

Chapter Four, in part, is currently being prepared for submission for publication of the material. Rosenblum, E., Gille, S., Lique, C. The dissertation author was the primary investigator and author of this paper.

Chapter Five, in part, is currently being prepared for submission for publication of the material. Rosenblum, E., Gille, S., Lique, C. The dissertation author was the primary investigator and author of this paper.

VITA

2011	Bachelor of Science in Physics Physics, Stony Brook University
2014	Master of Science in Mechanical Engineering Mechanical Engineering, University of California, San Diego
2014–2018	NSF Graduate Research Fellow and Chateaubriand Fellow, Scripps Institution of Oceanography, University of California, San Diego
2018	Doctor of Philosophy in Oceanography Scripps Institution of Oceanography University of California, San Diego

PUBLICATIONS

Sea Ice Trends in Climate Models Only Accurate in Runs with Biased Global Warming
Erica Rosenblum and Ian Eisenman
Journal of Climate, **2017**, *30*

Faster Arctic sea ice retreat in CMIP5 than in CMIP3 due to volcanoes
Erica Rosenblum and Ian Eisenman
Journal of Climate, **2016**, *29*

Turbulent mixing and layer formation in double-diffusive convection: 3D numerical simulations and theory
Erica Rosenblum, Pascale Garaud, Adrienne Traxler, and Stephan Stellmach
Astrophysical Journal, **2011**, *731*

ABSTRACT OF THE DISSERTATION

Arctic sea ice retreat and mixed-layer processes

by

Erica Jamie Rosenblum
Doctor of Philosophy in Oceanography
University of California, San Diego, 2018

Professor Ian Eisenman, Chair

Professor Sarah Gille, Co-Chair

Arctic sea ice retreat is a well-known signatures of climate change and is driving changes to the underlying ocean. Progress in modeling and observational systems have driven huge advances towards better understanding the complexities related to Arctic sea ice retreat and Arctic Ocean processes. The objective of this thesis is to incorporate the results of these studies into the development of simple but informative methods aimed at increasing our understanding of simulated sea ice evolution in climate models and ocean processes in observations.

Chapters 2 and 3 are focused on examining sea ice changes in climate models

with respect to simulated levels of global warming. In contrast to many previous studies that did not consider simulated global warming, we find that simulated internal variability cannot explain differences between observed and modeled sea ice retreat (Chapter 2). Next, we examine sea ice retreat in the two most recent generations of climate models and find that previously reported improvements in the simulated sea ice retreat was caused by an increase in the global warming bias, driven by the inclusion of simulated volcanic forcing (Chapter 3).

Chapters 4 and 5 are focused on examining changes in the mixed-layer evolution during the melt season in the Canada Basin in 1975, 2006, and 2007. Using a simplified salt budget, we find that recent increases in the seasonal mixed-layer freshening could mainly be a result of shallower mixed layers, which act to concentrate freshwater input within a smaller volume (Chapter 4). Motivated by this, we use a simplified energy budget to investigate factors driving differences in the mixed-layer depth evolution during the melt season in these three years. The results suggest that reduced ice-ocean drag may play a significant role in explaining shallower mixed layers in recent years (Chapter 5).

Chapter 1

Introduction

The rapid decline of Arctic sea ice cover is one of the most recognized signatures of climate change and is expected to have wide-reaching impacts on both regional and global scales (e.g., IPCC, 2013). Developments in numerical modeling and observational systems have opened new avenues for studying these phenomena. For example, since its origins in the mid-1990's, the Coupled Model Intercomparison Project (CMIP) has brought together modeling groups from around the world that develop state-of-the-art climate models (GCMs) to create a coordinated dataset of climate change simulations (Meehl *et al.*, 2007). CMIP3 and CMIP5 models have become an essential tool for assessing and predicting climate change and have been used extensively in the IPCC 4th and 5th assessment report (IPCC, 2007, 2013), respectively. There have also been a number of observational programs, providing valuable observations of the changing Arctic over the past decades, including a number of experiments carried out on occupied ice camps during the Arctic Ice Dynamics Joint Experiment (AIDJEX) (Maykut & McPhee, 1995) and more recently the Ice-Tethered Profiler (ITP) instrument system (Krishfield *et al.*, 2008) and the Ice Mass Balance (IMB) Buoy program (Perovich *et al.*, 2017), two systems made up of autonomous instruments that take oceanographic and ice thickness measurements throughout the

Arctic. These new tools have led to numerous studies that have increased our understanding of both simulated Arctic sea ice retreat in climate models (e.g., Stroeve & Notz, 2015) and the influence of these changes on the underlying ocean (e.g., Carmack *et al.*, 2015). This thesis is focused on incorporating several of these tools to increase our understanding of simulated sea ice evolution in climate models (Chapters 2-3) and ocean processes in observations (Chapters 4-5).

1.1 Simulated sea ice trends in climate models

While CMIP5 models simulate a faster sea ice retreat than CMIP3 models, both generations of climate models tend to underestimate the rate of sea ice retreat compared with the observations (Stroeve *et al.*, 2012; IPCC, 2013). These results raised two important questions: (1) Are the models inconsistent with the observations? (2) Why do CMIP5 models simulate a faster sea ice retreat that is more consistent with the observations than CMIP3 models?

Several studies suggest that models are still consistent with the observations after accounting for internal variability (Holland *et al.*, 2008; Kay *et al.*, 2011; Stroeve *et al.*, 2012; IPCC, 2013; Notz, 2014; Swart *et al.*, 2015) and that model improvements caused CMIP5 models to simulate a faster sea ice retreat than CMIP3 models (Stroeve *et al.*, 2012; Flato *et al.*, 2013). However, arriving at a firm answer to either of these questions is difficult given inter-model differences (Stroeve *et al.*, 2012; IPCC, 2013) and the wide range of processes that are expected to influence sea ice trends (e.g., Perovich *et al.*, 2011).

On the other hand, Winton (2011) suggested that these complications can be partially avoided by considering the sensitivity of the sea ice cover to global warming rather than sea ice retreat. This involved making the simplifying assumption that

changes in sea ice cover could approximately be described as

$$\Delta I = \frac{\Delta I}{\Delta T}\frac{\Delta T}{F}F, \tag{1.1}$$

where ΔI is the change in sea ice cover, ΔT is the change in global mean surface temperature, and F is the radiative forcing. By focusing on the "Sea Ice Sensitivity?" ($\frac{\Delta I}{\Delta T}$), Winton (2011) effectively factors out model differences, biases, and uncertainties that are related to the sensitivity of global temperature to radiative forcing.

Winton (2011) demonstrated that there was an approximately linear relationship between sea ice area and global temperatures in several CMIP3 models. This implies that simulations with more global warming also had more sea ice retreat. Further, he found that only simulations with more global warming than the observations could accurately simulate the Arctic sea ice retreat. That is, he found that the simulated Arctic sea ice cover was not as sensitive to global warming as the observations.

These results suggest that the models were not simulating the observed Arctic sea ice retreat for the right reasons, and therefore supported the view that the models and observations are not consistent even after accounting for internal variability. However, Winton (2011) pointed out that we cannot rule out the possibility that this discrepancy is related to internal variability, given the small number of simulations available and short observational record (he examined 1979-2009). That is, perhaps the range of sea ice trends possible under internal variability was not well represented.

In Chapter 2, the possibility that the 1979-2013 CMIP5 modeled and observed sea ice trends are consistent with each other after accounting for internal variability is revisited, following a similar methodology to Winton (2011). There are approximately three times as many CMIP5 simulations as there were CMIP3 simulations. The Community Earth System Model Large Ensemble is also examined, which provides

30 simulations from a single model that vary only due to internal variability. In Chapter 3, factors that caused CMIP5 models to simulate a faster Arctic sea ice retreat than CMIP3 models are investigated by examining changes in the simulated sea ice sensitivity to global warming in the two sets of models.

1.2 Arctic Mixed Layer Evolution

Under the Arctic sea ice, warm salty water from the Atlantic and the Pacific Ocean subducts below cold, fresh surface waters of the Arctic Ocean. In the Canada Basin, the largest of the sub-basins in the Arctic Ocean, surface waters are separated from the underlying warmer waters by a strongly stratified permanent halocline, causing these two features to have limited interaction with each other (Timmermans *et al.*, 2008; Toole *et al.*, 2010). This implies that the surface of the ocean is mainly driven by sea ice and atmospheric processes on seasonal timescales.

One of the earliest year-long examinations of the Arctic Ocean below sea ice was occurred during the Arctic Ice Dynamics Joint Experiment (AIDJEX) in the Canada Basin between April 1975 and April 1976. During this program, scientists lived on four drifting ice camps while collecting observations of the sea ice, ocean, and atmosphere. At the time, the region was covered with thick, perennial sea ice cover that strongly limited any interaction between the atmosphere and underlying ocean. Yet, early observations indicated the presence of a near-freezing mixed-layer with a salinity and depth that evolved on seasonal timescales (McPhee & Smith, 1976; Morison & Smith, 1981).

Qualitatively, this suggested that sea ice melt and formation were driving seasonal variations in the mixed-layer salinity and mixed-layer depth. In the fall and winter, brine rejection from sea ice formation would increase the salt content in the mixed layer (to $\sim$31 psu) and cause convectively-driven mixed layer deepening (to

$\sim$60m). In the spring and summer, freshwater flux from sea ice melt caused the mixed-layer salinity to decrease (to $\sim$30 psu), and the added buoyancy would lead to a shallower mixed-layer depth (to $\sim$20m) (Lemke & Manley, 1984).

Lemke & Manley (1984) presented one of the earliest under-ice seasonal mixed-layer models. It was an idealized, one-dimensional model that built off of an early model of the seasonal thermocline in mid-latitudes (Kraus & Turner, 1967). The model considered a mixed layer that was driven by kinetic energy from keel-stirring and salinity surface fluxes from sea-ice growth and sea-ice melt. This simplified model was shown to be consistent with observations from AIDJEX and has since been used as a basis for many other polar mixed-layer modeling studies (e.g., Lemke, 1987; Martinson, 1990; Björk, 2002; Petty *et al.*, 2013).

Since the AIDJEX experiment, the Arctic Ocean has undergone dramatic changes. This is particularly true of the Canada Basin (Peralta-Ferriz & Woodgate, 2015*a*), which has lost more first-year and multi-year sea ice than any other Arctic sub-basin (McLaughlin *et al.*, 2011). Confirming how this has influenced the ocean mixed layer is difficult given the observational constraints. The majority of the observations taken in the years following AIDJEX come from hydrographic measurements, which are intermittent and tend to take place in areas of low sea ice cover (Carmack *et al.*, 2015; Peralta-Ferriz & Woodgate, 2015*a*). As a result, for more than 20 years, there were few data available to compare with the AIDJEX dataset (McPhee *et al.*, 1998).

After AIDJEX, the first major US effort to collect ocean observations below Arctic sea ice for more than a year was the Surface Heat Budget of the Arctic (SHEBA) project in 1997. Similar to AIDJEX, the experiment platform drifted passively through the Canada Basin collecting oceanographic measurements. Comparisons of oceanic profiles from SHEBA in 1997 and AIDJEX in 1975 revealed dramatic

changes to the ocean mixed layer (McPhee *et al.*, 1998). Specifically, McPhee *et al.* (1998) found evidence suggesting significant increases in both the heat and freshwater fluxes that occurred during the melt season. However, a clear comparison between the two years still proved difficult given that the icebreaker drifted much further north of the AIDJEX ice camp locations fairly early in the experiment. McPhee *et al.* (1998) were therefore only able to compare profiles from November 1997 to profiles from July 1975.

More recently, the Ice-Tethered Profiler (ITP) instrument system (Krishfield *et al.*, 2008) has collected over 100,000 profilers below sea ice throughout the Arctic since 2004. The ITP instrument system is made up of a series of autonomous buoys that are frozen into sea ice floes throughout the Arctic. The buoys are connected to 800m wires and have profilers that move up and down 2-3 times per day collecting ocean measurements. Detailed studies of observations in conjunction with observations of sea ice thickness evolution and one-dimensional models have provided valuable insight into the underlying processes driving seasonal mixed-layer evolution in the Canada Basin in recent years (Toole *et al.*, 2010; Jackson *et al.*, 2011; Gallaher *et al.*, 2016).

Comparisons of ITP profiles that occurred in similar locations to the AIDJEX dataset also revealed anecdotal evidence of a trend toward warmer and fresher mixed layers (Toole *et al.*, 2010; McPhee, 2012), similar to the comparison with SHEBA data (McPhee *et al.*, 1998). The possibility that the surface mixed layer is undergoing significant changes has since been further supported by Peralta-Ferriz & Woodgate (2015*a*), who analyzed over 21,000 hydrographic profiles collected throughout the Arctic between 1979-2012 (though this study did not include AIDJEX or ITP data). Their results revealed clear 30-year trends towards warmer, fresher, and shallower mixed layers throughout the Arctic, with particularly large signals in the Canada

Basin.

These decadal changes in the seasonal mixed-layer evolution could signal a growing influence of the ocean mixed layer on Arctic sea ice evolution (e.g., Jackson *et al.*, 2010; Toole *et al.*, 2010; Jackson *et al.*, 2011; Steele *et al.*, 2011; Timmermans, 2015; Perovich & Richter-Menge, 2015; Carmack *et al.*, 2015; Gallaher *et al.*, 2016). Previous studies have provided significant insight into the processes controlling seasonal mixed-layer evolution in 1975 using AIDJEX data (Lemke & Manley, 1984; Maykut & McPhee, 1995), and other previous studies have provided significant insight into the processes controlling seasonal mixed-layer evolution in the 2000's using ITP data (Jackson *et al.*, 2010; Toole *et al.*, 2010; Gallaher *et al.*, 2017, 2016). Mechanisms driving decadal changes to seasonal mixed-layer evolution are investigated using a single simplified framework to examine seasonal mixed-layer evolution in both AIDJEX and ITP data in Chapters 4 and 5.

Chapter 2

Sea ice trends in climate models only accurate in runs with biased global warming

2.1 Abstract

Observations indicate that the Arctic sea ice cover is rapidly retreating while the Antarctic sea ice cover is steadily expanding. State-of-the-art climate models, by contrast, typically simulate a moderate decrease in both the Arctic and Antarctic sea ice covers. However, in each hemisphere there is a small subset of model simulations that have sea ice trends similar to the observations. Based on this, a number of recent studies have suggested that the models are consistent with the observations in each hemisphere when simulated internal climate variability is taken into account. Here we examine sea ice changes during 1979-2013 in simulations from the most recent Coupled Model Intercomparison Project (CMIP5) as well as the Community Earth System Model Large Ensemble (CESM-LE), drawing on previous work that found a

close relationship in climate models between global-mean surface temperature and sea ice extent. We find that all of the simulations with 1979-2013 Arctic sea ice retreat as fast as observed have considerably more global warming than observations during this time period. Using two separate methods to estimate the sea ice retreat that would occur under the observed level of global warming in each simulation in both ensembles, we find that simulated Arctic sea ice retreat as fast as observed would occur less than 1% of the time. This implies that the models are not consistent with the observations. In the Antarctic, we find that simulated sea ice expansion as fast as observed typically corresponds with too little global warming, although these results are more equivocal. We show that because of this, the simulations do not capture the observed asymmetry between Arctic and Antarctic sea ice trends. This suggests that the models may be getting the right sea ice trends for the wrong reasons in both polar regions.

2.2 Introduction

In comprehensive climate model simulations of long-term climate change, individual models are often used to carry out multiple simulations that differ only in their initial conditions. The spread among the simulations approximates the range of possible realizations of internal variability in the climate system. Therefore an individual simulation would not typically match the observations on decadal timescales even if the model were perfect, but the observations are expected to fall within the range of the ensemble of simulations.

Modeling groups from around the world have contributed to each phase of the Coupled Model Intercomparison Project (CMIP). In the previous phase, CMIP3 (Meehl *et al.*, 2007), virtually none of the models simulated a summer Arctic sea ice cover that diminished as fast as in the observations under historical natural and

anthropogenic climate forcing (Stroeve *et al.*, 2007). However, Stroeve *et al.* (2007) suggested the possibility that the observed Arctic sea ice retreat may represent a rare realization of internal variability that would be captured in only a small fraction of simulations. The CMIP3 models simulated sea ice trends that were more consistent with observations in the Antarctic than in the Arctic (Stroeve *et al.*, 2007; IPCC, 2007).

In the current phase, CMIP5 (Taylor *et al.*, 2012), the simulated rate of Arctic sea ice retreat is closer to the observations (Stroeve *et al.*, 2012; IPCC, 2013). The cause of this reduction in model bias is analyzed in a companion paper (Rosenblum & Eisenman, 2016). The ensemble-mean Arctic sea ice trend in CMIP5 is still slower than observed (Stroeve *et al.*, 2012; IPCC, 2013), but the observations fall within the range of simulations (Figures 2.1b,e). Therefore, many recent studies have suggested that the Arctic sea ice retreat simulated in this newer generation of climate models is consistent with observations when simulated internal climate variability is taken into account (Holland *et al.*, 2008; Kay *et al.*, 2011; Stroeve *et al.*, 2012; IPCC, 2013; Notz, 2014; Swart *et al.*, 2015). Given the CMIP5 ensemble-mean results, this would imply that climate forcing has caused some of the observed Arctic sea ice retreat, with the remainder caused by decadal-scale internal variability.

During the past several years, the observed trend toward Antarctic sea ice expansion has become substantially larger and crossed the threshold of statistical significance (Comiso & Nishio, 2008; IPCC, 2013), which was related to a recent update in the way the satellite sea ice observations are processed (Eisenman *et al.*, 2014). Most CMIP5 models do not simulate this trend (Figures 2.1c,f) (e.g., Turner *et al.*, 2013; Zunz *et al.*, 2013; IPCC, 2013), contributing to a consensus view that there is "low confidence" in the scientific understanding of the observed Antarctic sea ice expansion (IPCC, 2013). Nonetheless, a number of recent studies have argued

that the models are still at least marginally consistent with observations when the range of internal climate variability is considered (Turner *et al.*, 2013; Swart & Fyfe, 2013; Zunz *et al.*, 2013; Mahlstein *et al.*, 2013; Polvani & Smith, 2013; Goosse & Zunz, 2014; Gagné *et al.*, 2015; Fan *et al.*, 2014; Turner *et al.*, 2015; Purich *et al.*, 2016; Jones *et al.*, 2016). In this view, the observed Antarctic sea ice expansion is the result of internal climate variability overwhelming the sea ice retreat that would have occurred due to climate forcing.

Consequently, these recent studies suggest that simulated internal variability can explain the differences between typical state-of-the-art climate model simulations and observed sea ice trends in both the Arctic and the Antarctic. However, a number of previous studies have found that Arctic sea ice cover is approximately linearly related to global-mean surface temperature in climate models (Gregory *et al.*, 2002; Winton, 2011; Mahlstein & Knutti, 2012; Stroeve & Notz, 2015). This suggests that it may be important to consider global-mean surface temperature trends when comparing sea ice trends with observations.

Here, we examine the relationship between global-mean surface temperature and sea ice extent in each hemisphere in all available CMIP5 simulations of years 1979-2013, and we compare this with observations. There are 40 different climate models, many of which submitted multiple simulations with differing initial conditions, leading to a total of 118 ensemble members. Hence the CMIP5 ensemble members differ due to both inter-model differences and realizations of internal variability. In order to isolate the influence of internal variability alone, we also consider simulations from the Community Earth System Model Large Ensemble (CESM-LE) (Kay *et al.*, 2015), which includes 30 ensemble members that are all generated with the same model and differ only in initial conditions. See Table S1 for a list of models and Appendix A for details regarding the processing of the simulation output and the observations.

Some previous studies have focused on the September or March sea ice trend, whereas others have considered the annual-mean trend. Here we focus on annual-mean trends, thereby averaging over seasonal variability that may be unrelated to long-term changes.

2.3 Observed and simulated sea ice trends

As a starting point, we consider the extent to which the observations lie within the distribution of CMIP5 simulated 1979-2013 Arctic and Antarctic sea ice trends. Each distribution approximates the range of sea ice trends allowed by internal climate variability and differences in model physics. Examining each hemisphere individually, we find that in both cases the observed sea ice trend lands within the overall range of the CMIP5 distribution (Figure 2.1e-f).

To quantify the level of agreement, we determine the number of simulated trends that are at least as far in the tail of the CMIP5 distribution as the observed trend. We find that 13 of the 118 simulations have Arctic sea ice retreat at least as fast as the observations and 3 of the 118 simulations have Antarctic sea ice expansion at least as fast as the observations (Table 1). This implies that if the CMIP5 models are correct, then the probability that the Arctic sea ice would retreat as fast as observed is 11%, and the probability that the Antarctic sea ice would expand as fast as observed is 2.5%. These results are approximately similar to previous studies that found that, after accounting for simulated internal variability, the models and observations are statistically consistent in the Arctic (Stroeve *et al.*, 2012; Notz, 2014; Swart *et al.*, 2015) and marginally consistent in the Antarctic (Swart & Fyfe, 2013; Turner *et al.*, 2013; Zunz *et al.*, 2013; Purich *et al.*, 2016; Jones *et al.*, 2016).

As an alternative method of assessing the level of agreement, we also consider Gaussian fits of the model distributions. This will be useful later in the analysis when

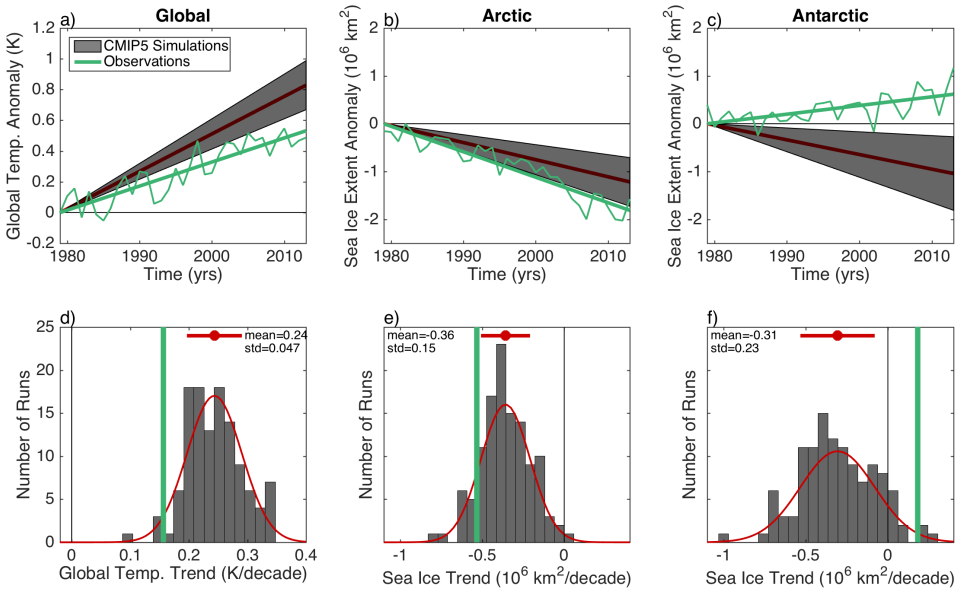

Figure 2.1: Observed and CMIP5 modeled linear trends in annual-mean (a,d) global-mean surface temperature, (b,e) Arctic sea ice extent, and (c,f) Antarctic sea ice extent. (a-c) Here the trends are illustrated as straight lines shifted vertically so that the trend lines go through zero in 1979. The dark red lines indicate the ensemble-mean trend, and the gray shadings indicate one standard deviation among the 118 CMIP5 trends. The observed time series is also included for each quantity (green). (bottom row) Histograms showing the distributions of CMIP5 modeled trends, with the observed trend indicated by a green line in each panel. The standard deviation of each distribution about the ensemble mean is indicated by a red error bar above the histogram, and a Gaussian fit to each distribution is plotted in red.

the observations fall deep within the tail of the distributions. We find that 12% of runs in the Gaussian distribution in Figure 2.1e have Arctic sea ice retreat at least as fast as the observations, and 1.6% of runs in the Gaussian distribution in Figure 2.1f have Antarctic sea ice expansion as fast as the observations, similar to the raw percentiles given above. It should be noted, however, that these distributions are not expected to be exactly Gaussian. They would be Gaussian, for example, if the simulated sea ice retreat were a linear trend in time at the same rate in all of the ensemble members with superimposed internal variability taking the form of realizations of white noise (e.g., Santer *et al.*, 2008). Under this construction, the center of the distribution is the response to climate forcing, and the width of the distribution represents the influence of internal variability.

2.4 Sea ice scales with global temperature

Previous studies have found an approximately linear relationship in many climate model simulations between global-mean surface temperature and sea ice extent in the Arctic (Gregory *et al.*, 2002; Winton, 2011; Mahlstein & Knutti, 2012; Stroeve & Notz, 2015) and Antarctic (e.g., Armour *et al.*, 2011), and the regression coefficient is often referred to as the "sea ice sensitivity" to global warming (Winton, 2011). We find that this applies to Arctic sea ice in the CESM-LE and CMIP5 ensembles (Figure A.1a): The annual-mean Arctic sea ice extent and annual-mean global-mean surface air temperature have an ensemble-mean correlation of -0.99 in the CESM-LE simulations of 1920-2100 and -0.94 in the CMIP5 simulations of 1900-2100 (Figure A.1c,e; see Appendix A for details). We find that the Antarctic sea ice extent has a similar relationship with global temperature (Figure A.1b), although the correlation is somewhat smaller at -0.98 and -0.86 in CESM-LE and CMIP5, respectively (Figure A.1d,f). These relationships imply that simulated 35-year global-mean surface temperature trends are related to sea ice trends in both hemispheres (scatter of black points in Figures A.3 and A.5a,b).

Although this study focuses primarily on CMIP5, we begin by using CESM-LE in order to assess how this relationship influences the distribution of 1979-2013 sea ice trends in realizations of a single model. In Figure 2.2a,b we plot the Arctic and Antarctic sea ice extent trend in each CESM-LE simulation versus the simulated trend in global-mean surface air temperature. This shows a clear relationship in which realizations of internal climate variability that have anomalously large levels of global warming during 1979-2013 also tend to have anomalously large levels of sea ice retreat during this period in both hemispheres. Two representative runs are plotted in Figure A.4 to further illustrate this point. This is consistent with Xie *et al.* (2016), who found that simulated internal variability in global-mean surface

temperature correlates substantially with temperatures in both polar regions.

The results in Figure 2.2 are also relevant to the recent study of Notz & Stroeve (2016), who propose a physical mechanism by which sea ice extent responds linearly to cumulative CO_2 emissions. This mechanism implies that the previously noted relationship between sea ice extent and global-mean surface temperature is actually an artifact of global temperature also depending linearly on cumulative CO_2 emissions. Since the CESM-LE simulations in Figure 2.2 each represent identical cumulative CO_2 emissions (i.e., each has identical forcing) and have a range of different global-mean temperature trends, they provide an ideal testing ground for this hypothesis. Hence the relationship between global-mean surface temperature trends and sea ice trends in Figure 2.2 represents a counterargument to the hypothesis that sea ice extent is fundamentally driven by cumulative CO_2 emissions (Notz & Stroeve, 2016). Rather, the results in Figure 2.2 suggest that the underlying mechanism for the linear relationship between sea ice extent and global-mean temperature must account for the relationship being robust to changes in global-mean temperature driven by internal climate variability (cf. Winton, 2011).

Next, we examine this relationship using CMIP5 simulations of 1979-2013 (Figure 2.3a-b). We find here also that higher levels of global warming tend to be associated with more rapid sea ice retreat, implying that some of the inter-model differences in sea ice trends may be associated with differences in the level of simulated global warming. Comparing with observations, we find that although some of the simulations in Figure 2.3a approximately match the observed sea ice retreat and others approximately match the observed level of global warming, there is a systematic bias in which none of the simulations match both observed rates. All of the simulations with Arctic sea ice trends similar to the observations have global warming rates that are approximately 1.4-2.1 times larger than the observed trend in Figure

2.3a. Similarly, each simulation with a temperature trend similar to the observations underestimates the Arctic sea ice retreat by at least 30%. By contrast, runs with approximately accurate levels of global warming tend to land closer to the observed Antarctic sea ice trend, although they still tend to simulate Antarctic sea ice retreat rather than the observed expansion (Figure 2.3b).

Note that the relationship between sea ice trends and global-mean surface temperature trends is less correlated in the CMIP5 simulations (correlations of -0.56 and -0.54 in Fig 2.3a and 2.3b, respectively) than in the CESM-LE simulations (correlations of -0.73 and -0.81 in the Fig 2.2a and 2.2b, respectively). This is consistent with the previous finding that the sea ice sensitivity to global warming remains relatively constant within a single model but can differ substantially from one model to another (Winton, 2011). On the other hand, however, sea ice and global temperature are typically less correlated under internal variability than under greenhouse-driven warming (Winton, 2011), which could be expected to cause simulations that differ only due to internal variability (Fig 2.2) to have a less correlated relationship than simulations with different levels of greenhouse-driven warming (Fig 2.3). The results of Fig 2.3a,b and 2.2a,b suggest that the former effect is the dominant factor here, and that the low correlation among the CMIP5 simulations (Figure 2.3) is largely due to inter-model differences in the sea ice sensitivity.

2.5 Effective sea ice trend

Motivated by the above result that biases in global-mean surface air temperature trends are related to both Arctic and Antarctic sea ice trends in these simulations, we consider a simple method to account for biases in the level of simulated global warming. This method leverages the approximately linear relationship between sea ice extent and global-mean surface temperature (Figure A.1), and it allows us to

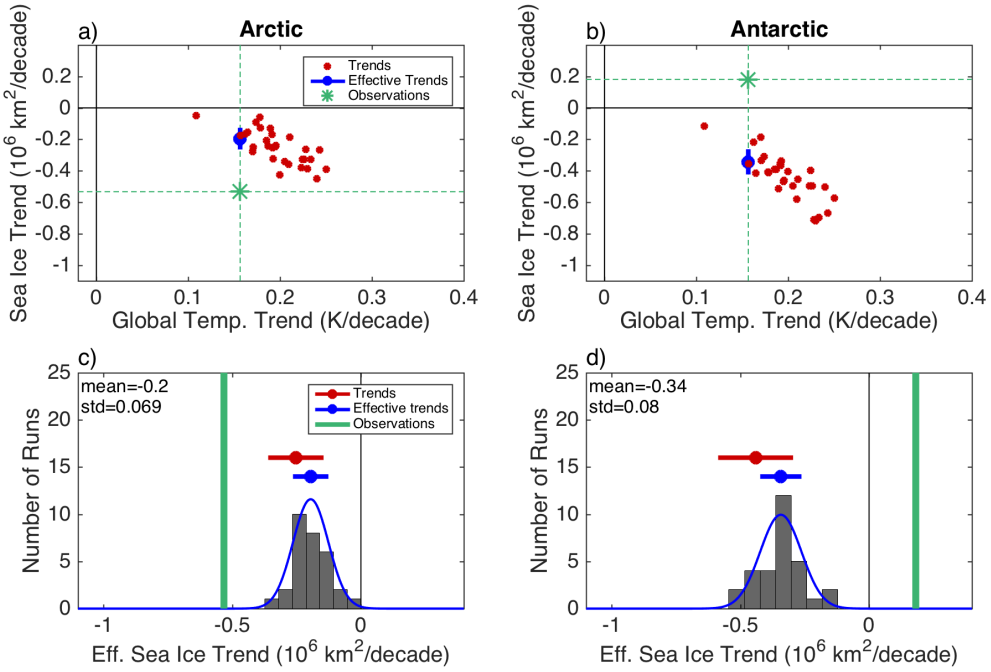

Figure 2.2: CESM-LE annual-mean sea ice trends (a) in the Arctic and (b) in the Antarctic plotted versus the global-mean surface temperature trend for each ensemble member (red points), with the observations indicated by green dashed horizontal and vertical lines. (c-d) The distribution of simulated effective sea ice trends (see text for details) from each CESM-LE simulation, with the observed trend indicated by a green vertical line. The mean and standard deviation of the distribution of simulated sea ice trends (red error bar, repeated from Figures 2.1e-f) and effective sea ice trends (blue error bar) are shown, as well as Gaussian fits to the effective sea ice trend distributions (blue curve). The mean and standard deviation of the effective trends are repeated for comparison in the top panel (blue vertical error bars).

approximately estimate the distribution of sea ice trends that the models would produce if they simulated a level of global warming during 1979-2013 that matched the observations. That is, we examine how the results presented in Section 2 are affected by the biases presented in Section 3.

Using the approximation that the ratio between trends in sea ice extent and trends in global temperature in each simulation does not depend on the level of global warming (which would hold if the relationship between sea ice extent and global-mean temperature were perfectly linear, i.e., if the sea ice sensitivity were constant), we can scale the sea ice trend in each simulation to account for the bias in global warming:

$$\left(\frac{dI}{dt}\right)_{\text{eff}} \equiv \left(\frac{dI}{dt} \Big/ \frac{dT}{dt}\right)_{\text{sim}} \left(\frac{dT}{dt}\right)_{\text{obs}}. \tag{2.1}$$

We define the term on the left-hand side as the "effective sea ice trend", which is computed for 1979-2013 in each simulation. The effective sea ice trend is meant to approximate what the value of the simulated sea ice trend would have been if the model had accurately captured the observed level of global warming. The quotient on the right-hand side is the simulated change in sea ice extent per degree of global warming (measured in km^2/K), which is a measure of the simulated sea ice sensitivity based on the ratio of simulated temporal trends (Winton, 2011). The sea ice sensitivity is then scaled by the observed global-mean surface temperature trend, which is the final term on the right-hand side.

This method can be visualized by drawing a line from the origin to each point in Figures 2.2a,b and 2.3a,b. The slope of this line is equivalent to the sea ice sensitivity, and the y-coordinate of the point where this line intersects the vertical dashed line (indicating the observed temperature trend) is equivalent to the effective sea ice trend. The spread in effective sea ice trends in each ensemble is shown by the vertical blue error bars in Figures 2.2a,b and 2.3a,b, which indicate that the effective

sea ice trends in the full ensemble are similar to the unadjusted sea ice trends in the subset of runs that have global temperature trends similar to the observations. This is consistent with the assumption of a linear relationship between sea ice area and global temperature and hence provides a validation of this method.

Using the effective sea ice trend causes the result presented in Section 2 to change substantially (compare red and blue confidence intervals in Figures 2.2c,d and 2.3c,d). First, the CMIP5 ensemble-mean effective sea ice retreat is slower in each hemisphere than the unadjusted sea ice trend by more than 35%. Second, the CMIP5 effective sea ice trend distribution is narrower than the distribution of unadjusted sea ice trends, implying that there is a smaller range of sea ice trends that can arise due to internal variability when constrained to match the observed level of recent global warming: the standard deviation of each distribution decreases by approximately 40%. Note that this may be partially related to the entire distribution being scaled by a constant value. As a result, we find that none of the 118 CMIP5 simulations have an Arctic effective sea ice retreat as fast as the observations. Similarly, none of the 118 CMIP5 simulations have an Antarctic effective sea ice expansion as large at the observations (Table 1).

Fitting a Gaussian to the distributions to approximately estimate values in the tails beyond what is populated by the 118 members, we find that the percentage of runs in the Gaussian distribution that have Arctic sea ice retreat as fast as the observations drops from 12% (Figure 2.1e) to 0.02% (Figure 2.3c). In the Antarctic, biases in the level of global warming appear to have a somewhat smaller effect. Although the center of the Antarctic distribution moves closer to the observed value, the width of the distribution decreases sufficiently to cause the percentage of runs in the distribution that have Antarctic sea ice expansion as large as the observations to drop from 1.6% (Figure 2.1f) to 0.37% (Figure 2.3d). Note that these results are

qualitatively consistent with the sea ice sensitivities reported by Purich *et al.* (2016) and Stroeve & Notz (2016).

It is noteworthy that the discrepancies between the models and observations have similar magnitudes in the Antarctic as the Arctic when using effective sea ice trends (Figure 2.3c,d), which is in contrast to the analysis of unadjusted sea ice trends, where the bias was larger in the Antarctic (Figure 2.1e,f). Note that a similar finding was reported for the sea ice sensitivity in CMIP3 (Eisenman *et al.*, 2011). This may be of interest, for example, because the different levels of consistency between the observed and modeled sea ice trends in the two hemispheres in CMIP5 contributed to the consensus view that there is low confidence in the scientific understanding of the observed Antarctic sea ice trend and high confidence in the scientific understanding of the observed Arctic sea ice trend (IPCC, 2013). Overall, the results of this section imply that the possibility that internal variability alone could explain the difference between the observed and modeled sea ice trends in either hemisphere decreases substantially after accounting for biases in the level of global warming.

2.6 Pseudo-ensemble from longer time period

Next, we explore an alternative method to estimate the distribution of sea ice trends that the CMIP5 models would simulate if each run had the observed level of global warming during 1979-2013. Here we assume that the relationship between global warming and sea ice changes is the same for all 35-year periods (which would hold if the relationship between sea ice extent and global-mean temperature were perfectly linear, i.e., if the sea ice sensitivity were exactly constant). We therefore examine the trends during each overlapping 35-year period in each of the CMIP5 simulations of 1900-2100. There are a total of 13,354 overlapping 35-year periods (some CMIP5 runs were excluded because data were not available for the entire

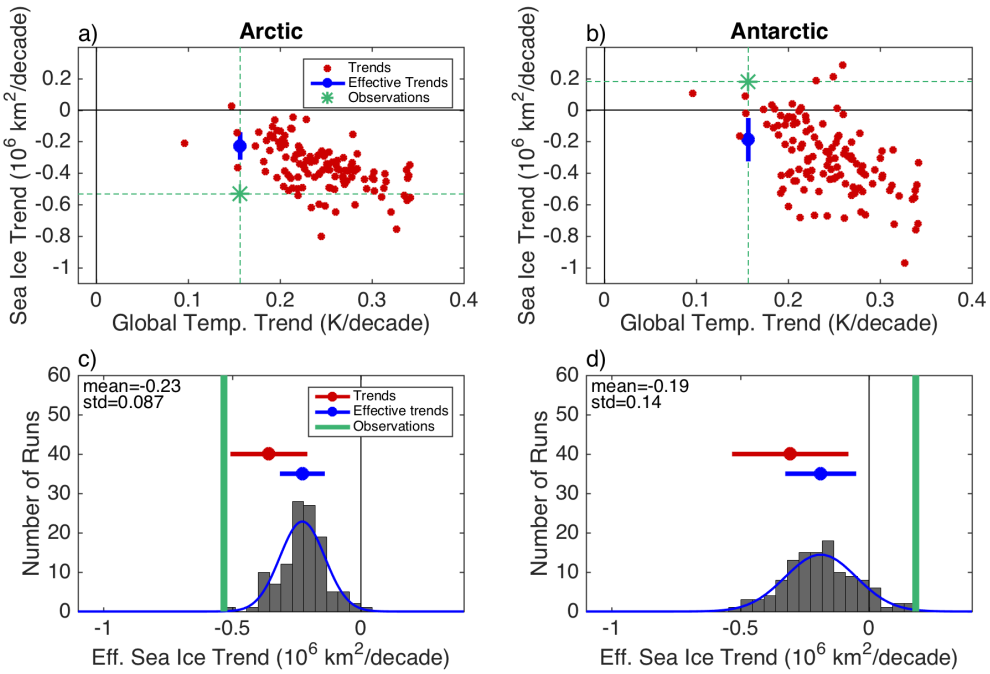

Figure 2.3: As in Figure 2.2, but using CMIP5 simulations instead of CESM-LE.

1900-2100 period; see Appendix A for details). Figure 3.4a-b shows a scatter of these 13,354 trends in annual-mean global-mean surface air temperature and sea ice extent. The trends during 1979-2013 are shown in red, illustrating the qualitatively similar relationship between trends in sea ice and global temperature during this period and other 35-year periods. That is, we find that higher levels of global warming are associated with faster sea ice retreat, even over this extended range of trends in global-mean surface temperature.

In order to validate whether this method can provide a meaningful approximation to the ensemble of 1979-2013 simulation results, we consider the distribution of sea ice trends during all 35-year periods that have levels of global warming similar to the simulated 1979-2013 distribution (i.e., similar to Figure 2.1d). Specifically, we select the 3,923 periods during 1900-2100 that have temperature trends within one standard deviation of the 1979-2013 ensemble mean (points that fall within the red shaded region in Figure A.3a,b), and we examine the histogram of the corresponding

sea ice trends (Figure A.3c,d). We find that the distribution of 3,923 trends in Figure A.3c,d does approximately match the mean and standard deviation of the smaller distribution of 118 simulated sea ice trends during 1979-2013 (Figure 2.1e,f): the red and black error bars in Figure A.3c,d are approximately aligned. This implies that this method allows us to build a far larger "pseudo-ensemble" by harvesting time periods with similar levels of global warming from the 200-year simulations.

Next, we create a pseudo-ensemble of time periods in the simulations that have global warming trends similar to the 1979-2013 observed value. This provides an approximation of the spread of simulated sea ice trends that would coincide with the observed level of global warming. Green shading in Figure 3.4a,b indicates 35-year global warming trends that are within the 68% linear regression confidence interval of the observed trend (using the method in Appendix B2 to account for autocorrelation). The pseudo-ensemble in Figure 3.4c,d is comprised of the distribution of 1,232 35-year periods that fall within this green shaded region. This approximates the ensemble of periods whose distribution of global warming trends are consistent with the observed trend.

Only 1 (0.08%) of the 1,232 sea ice trends from this pseudo-ensemble has an Arctic sea ice retreat that is as large as the observations (Table 1). Therefore, this analysis of years 1900-2100 in the simulations yields a similar result to the analysis in Section 5 that used the 1979-2013 effective sea ice trends. Consistent with this, the pseudo-ensemble distribution (Figure 3.4c) has a mean and standard deviation that are similar to the distribution of effective sea ice trends (Figure 2.3c), which can be seen by comparing the black and blue error bars in Figure 3.4c.

Note that increasing the range of global warming trends included in the pseudo-ensemble (i.e., widening the green shaded region in Figure 3.4a) does not substantially influence these results. Specifically, when we use the 95% autocorrelation-corrected

linear regression confidence interval of the observed trend rather than the 68% interval, we find that 6 (0.24%) of the 2,532 periods in the pseudo-ensemble have Arctic sea ice retreat as fast as the observations. See Appendix B3 for an alternative approach to generate a pseudo-ensemble that accurately captures the target distribution.

Similar to the comparison in Section 5 between the effective sea ice trend distribution and the unadjusted sea ice trend distribution, we next compare the pseudo-ensemble associated with the observed 1979-2013 level of global warming (Figure 3.4c) with the pseudo-ensemble associated with the ensemble of simulated 1979-2013 levels of global warming (Figure A.3c). First, whereas 9.0% of the Arctic sea ice trends in Figure A.3c are at least as negative as the observed value, this value drops to 0.08% in Figure 3.4c. Second, the mean Arctic sea ice trend in the pseudo-ensemble associated with the simulated level of 1979-2013 global warming (Figure A.3c) is approximately 25% larger than in the pseudo-ensemble associated with the observed level of global warming (Figure 3.4c). The results are approximately similar to the effective sea ice trend results in Section 5.

Turning to the Antarctic, we find some qualitative similarities with the Arctic results. First, the mean of the Antarctic sea ice trends in the pseudo-ensemble associated with the observed level of global warming is similar to the ensemble mean of Antarctic effective sea ice trends, although the standard deviations of the two distributions are somewhat different (compare error bars in Figure 3.4d). Second, the mean Antarctic sea ice trend in the pseudo-ensemble associated with the observed level of global warming (Figure 3.4d) is about 30% smaller than in the pseudo-ensemble associated with the CMIP5 simulated level of global warming (Figure A.3d). A notable difference compared with the Arctic results is that 3.7% of the periods in the pseudo-ensemble associated with the observed level of global warming have Antarctic sea ice expansion as large as the observations (Table 2.1, Figure 3.4d), compared to 1.6%

of the periods in the pseudo-ensemble associated with the CMIP5 simulated level of warming (Figure A.3d). This is in contrast with the effective sea ice trend results in Section 5, where the fraction of Antarctic sea ice trends as positive as the observations was found to be smaller for the effective sea ice trend than for the unadjusted sea ice trend. The reason for this discrepancy between the pseudo-ensemble result here and the effective trend result in Section 5 may be related to issues with the Antarctic sea ice sensitivity varying during the 1900-2100 period. In Figures A.1b, the Antarctic sea ice sensitivity in CESM-LE can be seen to be larger during 1900-2000 (top left part of plot: small warming leads to large sea ice retreat) than during 2001-2100 (remainder of plot: further warming leads to more gradual sea ice retreat). This may be associated with the Antarctic sea ice sensitivity being influenced by ozone forcing or other local processes that do not scale with greenhouse forcing during 1900-2100. The sea ice sensitivity in CESM-LE is more constant in the Arctic during 1900-2100 (Figure A.1a). This may cause the pseudo-ensemble approach, which assumes constant sea ice sensitivity during 1900-2100, to be less accurate in the Antarctic than the Arctic (cf. Figure A.2).

2.7 Discussion

The relationship between the global-mean surface air temperature trend and both the Arctic and Antarctic sea ice trends in these simulations implies that the models do not capture the hemispheric asymmetry of the observed sea ice trends during 1979-2013. This is illustrated in Figure 2.5a, which indicates a substantial systematic bias in the CESM-LE simulations compared with observations. The sea ice trend may be more accurately simulated in one hemisphere only at the cost of accuracy in the other. This is closely related to the temperature trend in each realization of internal variability (colors of points in Figure 2.5a). Realizations that warm most rapidly

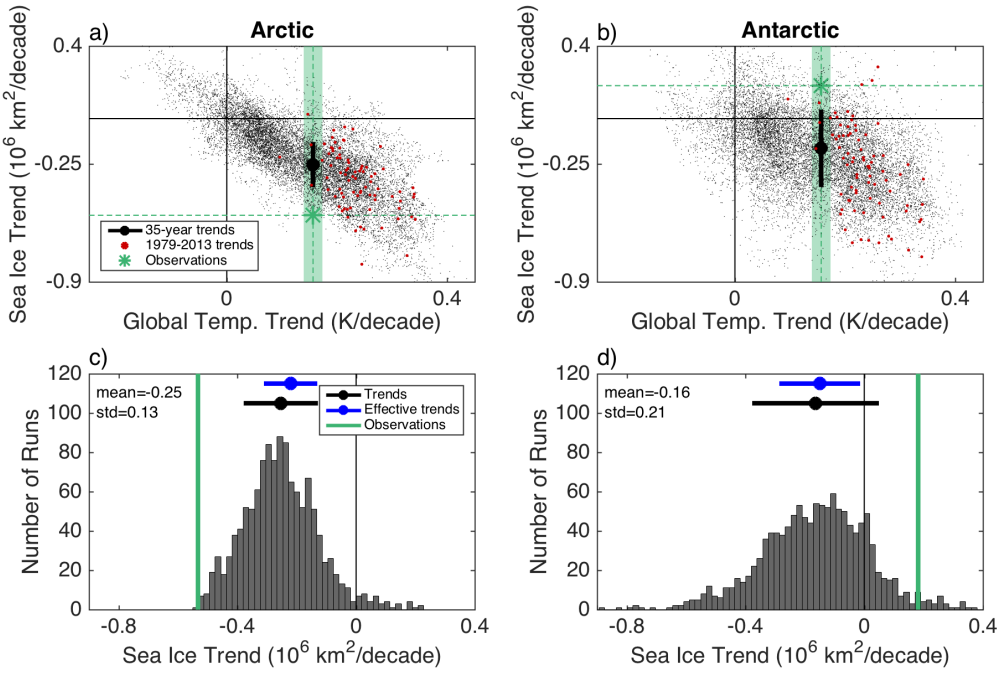

Figure 2.4: Scatter of observed and simulated annual-mean (a) Arctic sea ice trends and (b) Antarctic sea ice trends versus the global-mean surface temperature trends from all overlapping 35-year periods in 73 CMIP5 simulations of 1900-2100 (12,024 points in total); the 1979-2013 trends are indicated in red (as in Figure 2.3a-b). Green dashed horizontal and vertical lines represent the observed trends. Global-mean surface temperature trends that are within one standard deviation of the observed trend are highlighted in green. Sea ice trends from periods that fall within the highlighted regions are shown in histograms below (c,d), with the observed trend indicated by a thick green line. Standard deviations of this distribution (black) and the distribution of 1979-2013 effective sea ice trends (blue, as in Figure 2.3c-d) are also shown. The mean and standard deviation of the trends that fall within the highlighted regions are repeated for comparison in the top panel (black vertical error bars).

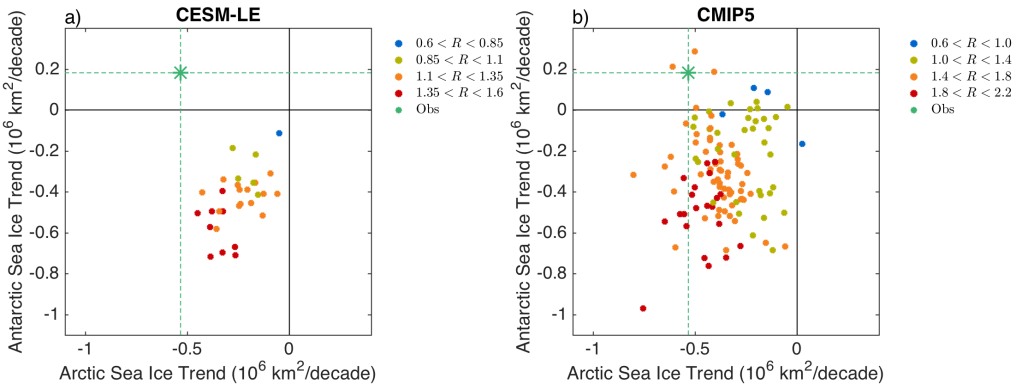

Figure 2.5: Simulated annual-mean Antarctic sea ice trend versus Arctic sea ice trend in each run in the (a) CESM-LE and (b) CMIP5 ensembles. The observed trends are indicated by green dashed horizontal and vertical lines. The color of each point indicates the ratio (R) between the simulated and observed values of the annual-mean global-mean surface temperature trend in each simulation.

compared to observations (red and orange points) tend to have more accurate Arctic sea ice trends but greater biases toward Antarctic sea ice retreat rather than expansion. The reverse also appears to be true (blue and yellow points), although there are far fewer simulations in CESM-LE that underestimate global warming trends. We repeat this analysis using CMIP5 in Figure 2.5b and find a similar result, although there is more spread, as expected from the comparison of Figure 2.2a,b with Figure 2.3a,b. Note that there are three simulations (from IPSL-CM5A-LR, MPI-ESM-MR, BCC-CSM1-1) that simulate sea ice retreat that is similar to the observations in both hemispheres, but they each overestimates the level of global warming by at least 40%.

The analyses in Sections 2.5 and 2.6 rely on the approximation that the relationship between simulated sea ice extent and global-mean surface air temperature is linear. The accuracy of this approximation for climate model simulations is demonstrated in Figure A.1. In the Arctic, simulated sea ice extent is highly correlated with global-mean temperature (left column of Figure A.1). This close relationship is consistent with the previous finding that the Arctic sea ice sensitivity in a given model does not to depend on the forcing scenario (Winton, 2011). While the Antarctic sea ice extent is not as highly correlated with global-mean temperature in many of

the models (right column of Figure A.1), the distributions in Figures 2.2b, 2.3b, and 3.4b suggest that the correlations between Antarctic sea ice extent and global-mean surface air temperature may be sufficiently large that the relationship between the trends of these two values during 35-year periods are directly related, causing simulated Antarctic sea ice expansion to occur more often in simulations with too little global warming.

We examine the extent to which internal climate variability weakens the relationship between sea ice extent and global-mean surface temperature over short time scales by evaluating the distribution of Arctic and Antarctic sea ice sensitivity in 30 CESM-LE simulations of 2006-2100 (Figure A.5e-f). This time period is chosen to avoid issues with the dependence of Antarctic sea ice sensitivity on the time period, as discussed in Section 6 above (Figure A.1b). We then compute the sea ice sensitivity of each overlapping 55-year period (Figure A.5c-d) and 35-year period (Figure A.5a-b). The greater widths of the latter distributions indicate the extent to which internal variability influences this relationship over shorter time periods. Figure A.5 indicates that even for 35-year time periods, the distributions of sea ice sensitivities in both hemispheres remain relatively narrow compared with the distance from the origin to the center of each distribution, that is, the fractional spreads remain relatively small.

Note that by approximating that sea ice extent varies linearly with global-mean temperature (Figures A.1) in the effective sea ice trend and pseudo-ensemble analyses (Sections 4 and 5), we approximate here that the sea ice sensitivity takes the same value in a given simulation whether the global warming occurs due to rising greenhouse forcing or internal variability (i.e., that the sea ice sensitivity is constant). However, it has previously been shown in a climate model that the magnitude of the Arctic sea ice sensitivity is somewhat larger in a control simulation than in a forced warming simulation (Winton, 2011). That is, they found that there was more sea

ice retreat under global warming caused by internal variability than under the same level of global warming caused by rising greenhouse forcing. This effect appears to also occur in the analysis presented here for both the Arctic and the Antarctic. In CESM-LE, all of the simulations of 1979-2013 have the same global warming due to greenhouse forcing since they are all from the same model with the same forcing scenario, but the temperature trends differ among the simulations due to internal variability. Hence a CESM-LE simulation with a larger temperature trend has more warming due to internal variability, and thus it should show a sea ice sensitivity with a larger magnitude. Indeed, points in Figure 2.2a-b that are farther to the right (i.e., runs with larger global temperature trends) have a ratio of the sea ice trend to the global temperature trend with a larger magnitude (i.e., the magnitude of the sea ice sensitivity is larger). Similar arguments imply that smaller temperature trends have a smaller magnitude of this ratio. This also occurs to a lesser extent in CMIP5 (Figure 2.3a-b), where the global warming due to greenhouse forcing varies among the runs. Hence this effect may explain why the scatterplots in Figures 2.2a-b and 2.3a-b do not appear to linearly extrapolate through the origin.

The central results of this study are relevant to previous studies that used control simulations with constant forcing to determine whether the observed Arctic and Antarctic sea ice trends could arise due to internal variability alone (Kay *et al.*, 2011; Polvani & Smith, 2013; Mahlstein *et al.*, 2013; Jones *et al.*, 2016, e.g.,). For example, Polvani & Smith (2013) found that 1979-2005 Antarctic sea ice trends that are up to three times as large as the observed trend can naturally emerge in control simulations. They suggest that this implies that the internal variability of this system is large enough to overwhelm the forced global warming signal, similar to arguments made by Mahlstein *et al.* (2013). However, the results presented here imply that periods in control simulations with expanding Antarctic sea ice are likely to have

global warming trends that are substantially below the 1979-2013 observed trend. Therefore, these results imply that when simulated global warming trends are not considered, neither the center nor the width of the distribution of sea ice trends in a control simulation should be expected to accurately reflect the range of possible sea ice trends that can emerge in climate models under the observed level of global warming.

We have examined the sensitivity of these results to adjustments in various details of the analysis, which is discussed in Appendix B. In Section B1, we evaluate the influence of using sea ice area in the models and observations, rather than sea ice extent as used in the main text. In Section B2, we repeat the analyses from Sections 2 and 5 using a framework in which each run is treated as a single realization from a unique ensemble, following Stroeve *et al.* (2012) and Santer *et al.* (2008); this is in contrast to the analysis in the main text, which treated all runs as realizations from a single ensemble. In Section B3, we carry out an alternative pseudo-ensemble approach that is more complicated than that used in Section 6 and may more accurately capture the target distribution. In Section B4, we repeat the effective sea ice trend analysis (Section 5) with the sea ice sensitivity in Eq. (1) computed using a total least squares regression, rather than the ratio of ice and temperature temporal trends. In Section B5, we repeat the effective trend analysis (Section 5) and the pseudo-ensemble analysis (Section 6) using the Hadley Centre Climatic Research Unit Version 4 (HadCRUT4) dataset (Morice *et al.*, 2012) for the global-mean surface temperature, rather than the GISTEMP dataset. Consistent with the central results of this study, in each case we find that after accounting for biases in the level of global warming, the possibility that internal variability alone could explain the difference between simulated and observed sea ice trends in either hemisphere becomes exceedingly small.

The results presented here stem from the point that the observed relationship

between sea ice extent and global-mean surface temperature, i.e., the observed sea ice sensitivity, is markedly different in each hemisphere from that simulated by climate models. It should be emphasized that the physical processes that determine the ice sensitivity are not well understood. Therefore, this bias may be related to issues in the atmosphere, ocean, or sea ice model components that are connected to the simulated sea ice changes or to the level of global warming. For example, several studies have identified model biases related to global warming trends (e.g., IPCC, 2013; Kosaka & Xie, 2013) and local processes that influence sea ice (Rampal *et al.*, 2011; Jahn *et al.*, 2012; Mahlstein & Knutti, 2012; Bintanja *et al.*, 2013; Mahlstein *et al.*, 2013; Zunz *et al.*, 2013; Uotila *et al.*, 2014; Haumann *et al.*, 2014; Purich *et al.*, 2016; Jones *et al.*, 2016). Additional studies have suggested that polar teleconnections may also have an important influence on sea ice trends in each hemisphere (Meehl *et al.*, 2016; Screen & Francis, 2016). Furthermore, errors in the observations could plausibly contribute to the discrepancy between observed and modeled sea ice sensitivity. For example, several studies have suggested that poorly sampled observations around the poles and in parts of Africa may help explain differences between observed and modeled global-mean surface temperature trends (Cowtan & Way, 2014; Richardson *et al.*, 2016; Karl *et al.*, 2015). Similarly, recent studies have highlighted uncertainties in the observed multi-decadal Antarctic sea ice extent trend due to changes in data sources (Screen *et al.*, 2011; Eisenman *et al.*, 2014). Lastly, we find that the observations show a correlation between sea ice extent and global-mean surface temperature that is similar to the models in the Arctic but not in the Antarctic (Figure A.6). This suggests that the discrepancy between the models and the observations in the Antarctic could be related to the models simulating an unrealistically tight relationship between Antarctic sea ice extent and global temperatures.

Table 2.1: Fraction of runs with simulated sea ice trends that are at least as extreme as the observations using the distribution of CMIP5 simulated trends (see Section 1), effective trends (see Section 4), and a pseudo-ensemble of 35-year periods that have similar levels of global warming to the observations (see Section 5). The first column is the fraction with Arctic sea ice retreat as rapid as the observations, and the second column is the fraction with Antarctic sea ice expansion as rapid as the observations. There are 118 simulations of 1979-2013 in the CMIP5 ensemble analyzed here and 1,232 overlapping 35-year periods in the pseudo-ensemble. Percentages are indicated to aid in comparison between the rows.

	Arctic	Antarctic
1979-2013 Trends	13/118 (11%)	3/118 (2.5%)
1979-2013 Effective Trends	0/118 (0%)	0/118 (0%)
Pseudo-ensemble	1/1,232 (0.1%)	45/1232 (3.7%)

2.8 Conclusion

In each hemisphere, the observed 1979-2013 trend in sea ice extent falls at least marginally within the distribution of the CMIP5 simulations (Figure 2.1b,c,e,f). Consistent with this, a number of previous studies have suggested that internal climate variability could explain the difference between the observed sea ice trend and the ensemble-mean simulated trend in each hemisphere (Holland *et al.*, 2008; Kay *et al.*, 2011; Stroeve *et al.*, 2012; Polvani & Smith, 2013; Mahlstein *et al.*, 2013; Turner *et al.*, 2013; Swart & Fyfe, 2013; Zunz *et al.*, 2013; IPCC, 2013; Fan *et al.*, 2014; Notz, 2014; Gagné *et al.*, 2015; Goosse & Zunz, 2014; Swart *et al.*, 2015; Purich *et al.*, 2016; Jones *et al.*, 2016).

The results presented here suggest that this viewpoint breaks down when we account for biases in simulated 1979-2013 global-mean surface temperature trends. We find that simulated Arctic sea ice retreat is accurate only in runs that have far too much global warming (Figure 2.2a, 2.3a, 3.4a). This suggests that the models may be getting the right Arctic sea ice retreat for the wrong reasons. Similarly, simulated periods with accurate Antarctic sea ice trends tend to have too little global warming, although these results are more equivocal (Figure 2.2b, 2.3b, 3.4b). Relatedly, the

simulations do not capture the observed asymmetry between Arctic and Antarctic sea ice trends (Figure 2.5).

We quantify how this bias influences the level of agreement between models and observations (Figure 2.1) by estimating what the simulated sea ice trend in each hemisphere would be in runs that matched the observed level of global warming (Table 1). This analysis relies on the approximately linear relationship between sea ice extent and global-mean surface temperature in the simulations (Figure A.1), which allow us to scale the results from simulations with varied levels of global warming (Figures 2.2c-d, 2.3c-d) and use simulations from different time periods (Figures 3.4c-d). These results suggest that the difference between observed and modeled sea ice trends in each hemisphere cannot be attributed to simulated internal climate variability alone. This implies systematic errors in the Arctic and Antarctic sea ice changes simulated with current models, or possibly errors in the observations.

2.A Methods

Here further details are given regarding the observations and the processing of the CMIP5 model output.

For the observed sea ice extent and sea ice area, we use monthly-mean data from the National Snow and Ice Data Center Sea Ice Index (Fetterer *et al.*, 2002), which uses the NASA Team algorithm to estimate sea ice concentration from satellite passive microwave measurements. We analyze years 1979-2013, since this was the period available at the time of analysis. We fill missing monthly values by interpolating between the same months in the previous and following years, and we then take annual averages. For the observed annual-mean global-mean surface temperature data, we use the Goddard Institute for Space Sciences Surface Temperature Analysis (GISTEMP) (Hansen *et al.*, 2010).

We analyze 118 simulations of years 1979-2013 from 40 CMIP5 models, using the Historical (1850-2005) and RCP4.5 (2006-2100) experiments; note that the choice of RCP scenario has minimal influence during 2006-2013. The models simulate surface air temperature at each horizontal atmospheric grid point, and sea ice concentration is simulated on the ocean grid in many of the models. Therefore, the areas of the cells in both grids are needed to compute the total Arctic and Antarctic sea ice areas as well as the global-mean temperature. The following models did not have grid cell areas reported in the CMIP5 archive: CanCM4 (surface air temperature), MPI-ESM-LR (surface air temperature), FIO-ESM (surface air temperature and sea ice). In these cases, grid cell areas were estimated from the reported locations of grid cell corners using the Haversine formula (note that this method requires a regular grid).

Simulations were not analyzed in this study when either surface air temperature output was not available during all of 1979-2013, sea ice output was not available during all of 1979-2013, dates reported in the file did not match the filename in the CMIP5 archive, or irregular grids were used but grid cell areas were not provided. The following runs each had at least one of these issues and hence were excluded: EC-EARTH runs 1,3-6,10; FIO-ESM run 2; MIROC-ESM-CHEM run 2; CESM1-CAM5-1-FV2 runs 1-4; GFDL-CM3 runs 2-5; GFDL-CMP2p1 runs 1-10; all runs from BCC-CSM1-1-M; and all runs from INMCM. GFDL-ESM2G run 1 is also excluded because the Antarctic sea ice extent gradually decreases and then increases during 1979-2013, leading to a highly autocorrelated time series of linear regression residuals with less than 2 effective degrees of freedom, which causes the standard error in the analysis in Appendix C to be complex (cf. eq. (4) in Santer *et al.*, 2008). Additional simulations were excluded from the analysis in Figures 3.4 and A.1e,f because data were not available for the entire 1900-2100 period.

2.B Robustness to changes in methods

2.B.1 Using ice area instead of ice extent

The results presented in the main text use sea ice extent as a measure of the sea ice cover. Here we briefly summarize the effect of instead using sea ice area in the models and observations. First, considering the Gaussian distribution of sea ice trends (as in Figure 2.1e-f), we find that 22% of the simulations would have Arctic sea ice retreat that is as large as the observations, and 1.5% would have Antarctic sea ice expansion as large as the observations, similar to the values of 12% and 1.6%, respectively, that we found for ice extent. When we use the Gaussian distribution of Arctic and Antarctic effective sea ice trends (as in Figure 2.3c-d), these values drop to 0.15% and 0.28% (similar to 0.02% and 0.37% for ice extent), respectively. Lastly, of the 2,532 overlapping 35-year periods that have global warming trends that are similar to the 1979-2013 observations (as in Figure 3.4c-d), 1.3% of the periods have Arctic sea ice trends as negative as the observed value, and 2.1% of the periods have Antarctic sea ice trends as positive as the observed value (similar to 0.24% and 2.7%, respectively, for ice extent).

2.B.2 Paired Trends Tests

In this section, we consider an alternative framework for the analysis in the main text: rather than treat each CMIP5 simulation as a realization from a single model, here we treat each simulation as a realization from a separate model. Following previous studies (Santer *et al.*, 2008; Stroeve *et al.*, 2012), we determine if each simulated trend is statistically different from the observed trend at the 95%

confidence level by using Welch's t-test statistic:

$$d = \frac{\beta_m - \beta_o}{\sqrt{\sigma_m^2 + \sigma_o^2}}. \tag{2.2}$$

Here β_m and β_o are the modeled and observed trends, respectively, and σ_m and σ_o are the associated standard errors, which are adjusted for autocorrelation following Santer *et al.* (2008). A value of $|d| > 1.96$ is equivalent to zero falling outside of the 95% confidence interval of a Gaussian distribution with a mean of $\beta_m - \beta_o$ and a standard deviation of $\sqrt{\sigma_m^2 + \sigma_o^2}$. In Figure A.7a-b, β_o and β_m are the observed and modeled sea ice trends, which are represented by a series of solid black dots (one for each simulation). The standard errors, σ_o and σ_m, are also shown. In Figure A.7c-d, β_m is the effective sea ice trend and σ_m is determined using error propagation:

$$\sigma_m = \sqrt{\left(\frac{\beta_m}{\beta_{I_t}}\sigma_{I_t}\right)^2 + \left(\frac{\beta_m}{\beta_{T_t}}\sigma_{T_t}\right)^2 + \left(\frac{\beta_m}{\beta_{T_t^o}}\sigma_{T_t^o}\right)^2}, \tag{2.3}$$

where β_{I_t}, β_{T_t}, and $\beta_{T_t^o}$ are the trends in simulated sea ice, simulated global-mean surface temperature, and observed global-mean surface temperature, and σ_{I_t}, σ_{T_t}, and σ_{I_t} are the associated standard errors.

We find that of the 118 simulations, 33% simulate sea ice trends that are statistically different from the observations at the 95% confidence level in the Arctic, and 80% in the Antarctic. On the other hand, 81% and 84% of the simulations have Arctic and Antarctic effective sea ice trends that are different from the observations at the 95% level, respectively.

2.B.3 Using scaled histograms in pseudo-ensemble analysis

In this appendix, we repeat the calculation in Section 6 (Figure 3.4a-b) using a somewhat more precise but less straightforward approach that involves a weighting

function rather than simply selecting the runs that fall within the shaded region. We begin with the distribution of 13,354 overlapping 35-year temperature trends during 1900-2100 as well as a Guassian distribution centered on the observed temperature trend with a width equal to the 68% linear regression confidence interval (which is adjusted for autocorrelation; see Appendix B2 for details). Next, we assign each 35-year period a weight equal to the height of the Guassian at the center of the histogram bin where the 35-year period falls divided by the number of runs in the histogram bin.

These weights scale the distribution of temperature trends during 1900-2100 to match a distribution consistent with the observed 1979-2013 temperature trend. Next, we create a histogram of sea ice trends with each 35-year period multiplied by its weight. Hence this approach asks what range of ice extent trends is consistent with the observed temperature trend under the assumptions described in Section 6. We find that the resulting distribution is approximately equivalent to the result of the simpler approach in Section 5 (Figure 3.4c-d): 0.32% of the 35-year periods have Arctic sea ice trends that are at least as negative as the observed value, and 5.2% have Antarctic sea ice trends at least as positive as the observed value, compared with 0.08% and 3.7%, respectively, reported in Section 5.

2.B.4 Using total least squares to compute sea ice sensitivity

Winton (2011) found that computing the sea ice sensitivity using a total least squares (TLS) regression between ice extent and global-mean surface air temperature leads to a slightly more accurate estimate than the ratio of ice and temperature temporal trends as in Eq. (1). We find that replacing the ratio of trends in Eq. (1) with a TLS regression between ice extent and global-mean surface air temperature yields similar results: using Gaussian fits to the distributions, we find that the probability

that the observations would land this far from the TLS effective sea ice trend ensemble mean is 0.02% in the Arctic and 0.08% in the Antarctic (similar to 0.02% and 0.37%, respectively, computed using the trend ratio).

2.B.5 Using HadCRUT4 instead of GISTEMP

The results presented in the main text use the GISTEMP dataset for the observed annual-mean global-mean surface temperature. Here we briefly summarize the effect of instead using the HadCRUT4 dataset (Morice *et al.*, 2012). This causes the 1979-2013 temperature trend to increase from 0.157 K/decade (GISTEMP) to 0.159 K/decade (HadCRUT4). Considering the Gaussian distribution of effective sea ice trends (as in Figure 2.3c-d), we find that this leads to 0.03% (HadCRUT4) instead of 0.02% (GISTEMP) of the simulations having Arctic sea ice retreat that is as fast as the observations, and 0.39% (HadCRU4) instead of 0.37% (GISTEMP) having Antarctic sea ice expansion as fast as the observations. Considering the 2,532 overlapping 35-year periods that have global warming trends similar to the 1979-2013 observations (as in Figure 3.4c-d), we find that this causes 0.31% (HadCRUT) instead of 0.24% (GISTEMP) of the periods to have Arctic sea ice trends as negative as observed, and 2.8% (HadCRUT) instead of 2.7% (GISTEMP) of the periods to have Antarctic sea ice trends as positive as observed. In summary, switching from GISTEMP to HadCRUT4 has little effect on the main results presented here.

Acknowledgements

The work was supported by the National Science Foundation (NSF) Graduate Research Fellowship and NSF grants ARC-1107795 and OCE-1357078. Without implying their endorsement, we are grateful to Sarah Gille, Art Miller, Paul Kushner,

Neil Tandon, Frédéric Laliberté, Till Wagner, and John Fyfe for helpful comments and discussions. We acknowledge the World Climate Research Programme's Working Group on Coupled Modelling, which is responsible for CMIP5, and we thank the climate modeling groups for producing and making available their model output. We also acknowledge the CESM Large Ensemble Community Project and supercomputing resources provided by NSF/CISL/Yellowstone. Processed CMIP5 data used in this study is available at http://eisenman.ucsd.edu/code.html.

Chapter Two, in full, is a reprint of the material as it appears in the Journal of Climate, 2017. Rosenblum, E. and Eisenman, I., (2017). Sea ice trends in climate models only accurate in runs with biased global warming. *Journal of Climate*, 30, 6265-6278. ©American Meteorological Society. Used with permission. The dissertation author was the primary investigator and author of this paper.

Chapter 3

Faster Arctic sea ice retreat in CMIP5 than in CMIP3 due to volcanoes

3.1 Abstract

The downward trend in Arctic sea ice extent is one of the most dramatic signals of climate change during recent decades. Comprehensive climate models have struggled to reproduce this trend, typically simulating a slower rate of sea ice retreat than has been observed. However, this bias has been widely noted to have decreased in models participating in the most recent phase of the Coupled Model Intercomparison Project (CMIP5) compared with the previous generation of models (CMIP3). Here we examine simulations from both CMIP3 and CMIP5. We find that simulated historical sea ice trends are influenced by volcanic forcing, which was included in all of the CMIP5 models but in only about half of the CMIP3 models. The volcanic forcing causes temporary simulated cooling in the 1980s and 1990s, which contributes

to raising the simulated 1979-2013 global-mean surface temperature trends to values substantially larger than observed. We show that this warming bias is accompanied by an enhanced rate of Arctic sea ice retreat and hence a simulated sea ice trend that is closer to the observed value, which is consistent with previous findings of an approximately linear relationship between sea ice extent and global-mean surface temperature. We find that both generations of climate models simulate Arctic sea ice that is substantially less sensitive to global warming than has been observed. The results imply that much of the difference in Arctic sea ice trends between CMIP3 and CMIP5 occurred due to the inclusion of volcanic forcing, rather than improved sea ice physics or model resolution.

3.2 Introduction

Modeling groups from around the world have contributed state-of-the-art climate model simulation results to the Coupled Model Intercomparison Project (CMIP). The simulations of the historical period have natural and anthropogenic forcing and can be compared with the instrumental record to assess how well the climate models perform. These simulations are then extended to project future climate change using several different greenhouse gas concentration trajectories. There have been several CMIP phases as comprehensive climate models have continued to be developed. The two most recent phases have been the CMIP3 (Meehl *et al.*, 2007) and CMIP5 (Taylor *et al.*, 2012) ensembles, which were used to project future climate change in the Intergovernmental Panel on Climate Change (IPCC) Fourth and Fifth Assessment Reports (AR4 and AR5), respectively.

The historical simulations have shown substantial bias in reproducing Arctic sea ice changes during the satellite record, with the models typically simulating a slower rate of sea ice retreat than has been observed (Stroeve *et al.*, 2007, 2012;

Winton, 2011; Kay *et al.*, 2011; Swart *et al.*, 2015). However, CMIP5 models tend to simulate faster sea ice trends that are more consistent with observations than CMIP3 (Stroeve *et al.*, 2012), as illustrated in Figure 3.1b,c. This has been a widely discussed feature of CMIP5, and it was highlighted in the Executive Summary of the IPCC AR5 chapter on the evaluation of climate models (Flato *et al.*, 2013). However, the cause of this apparent improvement has remained unresolved.

Here we focus on the influence of historical volcanic forcing, which was included in all of the CMIP5 models but only about half of the CMIP3 models. Volcanic eruptions perturb the climate by injecting gases into the stratosphere that produce short-lived sulfate aerosols which reflect and absorb solar radiation. This causes rapid global surface cooling that spans approximately two to three years, which is followed by a decade-long warming period in which the climate recovers (IPCC, 2013). This cooling due to volcanic eruptions has been found to be overestimated in climate models compared with observations, which can cause biases in simulated decade-scale trends (Schmidt *et al.*, 2014; Santer *et al.*, 2014). The CMIP3 models that include volcanic forcing tend to simulate global-mean surface air temperature changes that are fairly similar to the CMIP5 models, whereas CMIP3 models without volcanic forcing simulate global-mean surface air temperature changes that differ substantially from the CMIP5 simulations (e.g., Schmidt *et al.*, 2014; Knutson *et al.*, 2013; Marotzke & Forster, 2015).

Arctic sea ice extent has been found to be approximately linearly related to global-mean surface temperature in many of the CMIP3 and CMIP5 models (Gregory *et al.*, 2002; Winton, 2011; Mahlstein & Knutti, 2012; Stroeve & Notz, 2015), including over periods as brief as 1979-2013 (Rosenblum & Eisenman, 2016). This implies that volcano-related biases in simulated global warming during recent decades should be associated with biases in sea ice retreat. Consistent with this, a number of studies

have shown that volcanic forcing in climate model simulations can influence Arctic sea ice for a decade or more (Stenchikov *et al.*, 2009; Zhong *et al.*, 2011; Zanchettin *et al.*, 2012, 2013; Segschneider *et al.*, 2013; Zanchettin *et al.*, 2014). Taken together, the results of these previous studies raise the possibility that the inclusion of volcanic forcing in all of the CMIP5 models compared to only some of the CMIP3 models could have caused a systematic change in the distribution of simulated sea ice trends during the historical period. We examine this effect by analyzing simulations of 1979-2013 in 118 ensemble members from 40 CMIP5 models, as well as 38 ensemble members from 19 CMIP3 models, and comparing them with observations (see details in Appendix A). We use processed CMIP5 output from a previous study (Rosenblum & Eisenman, 2016), where we addressed whether simulated natural variability was sufficient to explain the biases in the CMIP5 ensemble-mean Arctic and Antarctic sea ice trends compared with observations.

3.3 Results

The distributions of September Arctic sea ice trends during 1979-2013 in the CMIP3 and CMIP5 simulations are plotted in Figure 3.1c,f. CMIP5 models tend to simulate a faster September Arctic sea ice retreat, which has a reduced bias compared with observations, as has been reported previously (Stroeve *et al.*, 2012; Flato *et al.*, 2013). The annual-mean sea ice trend behaves similarly (Figure 3.1b,e), with the ensemble mean falling closer to the observations in CMIP5 than in CMIP3.

It is noteworthy, however, that this decrease in bias in the simulated Arctic sea ice trend coincides with an increase in bias in the simulated annual-mean global-mean surface temperature trend compared to the observations during the same time period (Figure 3.1a,d). Although both generations of models tend to simulate too much warming, the observed global temperature trend during 1979-2013 falls less than one

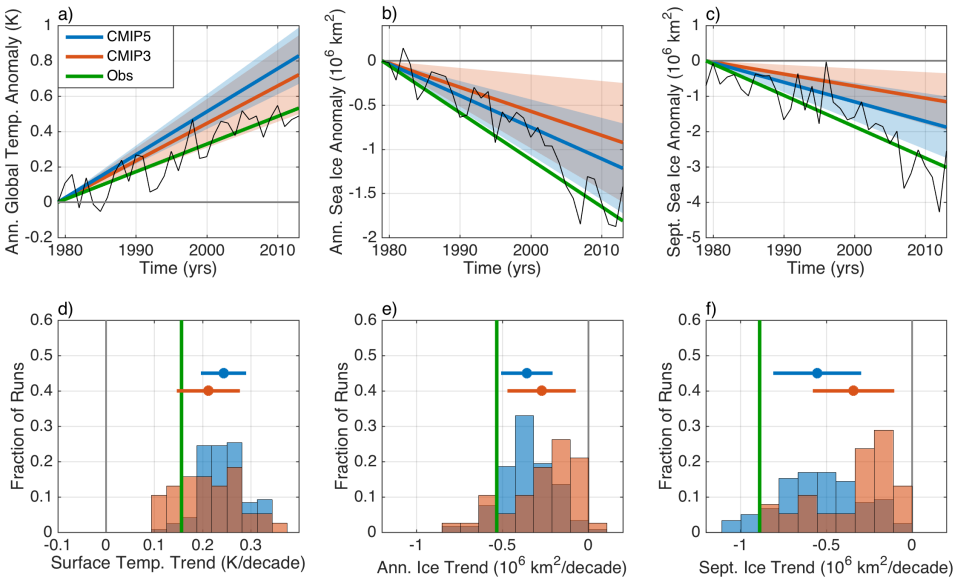

Figure 3.1: Observed as well as CMIP3 and CMIP5 modeled trends in (a,c) annual-mean global-mean surface temperature, (b,e) annual-mean Arctic sea ice extent, and (c,f) September Arctic sea ice extent. (a-c) Here the trends are illustrated as straight lines indicating the anomaly from 1979, and shadings indicate one standard deviation among the CMIP3 or CMIP5 trends around the ensemble means. The observed time series is also included (black, shifted vertically so linear trend goes through zero in 1979). (d-f) Histograms illustrating the distributions of CMIP3 and CMIP5 trends. Standard deviations among the distributions around the ensemble means are indicated by blue and red error bars above the distributions, and the observed trends are indicated by vertical green lines.

standard deviation below the mean in the CMIP3 distribution, whereas the CMIP5 distribution has a larger bias (error bars in Figure 3.1d).

This warming bias is partially related to both generations of models having a tendency to simulate too much global warming during the past 10-20 years, which has been attributed to a number of factors including internal variability (IPCC, 2013; Kosaka & Xie, 2013; Fyfe *et al.*, 2013). Additionally, the temperature trend during 1979-2013 is expected to be influenced by the eruptions of El Chichón in 1982 and Pinatubo in 1991. These events cause surface cooling in the 1980s and 1990s that has been found to be overestimated in climate models (Schmidt *et al.*, 2014; Knutson *et al.*, 2013; Marotzke & Forster, 2015). Figure 3.2a illustrates that the large negative temperature anomalies caused by these volcanoes lead to a larger over-

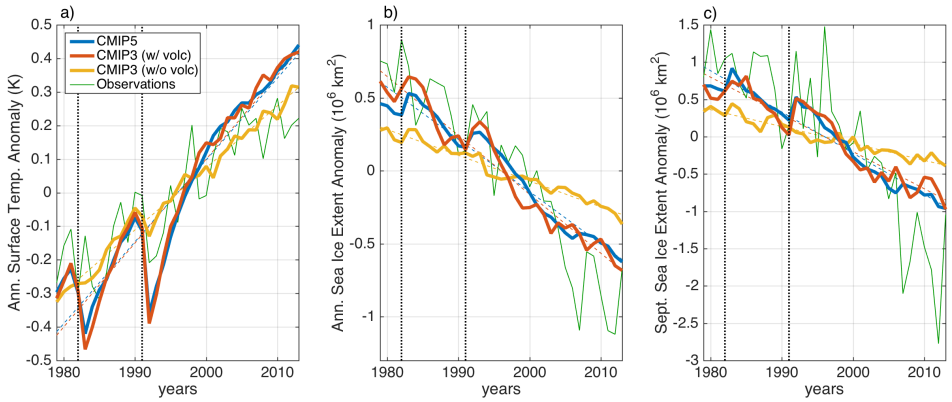

Figure 3.2: Observed and modeled (a) annual-mean global-mean surface temperature, (b) annual-mean Arctic sea ice area, and (c) September Arctic sea ice area. Anomalies from the average value during the plotted time period are shown for the observations (green), the CMIP5 ensemble mean (blue), and the ensemble mean of CMIP3 models with (red) and without (yellow) volcanic forcing. The linear trend associated with each time series is also indicated (dashed lines). This figure illustrates how the cooling effects associated with the eruptions of El Chichón (1982) and Pinatubo (1991) (vertical dotted lines) result in a faster global-mean temperature trends and sea ice cover trends.

all warming trend during this period. This suggests that one reason the CMIP5 ensemble-mean global warming trend during 1979-2013 is farther from the observations than in CMIP3 (Figure 3.1a,d) is because volcanic forcing is included in all of the CMIP5 models compared to about half of the CMIP3 models (Figure 3.2a and Table 3.1).

As expected from the approximately linear relationship between sea ice cover and annual-mean global-mean surface air temperature in many CMIP3 and CMIP5 models (Gregory *et al.*, 2002; Winton, 2011; Mahlstein & Knutti, 2012; Stroeve & Notz, 2015; Rosenblum & Eisenman, 2016), we find that the large negative temperature anomalies that are caused by simulated volcanic forcing are associated with concurrent positive sea ice cover anomalies (Figure 3.2). Similarly, we find that the decade-long warming periods following each eruption typically correspond with a drop in sea ice cover (Figure 3.2). Because these eruptions occur towards the beginning of the 1979-2013 period, they contribute to a larger overall rate of sea ice retreat (dashed-lines in Figure 3.2b,c). Therefore the bias in the models toward too much

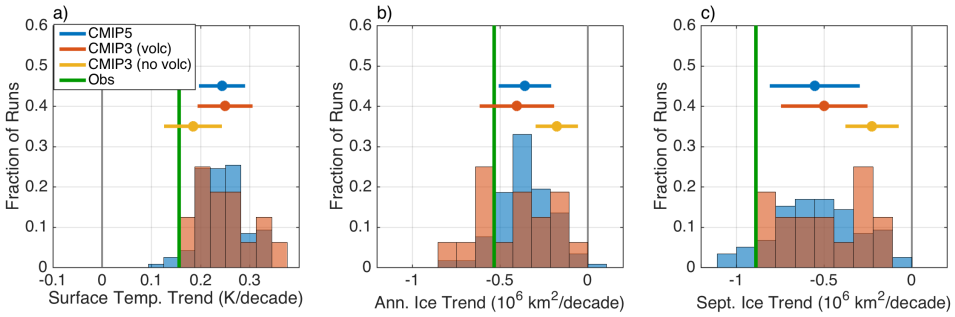

Figure 3.3: As in Figure 3.1d-f, but neglecting the CMIP3 simulations that do not include volcanic forcing. The ensemble mean and standard deviation of the CMIP3 simulations that do not include volcanic forcing are also indicated (yellow error bar).

1979-2013 global warming, which is elevated by volcanic forcing, appears to be associated with the larger simulated sea ice trends.

Consistent with this, we find that the major eruptions before 1979 in the CMIP3 and CMIP5 historical forcing scenarios are typically followed by a brief increase in the September and annual-mean Arctic sea ice (Figure B.1). Overall, this simulated historical Arctic sea ice response to volcanic eruptions is in agreement with previous modeling studies (Segschneider *et al.*, 2013; Zanchettin *et al.*, 2012; Stenchikov *et al.*, 2009; Zanchettin *et al.*, 2014).

By comparing CMIP5 models with the subset of CMIP3 models that include volcanic forcing, we find that both ensembles predict a more similar distribution of both global warming trends and sea ice trends (Figure 3.3a-c) than when all CMIP3 models are included (Figure 3.1d-f). Indeed, this difference in simulated volcanic forcing is typically accounted for in studies that compare simulated global warming between CMIP3 and CMIP5 (e.g., Knutson *et al.*, 2013; Watanabe *et al.*, 2013; Knutti & Sedláček, 2012).

Note that the influence of volcanoes is statistically significant in the CMIP3 results (red and yellow error bars in Figures 3.3a-c): using the Student t-test, we can reject the null hypothesis that the two sets of CMIP3 models simulate temperature trends that are drawn from distributions with the same mean at above the 99.9%

confidence level, and the same applies to the annual and September sea ice trends. It should be noted by caveat that this assessment relies on the relatively small ensemble of CMIP3 models that included volcanic forcing.

3.4 Discussion

Here we examine the results presented above in the context of sea ice sensitivity to global warming (Winton, 2011), drawing on methods developed in a previous study (Rosenblum & Eisenman, 2016).

3.4.1 Do volcanoes influence sea ice sensitivity?

The results above suggest that volcanic forcing artificially improved simulated sea ice trends by raising the level of global warming to values larger than observed. A simple interpretation of this is that the sea ice responds to the inclusion of volcanoes just as it does if the level of global warming increases due to other factors such as greenhouse gases or internal variability. Here we assess this possibility by investigating whether the inclusion of volcanic forcing affects the sensitivity of simulated sea ice cover to the level of global warming, or whether this sensitivity remains constant.

As in Rosenblum & Eisenman (2016), we consider the possibility that the relationship between global warming trends and sea ice trends remains approximately constant during all 35-year periods between 1900 and 2100 (which would exactly hold if this relationship were perfectly linear). We construct two distributions of 35-year sea ice trends and associated global-mean surface air temperature trends from models that include volcanic forcing: (1) using years 1979-2013, and (2) using all available overlapping 35-year periods during 1900-2100 that are not within 10 years of a major volcanic event (i.e., Santa Maria in 1902, Agung in 1963, El Chichón in 1982, and

Table 3.1: For each CMIP3 model, the number of runs, 1979-2013 annual-mean global-mean surface temperature trend (K/decade) averaged over the runs, and 1979-2013 annual-mean and September Arctic sea ice trends (10^6 km^2/decade) averaged over the runs. Note that similar information for the CMIP5 models is given in Table 1 of Rosenblum & Eisenman (2016).

Models with Volcanos	Number of Simulations	Annual Global Warming	Annual Ice Trend	September Ice Trend
gfdl-cm2-0	1	0.27	-0.72	-0.59
gfdl-cm2-1	1	0.28	-0.51	-0.68
giss-model-e-r	1	0.20	-0.14	-0.20
miroc3-2-hires	1	0.34	-0.54	-0.73
miroc3-2-medres	3	0.20	-0.26	-0.32
miub-echo-g	3	0.21	-0.28	-0.34
ncar-ccsm3-0	5	0.29	-0.45	-0.60
ukmo-hadgem1	1	0.25	-0.50	-0.67
all models w/ volc	16	0.25	-0.39	-0.49
Models without Volcanos	**Number of Simulations**	**Annual Global Warming**	**Annual Ice Trend**	**September Ice Trend**
bccr-bcm2-0	1	0.14	-0.27	-0.35
cccma-cgcm3-1	5	0.24	-0.15	-0.18
cccma-cgcm3-1-t63	1	0.29	-0.23	-0.24
cnrm-cm3	1	0.17	0.02	-0.25
csiro-mk3-5	1	0.21	-0.15	-0.26
giss-aom	2	0.14	-0.17	-0.23
inmcm3-0	1	0.26	-0.40	-0.53
ipsl-cm4	1	0.28	-0.49	-0.58
mpi-echam5	3	0.15	-0.21	-0.22
mri-cgcm2-3-2a	5	0.13	-0.10	-0.11
ukmo-hadcm3	1	0.16	-0.20	-0.29
all models w/o volc	22	0.18	-0.18	-0.23

Pinatubo in 1991). The first distribution is meant to characterize the distribution of sea ice trends that occur under global warming including the effects of volcanic forcing, while the second characterizes the distribution of sea ice trends that occur in the same models in the absence of volcanic forcing.

In Figure 3.4, the Arctic sea ice trend is plotted versus the annual-mean global-mean surface temperature trend, with each point representing a 35-year period in a simulation and colors representing the two distributions. By comparing the two distributions in each panel, we find that the influence of volcanic forcing has no visibly discernible impact on the sensitivity of the Arctic sea ice extent to the level of global warming. That is, for a given value on the horizontal axis in each panel of Figure 3.4, the blue points tend to be scattered around similar vertical locations as the red points, indicating that 35-year periods that undergo similar levels of global warming to those simulated for 1979-2013 typically have similar sea ice trends, even without volcanic eruptions. This implies that the influence of volcanic forcing on simulated sea ice trends can be approximately accounted for by considering only the effect on global-mean surface temperatures.

3.4.2 Comparing CMIP3 and CMIP5 sea ice sensitivities

The relationship between global-mean surface air temperature and Arctic sea ice cover implies that biases in simulated global warming trends should be associated with biases in sea ice trends (Winton, 2011). Therefore, similar to Rosenblum & Eisenman (2016), we examine the Arctic sea ice trend in each simulation versus the global-mean surface temperature trend. We find that both CMIP3 models and CMIP5 models that simulate larger (hence more accurate) annual-mean sea ice trends also tend to simulate larger (hence less accurate) global warming trends (Figure 3.5a and Table 1). While the CMIP3 models with volcanic forcing tend to fall in a different

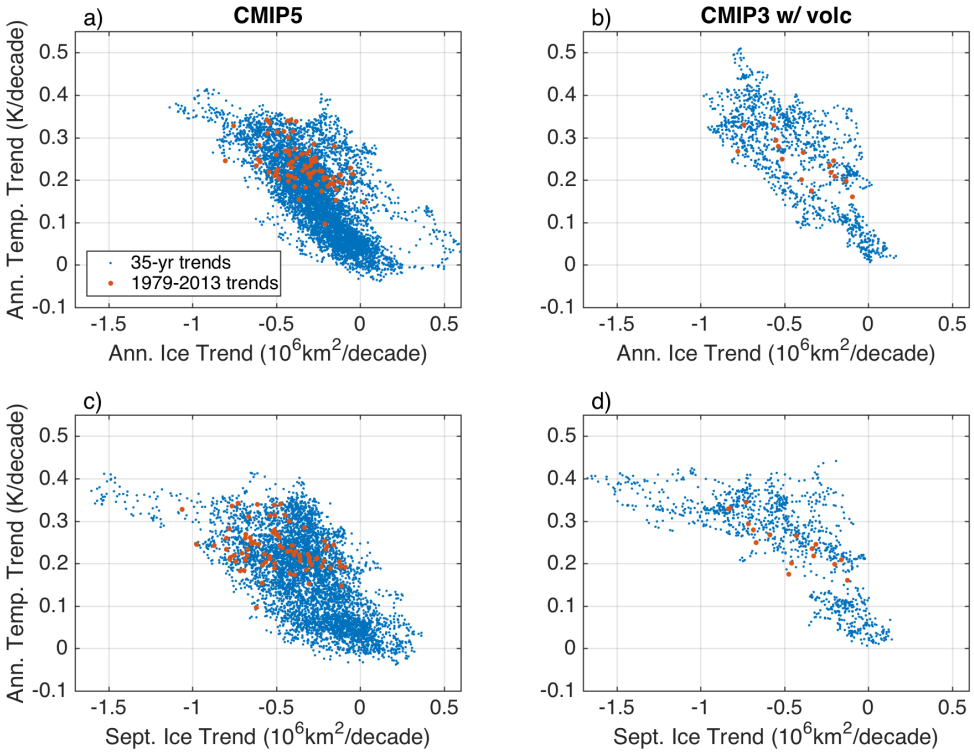

Figure 3.4: Simulated 35-year annual-mean global-mean temperature trends plotted versus the corresponding Arctic sea ice trends. Annual-mean sea ice trends are plotted in the top row, and September sea ice trends are plotted in the bottom row; CMIP5 models are plotted in the left column and CMIP3 models that included volcanic forcing are plotted in the right column. Trends from 1979-2013 are indicated in red, and all available 35-year time periods between 1900-2100 that were not within 10 years of a major volcanic event are indicated in blue. The major volcanic events are Santa Maria in 1902, Agung in 1963, El Chichón in 1982, and Pinatubo in 1991.

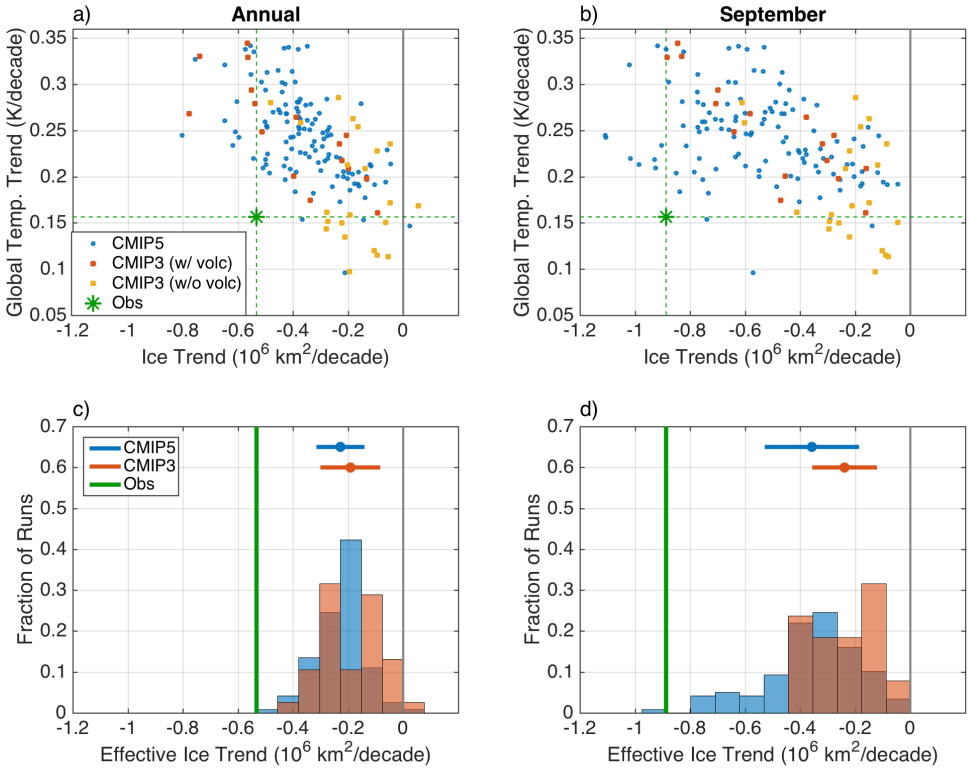

Figure 3.5: Observed and modeled annual-mean global-mean temperature trends plotted versus the corresponding Arctic (a) annual-mean sea ice trends and (b) September sea ice trends. CMIP5 models (blue), CMIP3 models with volcanic forcing (red), and CMIP3 models without volcanic forcing (yellow) are plotted, and dashed green lines represent the observed trend. The histograms show the Arctic (c) annual-mean effective sea ice trends and (d) September effective sea ice trends (see text for details), with the observed trend indicated by a thick green line. Standard deviations of the distributions around the ensemble means are also indicated. Note that the histograms in Fig. 3.1b,c describe the distributions of horizontal coordinate values in Fig. 3.5a,b.

region of the scatter plot than those without volcanic forcing (consistent with Figure 3.3), the points all fall near the same line. We find similar results using September sea ice trends (Figure 3.5b and Table 3.1), though this relationship appears noisier, perhaps due to a larger influence of internal variability.

We can approximately account for biases in the level of global warming by considering the Arctic "effective sea ice trend" (Rosenblum & Eisenman, 2016), which is defined as the simulated sea ice trend scaled by the bias in simulated global warming during the same time period (where the latter is calculated as the ratio of observed

to simulated annual-mean global-mean surface temperature trend; see Appendix A and Rosenblum & Eisenman (2016) for details). The effective sea ice trend is closely related to the sea ice sensitivity (Winton, 2011). It provides a rough estimate of what the sea ice trend would be in each run if the observed level of global warming had been simulated.

By comparing the distributions of modeled effective Arctic sea ice trends to the observed trend, the results in Figure 3.5c-d suggest that the modeled Arctic sea ice cover in both CMIP3 and CMIP5 would retreat far more gradually if the models simulated the observed level of global warming (see also Table 2, which includes both effective sea ice trends and sea ice sensitivities). The effective sea ice trend in CMIP5 is slightly closer to the observations than in CMIP3, especially in September, but the observed trend falls well outside both CMIP model distributions.

Note that this bias in simulated sea ice sensitivity is qualitatively consistent with Stroeve & Notz (2016), although there are quantitative differences due to factors including the availability of CMIP5 results at the time of each analysis and differing methods used to estimate the ice sensitivity (see Appendix A). The possibility that simulated natural variability could explain this bias is examined in a companion paper (Rosenblum & Eisenman, 2016).

3.5 Additional Points

Although Southern Hemisphere sea ice cover and annual-mean global-mean surface air temperatures are also approximately linearly related in these climate models (Rosenblum & Eisenman, 2016), we find that the influence of volcanoes does not appear to have the same impact on the evolution Antarctic sea ice (Figure B.2). This may be related to a range of factors, including that the aerosol forcing from both Pinatubo and El Chichón is more concentrated in the Northern Hemisphere than

Table 3.2: Observed as well as CMIP3 and CMIP5 ensemble-mean effective sea ice trends (10^6 km^2/decade) and ice sensitivity (10^6 km^2/K), as shown in Figure 3.5. The standard deviations among the ensemble members are indicated in parentheses. Note that the ice sensitivity is equal to the effective ice trend divided by the observed temperature trend, which is 0.16 K/decade.

	Ann. effective ice trend	Sept. effective ice trend
CMIP3	-0.19 (0.11)	-0.24 (0.12)
CMIP5	-0.23 (0.09)	-0.36 (0.17)
Observations	-0.53	-0.89
	Ann. ice sensitivity	Sept. ice sensitivity
CMIP3	-1.23 (0.69)	-1.53 (0.75)
CMIP5	-1.46 (0.56)	-2.29 (1.10)
Observations	-3.40	-5.67

the Southern Hemisphere in many datasets (Arfeuille *et al.*, 2014), that much of the temperature change caused by volcanoes has been suggested to occur at depth in the Southern Ocean (Fyfe, 2006), that Antarctic sea ice has been suggested to only respond to supervolcanoes (Zanchettin *et al.*, 2014), and that Antarctic sea ice extent is less correlated with annual-mean global-mean surface air temperature than Arctic sea ice extent (Rosenblum & Eisenman, 2016).

Previous studies have demonstrated that CMIP5 models simulate a smaller and more accurate climatological Arctic sea ice cover compared to CMIP3 (Stroeve *et al.*, 2012; Flato *et al.*, 2013). The possibility that this could be linked to sea ice trends has been considered previously, although no clear relationship was found (Massonnet *et al.*, 2012). Similarly, we find that the initial sea ice cover does not appear to be closely related to the sea ice trends (Figure B.3). This is consistent with the approximately linear relationship between simulated Arctic sea ice cover and annual-mean global-mean surface temperatures (Gregory *et al.*, 2002; Winton, 2011; Mahlstein & Knutti, 2012; Stroeve & Notz, 2015; Rosenblum & Eisenman, 2016). That is, if this were a perfectly linear relationship, a given amount of warming would

result in the same amount of ice loss regardless of the initial amount of sea ice cover. Note that although geographic muting effects due to the distribution of landmasses in the Arctic region (Eisenman, 2010) can cause a departure from this linearity for very large ice extents (Fig. S2 of Armour *et al.*, 2011), the relationship has been found to be approximately linear for annual-mean and September ice extents similar to and smaller than modern observed values (e.g., Fig. 2 of Armour *et al.*, 2011)).

The main results of this study are presented using sea ice extent. We find that analyzing observed and modeled sea ice area instead of extent leads to qualitatively similar results (Figures B.4-B.8).

Our estimate of the observed September sea ice sensitivity (-5.67×10^6 km^2/K) is more than twice as large as the number reported previously by Mahlstein & Knutti (2012) (-2.62×10^6 km^2/K), who used the ice sensitivity to make an observationally-based projection of how much global warming it would take for the September Arctic sea ice area to decline from its 1980-1999 mean value to the nearly ice-free value of 1×10^6 km^2. The difference between our estimate and that in Mahlstein & Knutti (2012) arises due to a number of factors. We use NASA Team sea ice extent (Fetterer *et al.*, 2002) during 1979-2013. By contrast, Mahlstein & Knutti (2012) use the coarser resolution Hadley Centre Sea Ice and Sea Surface Temperature (HadISST) (Rayner *et al.*, 2003) dataset, the observed ice area rather than ice extent, and a shorter observed time period (1980-2007). Further, they calculate the ice sensitivity using an ordinary least squares regression of ice on temperature (I. Mahlstein, personal communication May, 2016), which Winton (2011) found to give a less accurate estimate than the trend ratio method adopted here (see Appendix A).

Using CMIP3 simulations, Mahlstein & Knutti (2012) found that the ensemble-mean ice sensitivity during 2010-2100 was smaller than during 1980-2007 by a factor of 0.92, and hence they scaled the observed ice sensitivity by 0.92 to project the level

of future global warming at which the Arctic will become nearly seasonally ice-free. We repeat the calculation from Mahlstein & Knutti (2012) using an observed ice sensitivity of -5.67×10^6 km^2/K and the 1980-1999 mean September Arctic sea ice extent from the NASA Team dataset, rather than an observed sensitivity of -2.62×10^6 km^2/K and the 1980-1999 mean September Arctic sea ice area from the HadISST dataset. We find that in this case the level of global warming projected to cause a nearly ice-free Arctic Ocean is approximately 1°C, rather than approximately 2°C as reported in Mahlstein & Knutti (2012). Using NASA Team ice area rather than ice extent for the observed sensitivity and the 1980-1999 mean value yields a similar result of approximately 1°C.

3.6 Summary

CMIP5 models have been found to simulate Arctic sea ice retreat during 1979-2013 that is faster on average than in the CMIP3 models. At the same time, the CMIP5 ensemble-mean rate of global warming during 1979-2013 has been found to be larger than CMIP3. The difference in global warming has been previously attributed to historical volcanic forcing, which was included in all of the CMIP5 models but only about half of the CMIP3 models. However, the inclusion of volcanic forcing in the CMIP ensembles has not been considered, as far as the authors are aware, in previous analyses of the rate of simulated Arctic sea ice retreat. Here we show that a range of approaches all suggest that the change between CMIP5 and CMIP3 in the ensemble-mean 1979-2013 Arctic sea ice extent trend can also be largely attributed to the inclusion of volcanic forcing.

Specifically, major volcanic eruptions occur during the early part of this time period, and they cause temporary cooling and ice expansion. This exacerbates the model bias toward too much 1979-2013 global warming while reducing the model bias

toward too little Arctic sea ice retreat. These results are consistent with the sea ice sensitivity not being substantially influenced by volcanic eruptions, which would imply that the higher level of global warming caused by volcanoes should coincide with more sea ice retreat. This suggests that the reported improvement in simulated sea ice trends was largely an artifact of comparing simulations that had volcanic forcing with simulations that did not.

3.A Method

We analyze 118 simulations of years 1979-2013 from 40 CMIP5 models (Taylor *et al.*, 2012) with historical and RCP4.5 forcing as well 38 simulations from 19 CMIP3 models (Meehl *et al.*, 2007) with historical and SRES A1B forcing. The time period we analyze is chosen based on the availability of sea ice observations at the time of analysis. We use monthly-mean fields to compute values of global-mean surface air temperature, sea ice extent, and sea ice area. Grid cell area fields are used for models that provide them in the CMIP5 archive, and otherwise we estimate the grid cell areas based on the reported grid box vertices. For simplicity, in the distributions we treat each simulation as an ensemble member from an independent model, rather than considering which model each simulation comes from.

CMIP3 simulations were not used in this study when either (i) temperature and sea ice data were not both available during 1979-2013 or (ii) dates reported in the file did not match the filename in the CMIP3 archive. The following CMIP3 simulations each had at least one of these issues and were excluded: all runs of CSIRO-MK3-0; all runs of BCC-CM1; all runs of GISS-MODEL-E-H; CSIRO-MK3-5 runs 2 and 3; GISS-MODEL-E-R runs 2-9; all runs of INGIV-ECHAM; and NCAR-CCSM3.0 runs 3,4,8, and 9. We also exclude all runs of IAP-FGOALS because the simulated sea ice extent in both hemispheres is approximately twice as large as any other CMIP3

simulation. IPSL-CM4 reported grid cells with sea ice concentrations greater than 100%, which we replaced with 100%. Finally, note that the MRI-CGCM2-3-2a model reported having volcanic forcing in the CMIP3 documentation, but several studies found that it did not actually appear to include volcanic forcing (Knutson *et al.*, 2013; Sillmann *et al.*, 2013). We therefore considered this model to have not included volcanic forcing.

This study uses the processed CMIP5 values from Rosenblum & Eisenman (2016) (Ch. 2), where processing details are given. In the analysis of trends during years 1900-2100, we use only 80 CMIP5 simulations because 38 of the simulations do not report model output during the entirety of this longer time period.

We use observed monthly-mean sea ice extent and area from the National Snow and Ice Data Center Sea Ice Index (Fetterer *et al.*, 2002), which uses the NASA Team algorithm. Missing values are filled by linearly interpolating between the same month in the previous and following years. We use the Goddard Institute for Space Sciences Surface Temperature Analysis (GISTemp) (Hansen *et al.*, 2010) for the observed annual-mean global-mean surface temperature data.

All trends are computed using ordinary least squares regressions with time. For the sea ice sensitivity, the annual or September sea ice trend is divided by the annual global-mean surface air temperature trend. This method of estimating the sea ice sensitivity is sometimes referred to as the "trend ratio" (Winton, 2011). For the simulated effective sea ice trend, the simulated sea ice sensitivity is multiplied by the observed annual-mean global-mean surface temperature trend, as described in Rosenblum & Eisenman (2016). Note that for the observations, this leads to an effective sea ice trend which is equal to the actual sea ice trend. Winton (2011) suggests that total least squares (TLS) regression between ice and temperature leads to a slightly less biased estimate of the ice sensitivity, but we find that this has

a relatively small influence on the results presented here. For example, when we compute the observed Arctic sea ice sensitivity using TLS regression instead of the trend ratio, the ice sensitivity increases from -5.67×10^6 km^2/K to -5.69×10^6 km^2/K.

Acknowledgements

The work was supported a National Science Foundation Graduate Research Fellowship and National Science Foundation grants ARC-1107795 and OCE-1357078. Without implying their endorsement, we are grateful to Sarah Gille, Art Miller, Paul Kushner, Neil Tandon, Frédéric Laliberté, Till Wagner, and John Fyfe for helpful comments and discussions. Processed CMIP3 and CMIP5 data used in this study is available at http://eisenman.ucsd.edu/code.html.

Chapter Three, in full, is a reprint of the material as it appears in the Journal of Climate, 2016. Rosenblum, E. and Eisenman, I., (2016). Faster Arctic sea ice retreat in CMIP5 than in CMIP3 due to volcanoes. *Journal of Climate*, 29, 9179-9188. ©American Meteorological Society. Used with permission. The dissertation author was the primary investigator and author of this paper.

Chapter 4

Factors controlling seasonal mixed layer freshening in the Canada Basin during 1975, 2006, and 2007

4.1 Introduction

As the Arctic sea ice cover continues to recede, the underlying ocean mixed layer is warming, freshening, and shoaling throughout much of the Arctic (Peralta-Ferriz & Woodgate, 2015*a*; McPhee *et al.*, 1998; Toole *et al.*, 2010; Jackson *et al.*, 2010). Of all the Arctic regions, the Canada Basin has exhibited the largest mixed layer freshening trends (Peralta-Ferriz & Woodgate, 2015*a*) and the largest losses in both first-year and multi-year sea ice (McLaughlin *et al.*, 2011). Decadal trends toward fresher mixed layers have been attributed to reduced sea ice growth in the fall and winter (Yamamoto-Kawai *et al.*, 2009), increased freshwater transport from enhanced Ekman transport in the winter and early spring (Proshutinsky *et al.*, 2009), and increased sea ice melt in the spring and summer (Peralta-Ferriz & Woodgate,

2015*a*; Toole *et al.*, 2010; Lemke & Manley, 1984). Seasonal mixed layer freshening from sea ice melt increases seasonal halocline stratification, which can influence upper-ocean heat storage and consequently sea ice evolution (Jackson *et al.*, 2010; Ramudu *et al.*, 2018; Timmermans, 2015).

The Canada Basin mixed layer is relatively isolated from the influence of the underlying Pacific Water on seasonal timescales (Timmermans *et al.*, 2008; Toole *et al.*, 2010). However, a number of factors can influence the seasonal mixed layer freshening during the sea ice melt season. For example, warmer surface temperatures can lead to more mixed layer freshening by causing more sea ice bottom melt (Maykut & McPhee, 1995). Additionally, trends toward shallower mixed layers can cause freshwater input to be concentrated within a smaller volume, thereby raising the rate of mixed-layer freshening. On the other hand, reduced ice thickness and ice concentration can reduce the amount of freshening because there is less sea ice available to melt.

Here we examine how changes in mixed-layer temperatures, mixed-layer depth, and sea ice cover can influence seasonal mixed-layer freshening in the Canada Basin using observations and an idealized, one-dimensional framework. For 1975, 2006, and 2007, we examine melt-season observations that were collected in similar locations but under very different sea ice conditions (Figure 1). The observations used for the study are presented in Section 2, and the idealized framework is presented in Section 3. Results from the estimates of the idealized framework are presented in Section 4, discussed in Section 5, and summarized in Section 6.

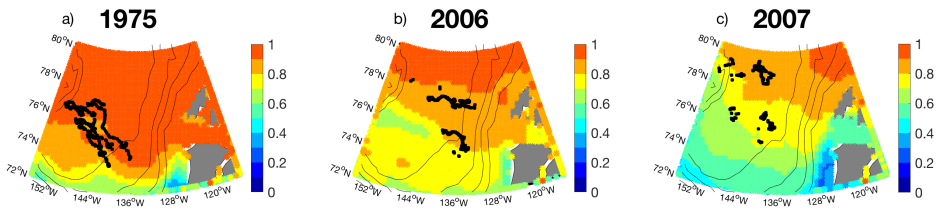

Figure 4.1: Position of ocean observations taken in the Canada Basin during May-August in (a) 1975, (b) 2006, and (c) 2007, overlaid on the average summer (May-August) sea ice concentration for each year. There are 433 profiles taken during this time period in 1975, 816 in 2006, and 444 in 2007. Note that observations of sea ice concentration for 1979 rather than 1975 are used for (a) due to data limitations (see Section 2 for details).

4.2 Observations

4.2.1 Oceanographic data

The Arctic Ice Dynamics Experiment (AIDJEX) program provided some of the earliest observations of seasonal mixed-layer evolution below what was then thick, perennial Arctic sea ice. A major component of the program consisted of four occupied, drifting ice camps that collected oceanographic data for one year between April 1975 and April 1976. Salinity and temperature profiles down to 750 m were measured daily at each camp, with a vertical resolution of 1-2 m using Plessey model 9040 STD and CTD systems, resulting in 1287 vertical profiles (Lemke & Manley, 1984). We examine all available data from this experiment.

The Ice Tethered Profiler (ITP) instrument system was deployed in 2004 and has since been recording temperature and salinity profiles with a vertical resolution of 25 cm throughout the Arctic. The system consists of a series of surface buoys that are frozen into drifting ice floes (Krishfield *et al.*, 2008). The buoys are connected to wires that are 800 meters long, attached to profilers that move up and down the wires collecting data approximately 3 times per day. A number of ITPs have been deployed

in the Canada Basin, and have collected oceanographic data in a similar region to that of AIDJEX, under now much thinner, more seasonal sea ice. We examine quality controlled data, identified as level 3 in the ITP data archives, which are available for 2004–2012. We consider only data within the Canada Basin, which we define as the region bounded by 72°N, 84°N, 130°W, and 155°W, following Peralta-Ferriz & Woodgate (2015*a*).

The aim of this study to examine the seasonal mixed-layer evolution during the melt season. We therefore take 10-day averages from May-September in the ITP and AIDJEX datasets, effectively removing smaller timescale variations and spatial variations. We only consider years where the 10-day averaged data are continuous throughout the melt season. We find that this condition holds for the entire AIDJEX dataset in 1975, and during 2006-2008 and 2011 in the ITP dataset (Figure S1). Based on the data availability related to the number of available observations, instrument drift, and locations, we focus our analysis on all the available ITP observations in 2006 and 2007 (see Appendix A for details). The analysis in this study focuses on 1975, 2006, and 2007 because these three years have been the subject of several upper-ocean studies in this region (e.g., Lemke & Manley, 1984; Maykut & McPhee, 1995; Perovich *et al.*, 2008; Toole *et al.*, 2010; Yamamoto-Kawai *et al.*, 2009; Timmermans, 2015), which is useful for validating the idealized framework. To assess the robustness of our results, we repeat our analysis using 2008, 2011, and the entire 2004-2012 ITP dataset in Section 5 and in the Supporting Information.

The mixed-layer depth of each profile is determined by the first depth at which the change in mixed-layer density exceeds 0.1 kg/m^3 from the shallowest observed value, following Peralta-Ferriz & Woodgate (2015*a*). Profiles were removed when a mixed layer was not detected or when the mixed layer depth was less than 2 meters from the shallowest observed value (following Jackson *et al.*, 2010). In addition to

these criteria, AIDJEX profiles were removed from the analysis when they contained zero values at every point or if the computed mixed-layer depth exceeded 100 meters, which only occurred when there were substantial data missing from the upper tens of meters. ITP profiles were also removed if the shallowest observed value was deeper than 10 meters (following Jackson *et al.*, 2010). These conditions reduced the AIDJEX dataset from 1287 profiles to 1261 profiles in 1975 and reduced the ITP dataset from 3294 profiles to 2613 profiles in 2006 and from 2828 profiles to 1747 profiles in 2007. We repeat our analysis using a different definition of the mixed-layer depth, (following Jackson *et al.*, 2010), in the Supporting Information.

4.2.2 Sea ice concentration data

Daily observations of sea ice concentration since 1979 are provided by the National Snow and Ice Data Center Sea Ice Index from satellite passive microwave measurements (Fetterer *et al.*, 2002). These observations were not available in 1975, so we instead use an estimate of sea ice concentration that was derived from the locations of the drifting AIDJEX ice camps (Maykut & McPhee, 1995). The derived sea ice concentration is higher than the basin average (Figure S4), likely due to the fact that the ice camps were sited in locations that were likely to survive the melt season, similar to the ice floes of ITPs. For consistency, we therefore estimate the average sea ice concentration associated with the ITP dataset by using the location of each ITP observation and finding the closest corresponding sea ice concentration data point. To examine the sensitivity of the results to this choice, we repeat our analysis in the Supporting Information using the basin average from satellite observations in 1979, 2006, and 2007.

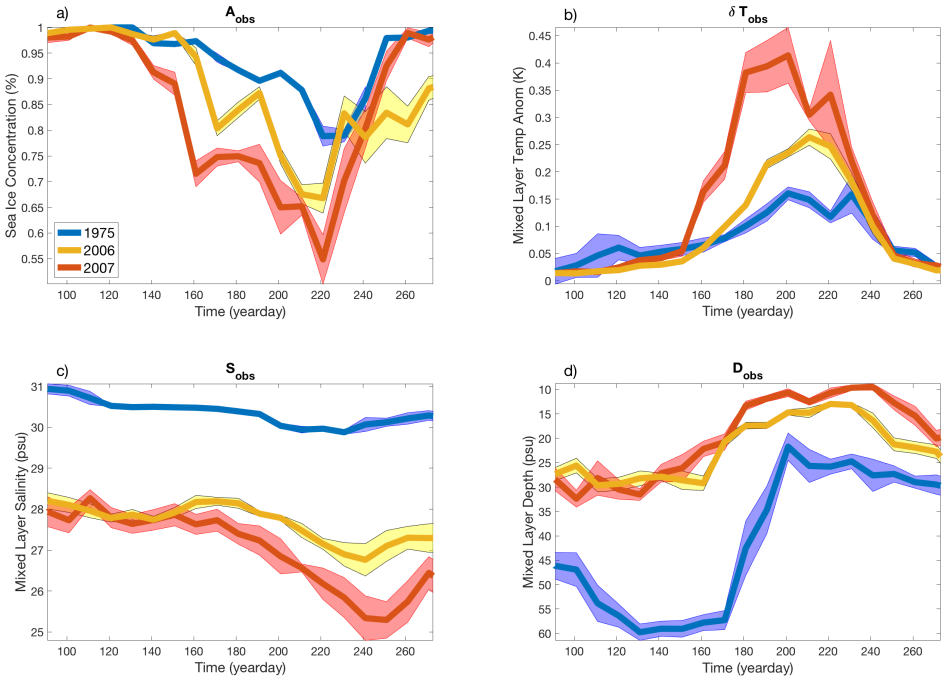

Figure 4.2: Seasonal evolution of the (a) sea ice concentration, (b) mixed-layer temperature anomaly from freezing, (c) mixed-layer salinity, and (d) mixed-layer depth in 1975 (blue), 2006 (yellow), and 2007 (red). Thick lines indicate the 10-day mean, and the shading indicates the standard error (see Appendix B).

4.2.3 Sea ice and mixed-layer evolution

We examine data collected during May-September in 1975, 2006, and 2007. Specifically, following the methods outlined above, we examine 433 profiles in 1975, 816 profiles in 2006, and 444 profiles in 2007 from all four AIDJEX ice camps and ITPs 1, 3, 5, 6, 8, 13, and 18 . The locations of these data and the average sea ice concentration during the same period are shown in Figure 4.1. The 10-day mean and standard error of the observed sea ice concentration, mixed-layer salinity, mixed-layer depth, and mixed-layer temperature anomaly from freezing are computed for each year (Figure 4.2). The method used for computing the standard error of these values are described in Appendix B.

During the course of the melt season, the sea ice concentration decreases and allows more solar radiation to warm the mixed layer, causing the mixed-layer temperature anomaly from freezing to increase. Warming mixed-layer temperatures and decreasing sea ice cover coincides with mixed-layer shoaling and freshening. We obtain a summer mixed layer of approximately 20 m in 1975, consistent with Lemke & Manley (1984), and a summer mixed layer of approximately 10-15 m in 2006 and 2007, somewhat consistent with Toole *et al.* (2010) ($\sim$16 m, using ITP data) and Peralta-Ferriz & Woodgate (2015*a*) ($\sim$9 m, using 30 years of hydrographic data). Figure 4.2 also reveals anecdotal evidence of the previously reported decadal trends towards warmer, fresher, and shallower mixed layers (Peralta-Ferriz & Woodgate, 2015*a*), as well as an increase in the amount of mixed-layer freshening that occurs over the course of a single melt season (Yamamoto-Kawai *et al.*, 2009).

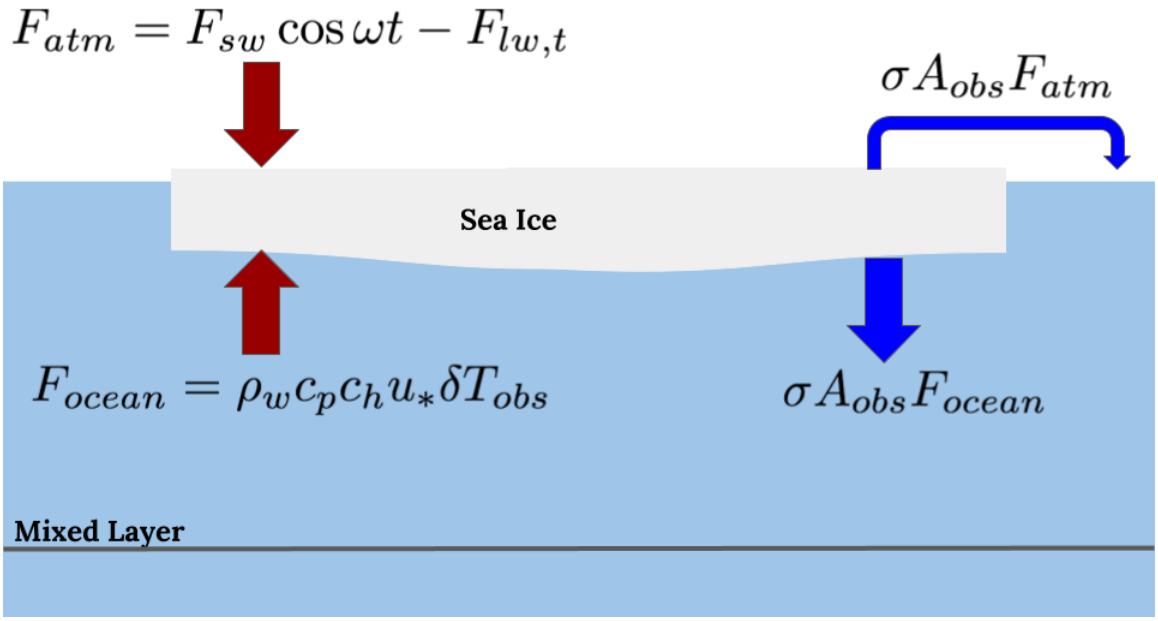

Figure 4.3: Schematic of the one-dimensional framework. Red arrows indicate heat flux to sea ice and blue arrows indicate resulting freshwater flux into the mixed layer from sea ice melt (see Section 5.5 for details).

4.3 Idealized Framework

Here, we present a simplified, one-dimensional framework to examine factors controlling seasonal mixed-layer freshening, illustrated in Figure 4.3. The framework is meant to represent the fundamental mechanisms controlling mixed-layer salinity evolution during the melt season by using observations of sea ice concentration (A_{obs}), mixed-layer depth (D_{obs}), and mixed-layer temperature anomalies from freezing (δT_{obs}) from 1975, 2006, and 2007 (Figures 5.2). The main assumptions used in this framework are motivated by previous observational studies in the Canada Basin.

First, the mixed layer is relatively isolated from underlying water (i.e Pacific Water and remnant mixed layers) during the melt season due to the strongly stratified seasonal and permanent halocline (Toole *et al.*, 2010). We therefore neglect exchanges between the the mixed layer and the underlying ocean and instead only consider a closed system between the mixed layer and the sea ice. We note that this is similar

to early models of the seasonal pycnocline (Kraus & Turner, 1967; Lemke & Manley, 1984).

Second, seasonal mixed layer freshening is driven primarily by thermodynamic seasonal sea ice melt (Peralta-Ferriz & Woodgate, 2015*a*; Lemke & Manley, 1984; Toole *et al.*, 2010). We therefore consider a system where the freshwater flux is only driven by sea ice melt.

Third, sea ice surface melt has remained relatively constant over the past several decades (1959-2014 average: 57±19 cm) compared to sea ice bottom melt, which has increased with time and has large inter-annual variations (1959-2014 average: 83±63 cm) (Perovich & Richter-Menge, 2015). We therefore consider a system in which the atmospheric heat flux to the top of the sea ice is the same in 1975, 2006, and 2007, while the oceanic heat flux to the sea ice fluctuates, depending on the observed mixed-layer temperature anomaly from freezing (δT_{obs}).

Finally, for simplicity, we consider large sea ice floes (with radii significantly larger than 30 m) and therefore neglect contributions from lateral sea ice melt (Steele, 1992). Each component of this framework and additional assumptions is outlined below.

4.3.1 Heat Fluxes

We choose an idealized representation of the atmospheric heat flux to the top of the sea ice that is roughly consistent with observations of the surface energy budget averaged over the past few decades and sea ice top melt, by considering the results of Serreze *et al.* (2007) and Perovich & Richter-Menge (2015). Observations indicate that the total downward heat flux is roughly sinusoidal during the melt season, and that it is driven mainly by a sinusoidally evolving shortwave radiative heat flux and by a smaller, less seasonally variable contribution from long-wave radiation and turbulent

heat fluxes (Serreze *et al.*, 2007, their Figure 3d). We therefore prescribe the following atmospheric heat flux to the top of the sea ice (F_{atm}):

$$F_{atm} = F_{sw} \cos \omega t - F_{lw,t}, \tag{4.1}$$

where $F_{lw,t}$ is a combination of the long-wave and turbulent heat flux components and $F_{sw} = (1 - \alpha_i)F_0$ is the shortwave component, which depends on the incoming solar radiation (F_0) and the sea ice albedo (α_i), and $\omega = 2\pi/\text{year}$ is the annual frequency. We set F_0 =200 W m^{-2} (similar to observations in the same region Timmermans, 2015), $\alpha_i = 0.6$ (following Wagner & Eisenman, 2015), and $F_{lw,t} = 50$ W m^{-2} (similar to observations from Serreze *et al.*, 2007). We find that these parameter choices for F_{atm} results in a change in sea ice thickness due to top melt that is consistent with the observed average top melt in the region over the past several decades (see Discussion for details).

The ocean driven heat flux to the sea ice is closely related to the mixed-layer temperature anomaly from freezing (Maykut & McPhee, 1995). We therefore use the observed mixed-layer temperature anomaly from freezing (δT_{obs}) to prescribe the ocean heat flux to the bottom of the sea ice as

$$F_{ocean} = k \delta T_{obs} \tag{4.2}$$

$$k = \rho_w c_p c_h u_*, \tag{4.3}$$

where ρ_w is the density of water, c_p is the uniform heat of fusion, c_h is a non-dimensional heat transfer coefficient, and u_* is the friction velocity. The parameters are set following Maykut & McPhee (1995): $\rho_w = 1026$ kg m^{-3}, $c_p = 3980$ J kg^{-1}, and $c_h = 0.006$. We set $u_* = 0.005$ m s^{-1}, similar to a number of observations in the Canada Basin using AIDJEX and ITP data (Maykut & McPhee, 1995; Gallaher

et al., 2016; Cole *et al.*, 2017).

The total estimated heat flux onto both interfaces of the sea ice in this idealized framework is then given by:

$$F_{est} = F_{atm} + k\delta T_{obs}. \tag{4.4}$$

4.3.2 Salt Budget

Applying the above heat fluxes to a simple model of sea ice the melt season, we derive the evolution of sea ice thickness, freshwater flux from sea ice melt, and the resulting mixed-layer salinity evolution in this idealized scenario.

First, we use the observed mixed-layer temperature anomaly from freezing (δT_{obs}) to estimate the evolution of the sea ice thickness (h_{est}) as

$$\rho_i L \frac{dh_{est}}{dt} = -(F_{atm} + k\delta T_{obs}), \tag{4.5}$$

where $L = 3.3 \cdot 10^5$ J kg^{-1} is the latent heat of fusion of sea ice and $\rho_i = 900$ kg m^{-3} is the density of sea ice.

Second, we use the observed sea ice concentration (A_{obs}) and the observed mixed-layer temperature anomaly from freezing (δT_{obs}) to estimate the evolution of the freshwater flux from sea ice melt in response to the applied heat fluxes alone (i.e. contributions from lateral melt are neglected) as $\phi = \sigma A_{obs} dh_{est}/dt$, or similarly

$$\phi = -\frac{\sigma A_{obs}}{\rho_i L}(F_{atm} + k\delta T_{obs}), \tag{4.6}$$

where $\sigma = 20$ psu is the difference between the salinity in the mixed layer and the salinity of the sea ice. Note that this is smaller than the typical value used in idealized studies of approximately 30 psu (Goosse & Zunz, 2014; Petty *et al.*, 2013; Martinson,

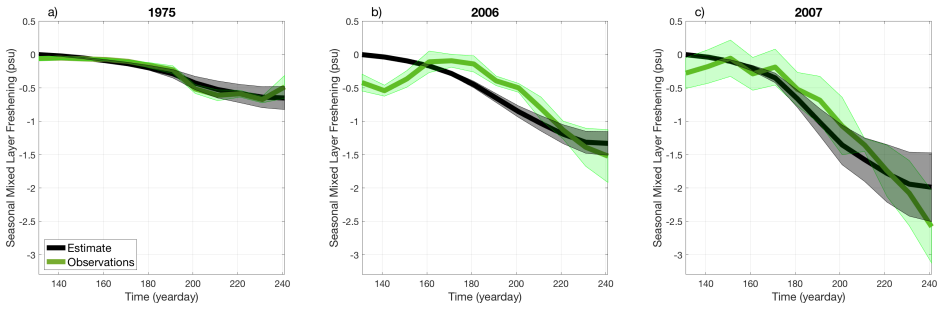

Figure 4.4: Observed (green) and estimated (black) seasonal mixed-layer freshening ($\mathfrak{F}$, eq. 4.9) in (a) 1975, (b) 2006, and (c) 2007. Thick lines indicate the 10-day mean, and the shading indicates the standard error.

1990) because the mixed-layer salinity drops as low as 25 psu in 2007 (Figure 1). We did not find that our subsequent analysis was sensitive to this parameter choice (not shown).

Finally, we use the observed mixed-layer depth (D_{obs}), the observed sea ice concentration (A_{obs}), and the observed mixed-layer temperature anomaly (δT_{obs}) to estimate the mixed-layer salinity (S_{est}) evolution as $D_{obs} dS_{est}/dt = \phi$, or similarly

$$D_{obs}\frac{dS_{est}}{dt} = \frac{\sigma A_{obs}}{\rho_i L}(F_{atm} + k\delta T_{obs}). \tag{4.7}$$

4.4 Results

4.4.1 Validation

As a starting point, we examine the extent to which this idealized, one-dimensional framework can explain differences in seasonal mixed-layer freshening between 1975, 2006, and 2007. We use the observed sea ice concentration (A_{obs}), the observed mixed layer depth (D_{obs}), and the observed mixed-layer temperature anomaly from freezing (δT_{obs}) shown in Figure 4.2 to estimate the mixed-layer salinity evolution during the melt season by integrating equation 4.7. That is, for each

year we compute

$$S_{est}(t) = -\frac{\sigma}{\rho_i L}\int_{t_0}^{t} \frac{A_{obs}}{D_{obs}}(F_{atm} + k\delta T_{obs}) \cdot dt + S_0, \tag{4.8}$$

where we have defined the melt season as the period of time during which $F_{est} > 0$, t_0 is the beginning of the melt season, and S_0 is the observed mixed-layer salinity at the start of the melt season in each year.

Next, we compute the observed and estimated seasonal mixed-layer freshening ($\mathfrak{F}$), which we define as the mixed-layer salinity anomaly relative to the melt-season average, offset by a constant. That is, for each year we compute:

$$\mathfrak{F}_{obs}(t) = S_{obs}(t) - \langle S_{obs} \rangle + S_{est}(t_0) \tag{4.9}$$

$$\mathfrak{F}_{est}(t) = S_{est}(t) - \langle S_{est} \rangle + S_{est}(t_0), \tag{4.10}$$

where the brackets represent the temporal mean during the melt season and S_{obs} is the observed mixed-layer salinity.

Figure 4.4 shows the observed and estimated seasonal mixed-layer freshening in 1975, 2006, and 2007. The estimated mixed-layer freshening, indicates gradual changes due to sea ice melt throughout the melt season. The observations, by contrast, are significantly noisier and even indicate that the mixed layer initially becomes saltier, likely due to entrainment, before freshening later in the melt season.

Despite the limited physics that is included in the idealized framework, we find that the estimate predicts a level of mixed-layer freshening by the end of the melt season that is similar to the observed freshening. In particular, we find that both the model estimate and the observations indicate approximately twice as much freshening in 2006 compared to 1975 and three to four times more freshening in 2007 compared to 1975 (Table 1).

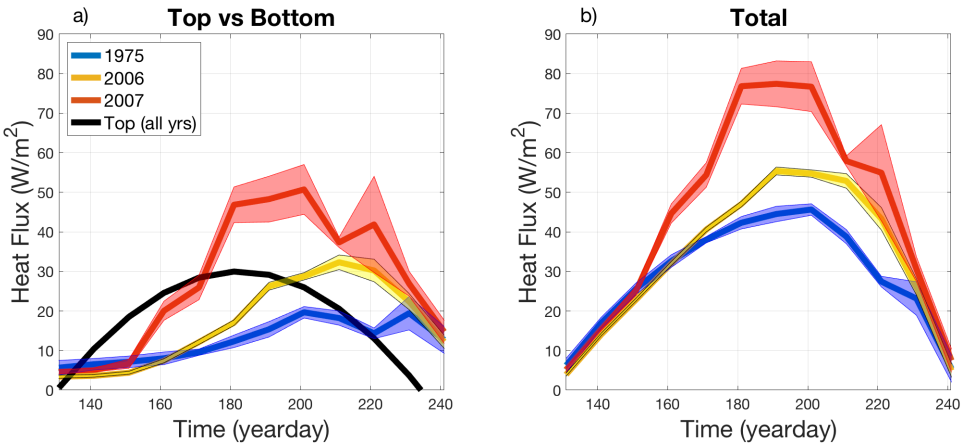

Figure 4.5: The estimated change in heat flux towards (a) the top of the sea ice (F_{atm}, eq. 4.1) and the bottom of the sea ice (F_{ocean}, eq. 4.2), and (b) their sum (F_{est}, eq. 4.4) is show during 1975 (blue), 2006 (yellow), and 2007 (red). The estimated heat flux to the top of the sea ice (black) is the same for each year, and is shown in each panel for reference. Thick lines indicate the 10-day mean, and the shading indicates the standard error.

To quantify the level of agreement between the estimate and observations, we examine the ratio of the maximum freshening in the models to the observations. That is, for each year, we compute:

$$\mathfrak{R} = \frac{\max(\mathfrak{F}_{obs}) - \min(\mathfrak{F}_{obs})}{\max(\mathfrak{F}_{est}) - \min(\mathfrak{F}_{est})}. \tag{4.11}$$

We find that the models and observations are in agreement within one standard error (Table 2). This suggests that our framework may include essential processes necessary to capture year-to-year variations in the seasonal mixed-layer freshening. Motivated by this, in the following subsections we break down this estimate into the components introduced in Section 3 to better understand what processes are driving the differences in the seasonal mixed-layer freshening between 1975, 2006, and 2007.

4.4.2 Heat Flux

Figure 4.5 shows the prescribed atmospheric heat flux to the top of the sea ice (F_{atm}, eq. 4.1), the estimated oceanic heat flux to the bottom of the sea ice

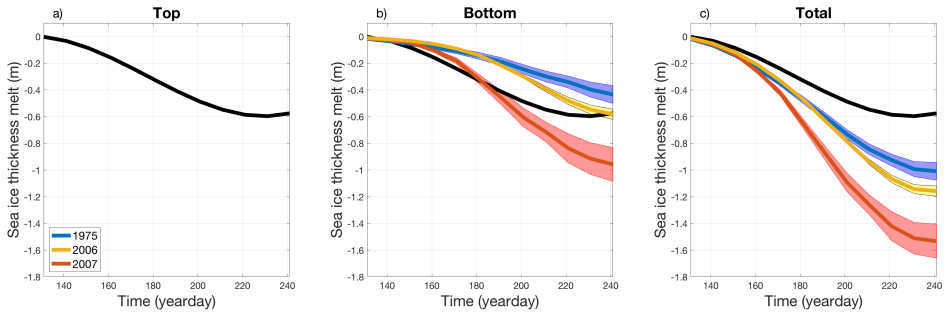

Figure 4.6: The estimated change in sea ice thickness due to (a) top melt (h_{top}, eq. 4.12), (b) bottom melt (h_{bot}, eq. 4.12), and (c) their sum (h_{est}, eq. 4.5) is shown during 1975 (blue), 2006 (yellow), and 2007 (red). The estimated sea ice thickness change due to top melt (black) is the same for each year, and is shown in each panel for reference. Thick lines indicate the 10-day mean, and the shading indicates the standard error.

(F_{ocean}, eq. 4.2), and their sum (F_{est}, eq. 4.4) for 1975, 2006, and 2007. The atmospheric heat flux is the same for each case, while the oceanic heat flux varies in each year, directly reflecting variations in the observed mixed-layer temperature anomaly relative to freezing (δT_{obs}, Figure 4.2b). The estimated total heat flux to the sea ice therefore also only differs in each year due to variations in the observed mixed-layer temperature relative to freezing.

We compare relative contributions of the atmospheric and ocean heat fluxes in each year (black vs colored lines, Figure 4.5a). In each case, the atmospheric heat flux has the largest influence on the total heat flux in spring, while the oceanic heat flux increases with time, reaching maximum values during the summer. In 1975, the atmospheric heat flux has the largest impact until August. By contrast, the atmospheric heat flux only has the largest impact until June in 2007 and until July in 2006, as a result of warmer mixed-layer temperatures.

Figure 4.5b shows the estimated influence of differences in the observed mixed-layer temperature anomaly from freezing on the total heat flux to the sea ice. Quantitatively, we find that the estimated total heat flux to the sea ice integrated over the melt season in 2007 is approximately 55% larger than in 1975, and 2006 is 17% larger than in 1975 (Table 1).

4.4.3 Sea Ice Thickness

We estimate the influence of oceanic heat flux on the sea ice thickness evolution during the melt season by integrating equation 4.5 and examining each term separately. That is, we examine the sea ice thickness changes due to top melt (h_{top}), the sea ice thickness changes due to bottom melt (h_{bot}), and their sum (h_{est}), where changes in sea ice thickness due to top and bottom melt are defined as:

$$h_{top}(t) = -\int_{t_0}^{t} \frac{F_{atm}}{\rho_i L} dt, \tag{4.12}$$

$$h_{bot}(t) = -\int_{t_0}^{t} \frac{k\delta T_{obs}}{\rho_i L} dt. \tag{4.13}$$

Figure 4.6 shows h_{top}, h_{bot}, and h_{est} for 1975, 2006, and 2007. The term h_{top} (black lines) is directly related to the atmospheric heat flux, and is therefore the same every year; h_{bot} varies each year, reflecting differences in the observed mixed-layer temperature anomaly from freezing (δT_{obs}, Fig. 4.2b); h_{est} therefore also differs in each year due to differences in the observed mixed-layer temperature anomaly from freezing (Figure 4.6c), similar to the estimated total heat flux to the sea ice (Figure 4.5b).

We compare relative contributions of the atmospheric and ocean heat fluxes to sea ice thickness evolution in each year (black vs colored lines, Figure 4.5b). We find that the sea ice melts mostly from the surface throughout most of the melt season in 1975 and 2006. In 2007, by contrast, the sea ice melts from the surface and the bottom at a similar rates in the spring, but melts mostly from the bottom in the summer.

Figure 4.6c shows the estimated influence of differences in the observed mixed-layer temperature anomaly from freezing on the total change in the sea ice thickness. Quantitatively, these estimates suggest that the sea ice thickness decreases 55% more

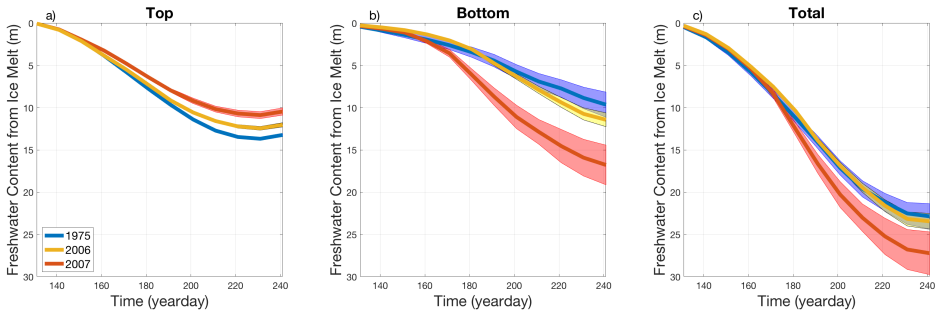

Figure 4.7: The estimated change in freshwater content from sea ice melt during the melt season due to (a) top melt (ϕ_{top}, eq. 4.14), (b) bottom melt (ϕ_{bot}, eq. 4.14), and (c) their sum (ϕ_{est}, eq. 4.6) during 1975 (blue), 2006 (yellow), and 2007 (red). Thick lines indicate the 10-day mean, and the shading indicates the standard error. Note that the y-axis is reversed here.

during the course of the melt season in 2007 compared to 1975 and 17% more in 2006 compared to 1975 (Figure 4.6c, Table 1), consistent with estimated year-to-year changes in heat flux to the sea ice integrated over the melt season (Figure 4.5c, Table 1).

4.4.4 Freshwater content from ice melt

Increased heat flux to the sea ice does not necessarily result in increased freshwater input from sea ice melt. Instead, our idealized framework suggests that there are two competing factors that can modulate the amount of freshwater content from sea ice melt (ϕ_{est}, eq. 4.6). These are related to the difference between the observed mixed-layer temperature and freezing (δT_{obs}, Fig. 4.2b) and the observed sea ice concentration (A_{obs}, Fig. 4.2a). Under less sea ice cover, (1) surface temperatures are warmer and cause more sea ice bottom melt. By contrast (2) lower sea ice cover causes less sea ice melt by limiting the amount of sea ice that is available to melt.

We examine how these factors play out in 1975, 2006, and 2007, estimating the change in freshwater content due to sea ice melt by integrating equation 4.6 and examining each term separately. That is, we estimate the change in freshwater content due to sea ice bottom melt (ϕ_{bot}), due to sea ice top melt (ϕ_{top}), and their sum (ϕ_{est}):

$$\phi_{top}(t) = -\int_{t_0}^{t} \frac{A_{obs} F_{atm}}{\rho_i L} dt \quad (4.14)$$

$$\phi_{bot}(t) = -\int_{t_0}^{t} \frac{A_{obs} k \delta T_{obs}}{\rho_i L} dt. \quad (4.15)$$

Figure 4.7a shows the estimated freshwater content change due to top melt (ϕ_{top}) for 1975, 2006, and 2007. The term ϕ_{top} is only a function of the observed sea ice concentration (A_{obs}). Therefore, less sea ice cover in 2006 and 2007 compared to 1975 (Fig. 4.2a) implies that the contribution from ϕ_{top} is also lower in 2006 and 2007 compared to 1975.

Figure 4.7b shows the estimated freshwater content change due to bottom melt (ϕ_{bot}) for 1975, 2006, and 2007. Here ϕ_{bot} is a function of both the observed sea ice concentration (A_{obs}) and the observed mixed-layer temperature anomaly relative to freezing (δT_{obs}). While A_{obs} is smaller in 2006 and 2007 than in 1975 (Fig. 5.2a), δT_{obs} is larger (Fig. 4.2c). Figure 4.7b shows that ϕ_{bot} is larger in 2006 and 2007 than in 1975, indicating that the ocean heat flux to the sea ice has increased enough to cause the freshwater flux due to sea ice melt to increase, even though there is less sea ice available to melt in more recent years.

To summarize, we find that lower sea ice cover and higher surface temperatures in recent years correspond to less freshwater input from sea ice surface melt and more freshwater input from sea ice bottom melt (Fig. 4.7a-b). As a result, the total change in freshwater content is 25% larger during the melt season in 2007 compared to 1975 and 8% larger in 2006 compared to 1975 (Fig. 4.7c). This is approximately half as much as the change in sea ice thickness melt and heat flux during the same years (Table 1).

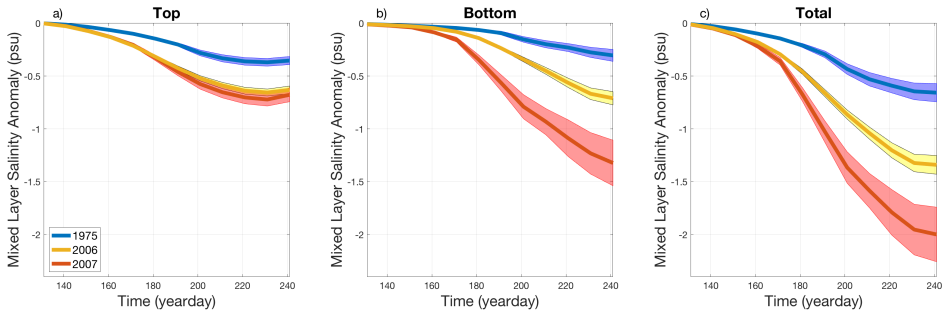

Figure 4.8: The estimated change in mixed layer salinity during the melt season due to (a) top melt (S_{top}, eq. 4.16), (b) bottom melt (S_{bot}, eq. 4.16), and (c) their sum (S_{est}, eq. 4.7) during 1975 (blue), 2006 (yellow), and 2007 (red). Thick lines indicate the 10-day mean, and the shading indicates the standard error.

4.4.5 Mixed-Layer Salinity

Modest changes in the freshwater input from sea ice melt do not necessarily imply modest changes in the mixed-layer salinity. Instead, our idealized framework suggests that there are three factors influencing mixed-layer salinity evolution (S_{est}, eq. 4.7), which are related to the observed mixed-layer temperature anomaly from freezing (δT_{obs}, Fig. 4.2b), the observed sea ice concentration (A_{obs}, Fig. 4.2a), the observed mixed-layer depth (D_{obs}, Fig. 4.2d). Under lower sea ice cover, (1) surface temperatures are warmer and cause more freshening through sea ice bottom melt, (2) lower sea ice cover causes less freshening by limiting the amount of sea ice that is available to melt, and (3) shallower D_{obs} causes more freshening by concentrating the freshwater within a smaller volume.

We examine how these three factors play out by estimating the seasonal mixed-layer freshening in 1975, 2006, and 2007 by integrating equation 4.7 and examining each term separately. That is, we examine the mixed-layer salinity changes due to top melt (S_{top}), mixed-layer salinity changes due to bottom melt (S_{bot}), and their sum

(S_{est}):

$$S_{top}(t) = -\frac{\sigma}{\rho_i L}\int_{t_0}^{t}\frac{A_{obs}F_{atm}}{D_{obs}}dt + S_0 \quad (4.16)$$

$$S_{bot}(t) = -\frac{\sigma}{\rho_i L}\int_{t_0}^{t}\frac{A_{obs}k\delta T_{obs}}{D_{obs}}dt + S_0. \quad (4.17)$$

Figure 4.8a shows the mixed-layer freshening due to sea ice top melt (S_{top}) in 1975, 2006, and 2007. S_{top} is a function of the observed sea ice concentration (A_{obs}) and the observed mixed-layer depth (D_{obs}). We find that the influence of the shallower mixed layers is somewhat larger than the influence of lower sea ice concentration, causing seasonal mixed-layer freshening due to top melt to increase moderately with time. Note that this is in contrast to changes in the freshwater content due to top melt, which decreased with time (Figure 4.7a).

Figure 4.8b shows the mixed-layer freshening due to sea ice bottom melt (S_{bot}) in 1975, 2006, and 2007. S_{bot} is a function of the observed mixed-layer temperature anomaly from freezing (δT_{obs}) in addition to the observed mixed-layer depth (D_{obs}) and sea ice concentration (A_{obs}). Variations in δT_{obs}, which do not influence S_{top}, cause S_{bot} to increase from one year to the next significantly more than S_{top} (compare Figure 4.8a to Figure 4.8b).

Compared to freshwater content from sea ice melt, mixed-layer freshening varies from one year to the next significantly more than sea ice melt (compare Fig. 4.8c and 4.7c). Quantitatively, our estimate suggests that the mixed layer undergoes approximately 3 times more freshening in 2007 and two times more freshening in 2006 compared to 1975 (Table 1), similar to the observations (Figure 4.4). This is several times larger than the change in the freshwater content from sea ice melt between 1975, 2006, and 2007 (Table 1). This suggests that mixed-layer shoaling, rather than increased freshwater input from sea ice melt, drives changes to seasonal mixed-layer

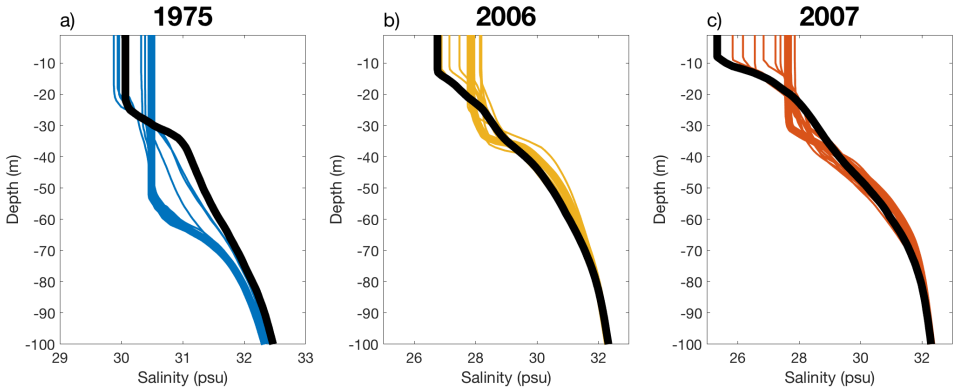

Figure 4.9: 10-day mean salinity profile during the melt season in (a) 1975, (b) 2006, and (c) 2007. Thick colored lines indicate first profile of the melt season, and thick black lines indicate the last profile of the melt season (see Section 5a for details).

freshening.

4.5 Discussion

4.5.1 Observed Salinity Profiles

The framework presented here describes a simplified scenario in which all the freshwater input from sea ice melt is stored locally within the mixed layer (i.e. the contribution from horizontal and vertical advection is neglected). Here, we aim to qualitatively assess this possibility by examining the observed evolution of the salinity profiles during the melt season in 1975, 2006, and 2007. A more quantitative analysis of the mixed layer dynamics and the influence of sea ice bottom melt is carried out in a companion paper (Rosenblum et al., in prep).

Here, we linearly interpolate each observed profile onto a 1 m resolution grid that runs from the surface to a depth of 70 meters. The shallowest recorded depths vary depending on the profiles. For illustrative purposes, values shallower than the mixed-layer depth are assigned a salinity that is equivalent to the mixed-layer salinity (See Section 2 for details). Figure 4.9 shows the 10-day average profiles computed

during the melt season in 1975, 2006, and 2007, with the first profile shown as a thick colored line and last profile shown in a thick black line.

In general, Figure 4.9 indicates that freshening mainly occurs within the summer mixed layer, while the remnant winter mixed layer appears to become progressively saltier, and the values deeper than the winter mixed layer remain fairly constant. This is consistent with the more comprehensive analysis presented by Toole *et al.* (2010), who found that mixed-layer freshening creates a strongly stratified seasonal halocline that inhibits mixed-layer deepening and therefore limits the influence of entrainment of the underlying water during the melt season. It is also consistent with Peralta-Ferriz & Woodgate (2015*a*), who found that approximately 70% of the freshwater change over the past 30 years occurred above the winter mixed-layer depth. Together this suggests that our idealized framework, despite its simplicity, may be capturing leading order processes controlling seasonal mixed-layer freshening.

4.5.2 Comparisons with other studies

The results using this idealized framework are consistent with a number of previous observational studies. First, similar to Maykut & McPhee (1995), we estimate an ocean heat flux to the sea ice of approximately 10-20 W m^{-2} in 1975. Both estimates use AIDJEX data, but our estimate assumes that u_* is a constant. Second we find that our estimated changes in sea ice thickness due to bottom melt are roughly consistent with observations from Ice Mass Balance Buoys (IMBs) during the same time period in this region. Perovich & Richter-Menge (2015) reported 34 cm of bottom melt in 1975 compared to our estimate of 42 cm. Timmermans (2015) report approximately 60 cm and 80 cm of bottom melt in 2006 and 2007, respectively (their Figure 2). This is similar to our estimate of 58 cm and 96 cm in 2006 and 2007, respectively. We note that our values for ocean heat flux and sea ice bottom melt

are significantly smaller than those reported by Toole *et al.* (2010), using data in a similar region in 2007. However, Timmermans (2015) showed that these values are anomalously large compared to other observations in that region. Third, we estimate a sea ice thickness change due to top melt of 60 cm, which is consistent with the observed 1959-2014 average in the region of 57 $\pm$ 19 cm. (Perovich & Richter-Menge, 2015).

Our results are also consistent with one previous study that used a regional ice-ocean model to examine the heat and salt budget during the summer in the Pacific sector of the Arctic during 2000-2007 (Steele *et al.*, 2010). They showed that top melt tends to have the largest influence on sea ice melt early in the melt season, while bottom melt tends to have the largest influence toward the end of the melt season, similar to our results (Figures 4.5b,4.6b). Further, they found that 2007 differs from previous years because of early sea ice retreat, which causes enhanced bottom melt. Yet, similar to our results (Figure 4.7c), they find that this has only a modest effect of the freshwater flux from sea ice melt in the region. Similarly, Yamamoto-Kawai *et al.* (2009) found the freshwater content from sea ice melt over the top 50 meters in the Canada Basin to remain relatively constant (i.e. no discernible trend in time) between 1987 and 2003-2007.

In terms of mixed-layer evolution, our analysis is consistent with previous studies that used observations from the Canada Basin that spanned several decades (Peralta-Ferriz & Woodgate, 2015*a*; Yamamoto-Kawai *et al.*, 2009), a one-dimensional model using AIDJEX data (Lemke & Manley, 1984), and a one-dimensional model using ITP data (Toole *et al.*, 2010). That is, we find that (1) the mixed-layer salinity evolution during the melt season can be roughly explained by sea melt alone (Peralta-Ferriz & Woodgate, 2015*a*; Lemke & Manley, 1984; Toole *et al.*, 2010) and (2) the mixed-layer depth is very sensitive to small changes in the buoyancy flux (Peralta-

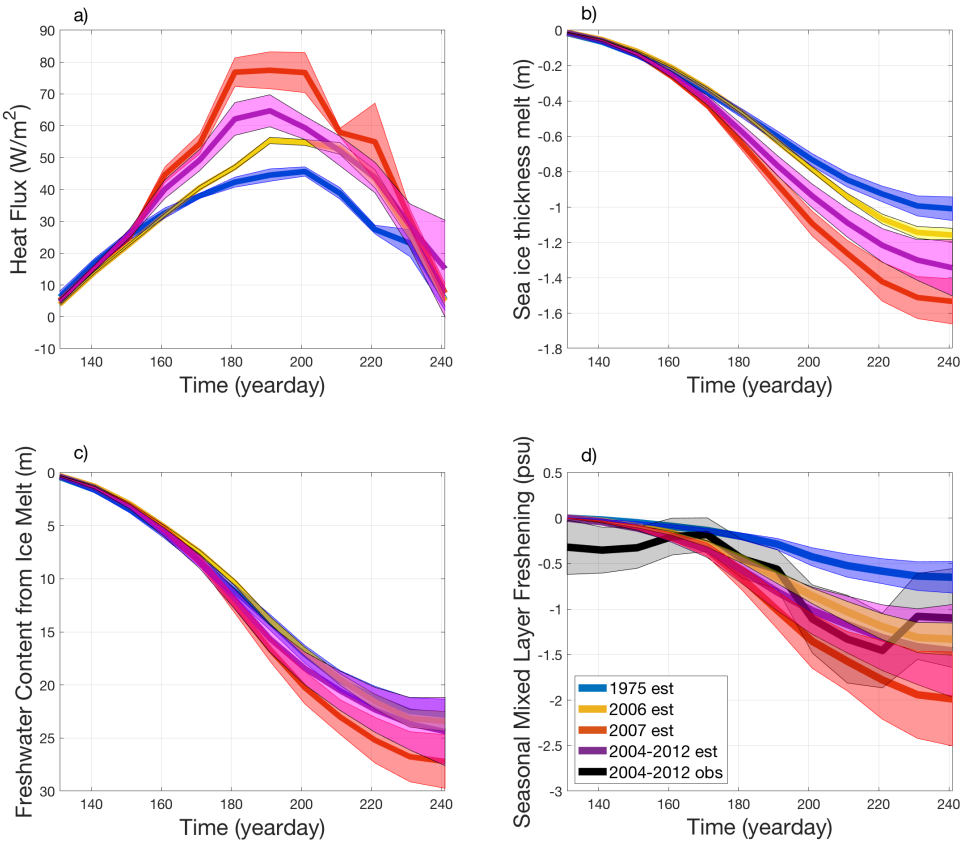

Figure 4.10: 1975 (blue), 2006 (yellow), 2007 (red), and 2004-2012 (magenta) estimated heat flux, estimated sea ice thickness, estimated freshwater content, and estimated seasonal mixed-layer freshening as well as the observed 2004-2012 mixed-layer freshening (black). Solid lines indicate the mean, and shading indicates one standard error.

Ferriz & Woodgate, 2015*a*; Yamamoto-Kawai *et al.*, 2009).

4.5.3 Sensitivity to Methods

The aim of Chapter 4 is to better understand fundamental processes controlling decadal changes to the surface mixed layer in the Canada Basin. However, we have focused on 3 years of data, and it is difficult to discern the extent to which these years are representative of typical processes controlling mixed-layer freshening in this region over the past few decades. Further, our results rely on the observed sea ice

concentration and mixed-layer depth, which depend on our method for computing these quantities. In the Supplementary Material, we examine the sensitivity of our results to these choices by repeating the analysis using different observations and by using different methods to estimate the observed sea ice concentration and mixed-layer depth.

First, we repeat our analysis in using the basin average sea ice concentration (defined as the area bounded between 72N, 81N, 130W, and 155W) in 1975, 2006, and 2007 (Figures C.4,C.5). A comparison of the resulting sea ice concentration evolution from the different methods is shown in Figure C.6. Second, we repeat our analysis by defining the mixed-layer depth as the shallowest depth at which the mixed-layer density exceeds 0.1 kg m^{-3} from the surface, following Toole *et al.* (2010) (Figure C.7,C.8). Third, we repeat our analysis using years 2008, 2011, and the entire ITP dataset which spans 2004-2012 (Figures 4.10, C.9,C.10).

In each case, our main results hold. That is, compared to 1975, more recent years have: (1) a mixed layer that freshens 2-4 times more during the melt season than in 1975, (2) higher mixed-layer temperatures that raise the estimated heat flux toward the sea ice, (3) a similar amount of estimated freshwater flux from sea ice melt. Together, these results suggest that shallower mixed-layer depths could explain why recent years undergo more mixed-layer freshening than 1975 did.

The extent to which the estimated mixed-layer freshening is consistent with the observed mixed-layer freshening is somewhat more sensitive to the methods. We find that the estimate is consistent with the observations in 1975 and 2006, regardless of the method used to compute the mixed-layer depth and the sea ice concentration. However, the 2007 estimate is less consistent with the observations in each case. This is likely because there is more freshwater trapped at the surface in 2007 and because the basin average sea ice concentration varies more significantly during the melt season

in 2007 compared to the other years (Figure C.6). The estimate is consistent with the observations in 2008 and the 2004-2012 average, but not in 2011 (Figure 4.10, Figure C.9-C.10). This is likely due to the large spatial variability exhibited in the ITP dataset for each of the years (Figure C.11-C.15), implying that the consistency between the observed and estimated freshening can depend significantly on the the location of the ITPs during the melt season.

4.5.4 Additional points

This analysis has several potential limitations. First, we have neglected important factors that contribute to the freshwater input in this region, including horizontal advection of freshwater and freshwater input from river runoff, which are likely to influence seasonal mixed-layer salinity evolution (Peralta-Ferriz & Woodgate, 2015*a*), particularly in 2007 (Yamamoto-Kawai *et al.*, 2009; Proshutinsky *et al.*, 2009). Second, the ITP instrument system is likely to have mixed-layer depths that are biased too deep in the summer (Toole *et al.*, 2010) and may incorrectly indicate that mixed-layer shoaling occurs as much as two weeks later than in reality (Gallaher *et al.*, 2017). Hence, these factors could potentially lead us to underestimate the influence of mixed-layer dynamics on mixed-layer freshening. Third, this idealized representation of the mixed-layer salinity evolution does not include entrainment, which appears to be an important component controlling mixed-layer salinity evolution toward the beginning of the melt season (Fig. 5.2, 4.4). Fourth, the friction velocity (u_*) was set to a constant throughout the analysis, though it is possible that this factor may decrease with time as a result of changing sea ice conditions or that it varies significantly in both space and time (Cole *et al.*, 2017).

4.6 Summary

Over the past few decades, the Arctic sea ice cover has receded dramatically in the Canada Basin. This reduction in sea ice has coincided with a significant trend toward warmer, fresher, and shallower mixed layers (Peralta-Ferriz & Woodgate, 2015*a*) (e.g., Fig. 4.2). Here, we have presented an idealized model that allows us to examine the relative contributions of warmer mixed layers (which increase sea ice bottom melt), lower sea ice cover (which limits the amount of available to melt), and shallower mixed layers (which concentrate freshwater input over a smaller volume) on mixed-layer freshening during the melt season in 1975, 2006, and 2007.

We find that our idealized framework provides an estimate of the seasonal mixed-layer freshening that is roughly consistent with the observations (Fig. 4.4, Table 2). Our estimate suggests that while ocean-driven heat flux to the sea ice has increased significantly in 2006 and 2007 compared to 1975 (Fig. 4.5, Table1), the amount of ice available to melt has also decreased significantly (Fig 4.2a). As a result, we find only very modest changes in the freshwater flux due to sea ice melt (Fig. 4.7c). By contrast, we estimate that the mixed layer freshens 3 times as much in 2007 as in 1975 and twice as much in 2006 as in 1975, similar to the observations (Fig. 4.8, Table 1). We suggest that this is mainly due to the shallower mixed layers (Fig. 4.2d), which coincide with a more strongly stratified upper ocean (Fig. 4.9). That is, we suggest that changes to the upper-ocean structure cause similar levels of freshwater input from sea ice melt to be concentrated over a much smaller volume, which ultimately drives enhanced seasonal mixed layer freshening. We arrive at similar results when comparing 1975 to the 2004-2012 average (Figure 4.10). This suggest that, while observational limitations make it difficult to draw significant conclusions regarding decadal changes to the seasonal processes, changes the upper-ocean structure may be driving changes to seasonal mixed-layer freshening in the Canada Basin.

4.A Method for data selection

For each 10-day interval during each of the 5 years (1975, 2006-2008, and 2011), we investigate the number of observations, the average distance between points, and the average drift, which we define as the change in the mean location in January 1 as a function of time (Figure C.2). Focusing on the ITP dataset, both the number of observations and the average distance between observations can vary substantially throughout the year, particularly during the melt season, when new ITPs are deployed and older ITPs are lost as a result of melting ice floes. The average and standard deviation during May-September are shown in Table S1.

First, we find that while each of the four years have a similar number of observations, the average distance between observations is approximately twice as large in 2008 compared with 2006-2007. Second, we find that the ITPs in 2011 drift approximately twice as much as in 2006-2007, as a result of an increase in the number of instruments toward the end of the melt season. Third, we find that reducing the ITP dataset to only ITPs that sample throughout the melt season would roughly halve the amount of data available in 2008 and 2011, would eliminate 2007 from the analysis because it would no longer have continuous data throughout the melt season, would cause the amount of drift to increase in 2006 and 2008, and would still result in significantly larger distances between observations in 2008 compared to 2006. We therefore focus our analysis on all the available ITP observations in 2006 and 2007 in the main text.

4.B Standard Error

We found a that the mixed layer and sea ice evolution exhibited a decorrelation scale of 2. Based on this, for each 10-day bin, we computed the effective degrees of

freedom as the number of measurements divided by twice the number of instruments. The standard error for the observed sea ice concentration and mixed layer salinity, depth, and temperature anomaly from freezing for each 10-day interval was given by the standard deviation divided by the square root of the effective degrees of freedom for that bin. Standard errors for the model estimates are then computed by error propagation of the observed variables.

Acknowledgements

This work was supported a National Science Foundation Graduate Research Fellowship and a Chateaubriand Research Fellowship.

Chapter Four, in part, is currently being prepared for submission for publication of the material. Rosenblum, E., Gille, S., Lique, C. The dissertation author was the primary investigator and author of this paper.

Chapter 5

Factors controlling seasonal halocline stratification in the Canada Basin during 1975, 2006, and 2007

5.1 Introduction

Upper ocean heat storage in the Canada Basin has undergone dramatic changes over the past few decades as a result of the reduced sea ice cover. In particular, the heat stored in the Near-Surface Temperature Maximum (NSTM) layer has increased, as has the strength of the seasonal halocline stratification (Jackson *et al.*, 2010, 2011; Steele *et al.*, 2011; Carmack *et al.*, 2015; Gallaher *et al.*, 2017, 2016). The increase in seasonal halocline stratification inhibits mixed-layer deepening (Peralta-Ferriz & Woodgate, 2015*a*; Toole *et al.*, 2010) and has been suggested to, in part, explain why the NSTM has been able to survive into the fall and winter in recent years (Jackson

et al., 2010, 2011; Steele *et al.*, 2011; Carmack *et al.*, 2015; Gallaher *et al.*, 2017, 2016). Surface freshening trends, primarily driven by sea ice melt, are expected to be the main component driving the increase in stratification (Jackson *et al.*, 2010, 2011; Steele *et al.*, 2011; Carmack *et al.*, 2015; Peralta-Ferriz & Woodgate, 2015*a*; Yamamoto-Kawai *et al.*, 2009).

However, the kinetic energy input from the wind is also expected to have a significant influence on mixed-layer evolution and seasonal halocline formation (Kraus & Turner, 1967; Lemke & Manley, 1984; Peralta-Ferriz & Woodgate, 2015*a*). In sea ice-covered oceans, the wind imparts momentum to the sea ice, which in turn can mix the underlying ocean through keel stirring. How the effectiveness of keel-stirring changes under different sea ice conditions is not well-understood due to observational limitations. However previous modeling and observational studies suggest that the momentum transfer to the underlying ocean may decrease in areas that are transitioning from multi-year sea ice cover to first-year sea ice cover, as in the Canada Basin (Martin *et al.*, 2016; McPhee, 2012; Cole *et al.*, 2017). In particular, sea ice roughness is expected to decrease in first-year ice as a result of less ridging, that can develop over the course of multiple winters (Martin *et al.*, 2016; McPhee, 2012). Further, increased underlying stratification can decrease turbulent length scales, allowing sea ice motion to cause less momentum exchange with the ocean (McPhee, 2012). Based on these ideas, McPhee (2012) predicts that a transition from multi-year ice to first-year ice can cause the sea ice to exert approximately half as much drag on the underlying ocean. Somewhat consistent with this prediction, a recent study examining momentum transfer in the Canada Basin in 2014 observed frictional velocities that were approximately half the magnitude of those observed in 1975 (Cole *et al.*, 2017).

Here, we examine the relative influence of the freshwater flux and kinetic energy input on mixed-layer evolution and seasonal halocline formation in the Canada

Basin during 1975, 2006, and 2007. In 1975, the heat stored in the NSTM was small and quickly eroded following its formation (Maykut & McPhee, 1995). The NSTM was first observed to survive for an entire year following the summer of 2007 (Jackson *et al.*, 2010; Toole *et al.*, 2010; Steele *et al.*, 2011; Carmack *et al.*, 2015). This stored heat caused an estimated 25% decrease in sea ice thickness in the following winter from entrainment of the NSTM due to brine rejection (Jackson *et al.*, 2010; Steele *et al.*, 2011; Timmermans, 2015). Here, we aim to examine what factors cause the difference in seasonal halocline stratification that resulted in this change in NSTM heat storage.

The methods are presented in Section 5.2, and observations of the mixed layer and seasonal pycnocline in 1975, 2006, and 2007 are presented in Section 5.3. In Section 5.4, we quantify the strength of the seasonal halocline during each of the three years by estimating the change potential energy required to erode the seasonal halocline (ΔPE). Additionally, we examine the extent to which variations in the ΔPE are due to differences in the mixed-layer evolution alone. In Section 5.5 we present a simplified framework for examining the relative influence of freshwater flux and kinetic energy input on the mixed layer evolution and seasonal halocline formation during the melt season. We test this framework against the observations in Section 5.6. In Section 5.7, we use the framework to examine the possibility that either changes in the kinetic energy or changes in the freshwater flux alone could explain differences in the mixed-layer and ΔPE evolution in 1975, 2006, and 2007. These results are discussed in Section 5.8 and summarized in Section 5.9.

5.2 Methods

We examine ocean mixed-layer and sea ice observations from 1975, 2006, and 2007, using data from the Ice-Tethered Profiler (ITP) instrument system (Krishfield

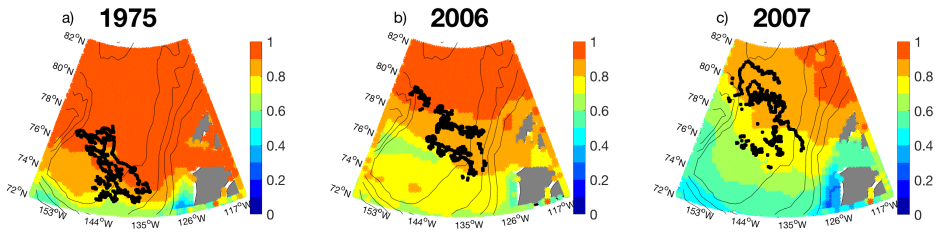

Figure 5.1: Location of ocean observations during (a) 1975, (b) 2006, and (c) 2007 in the Canada Basin. The average summer (July-September) sea ice concentration for each year is also shown. Note that the 1979 sea ice concentration is shown instead of 1975, due to data restrictions (see Section 2 for details).

et al., 2008), the AIDJEX program (Lemke & Manley, 1984), and the daily sea ice concentration from the National Snow and Ice Data Center Sea Ice Index from the satellite passive microwave measurements (Fetterer *et al.*, 2002). Details on the observations, methods, and data choices are outlined in Chapter 4, some of which are repeated here for completeness. Satellite passive microwave measurements are only available starting in 1979. We, therefore, use an estimate of the sea ice concentration from the AIDJEX ice camps (Maykut & McPhee, 1995).

We examine all available level 3 processed ITP data in 2006 and 2007 from the Canada Basin, which we define as the region bounded by 72N, 84N, 130W, and 155W, following Peralta-Ferriz & Woodgate (2015*a*) and all available AIDJEX ocean data from April 1975 through April 1976 (since the focus of the analysis will be on the melt season, we will refer to observations from this time period as data from 1975). The mixed-layer depth in each profile is determined by the depth at which the the density change from the surface exceeds 0.1 kg/m^3, following Peralta-Ferriz & Woodgate (2015*a*). Each salinity profile is interpolated onto a 1-meter grid. Additionally, because the profiles begin at different depths, all values shallower than the mixed-layer depth are given a value equivalent to the computed mixed-layer salinity and

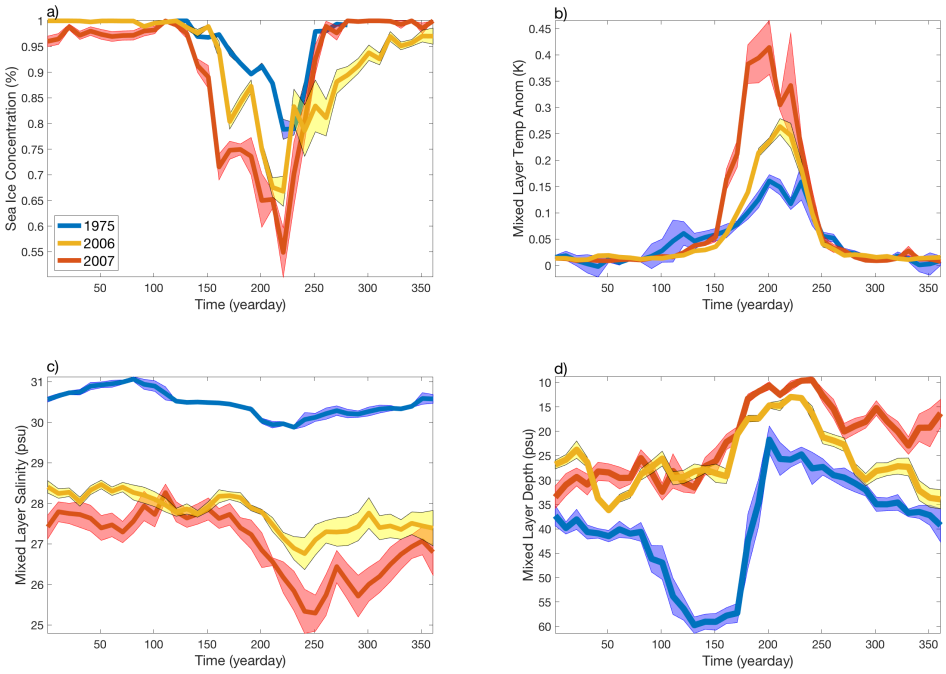

Figure 5.2: Seasonal evolution of the (a) sea ice concentration, (b) mixed layer temperature anomaly from freezing, (c) mixed layer salinity, and (d) mixed layer depth in 1975 (blue), 2006 (yellow), and 2007 (red). Thick lines indicate the 10-day mean and the shading indicates the standard error.

mixed-layer temperature. Figure 5.1 shows the location of the 1261 profiles in 1975, the 2613 profiles in 2006, and the 1746 profiles in 2007, following data processing.

5.3 Observations

In the Canada Basin, observations indicate that surface forcing is the primary driver of the ocean mixed-layer evolution (Peralta-Ferriz & Woodgate, 2015*b*; Lemke & Manley, 1984; Toole *et al.*, 2010). During the fall and winter, the mixed layer cools, and brine rejection from sea ice formation increases upper-ocean salt content, causing convection and mixed-layer deepening. Conversely, spring and summer sea ice melt allows solar heating to raise the mixed-layer temperature and adds fresh water to the upper ocean, causing the mixed layer to shoal.

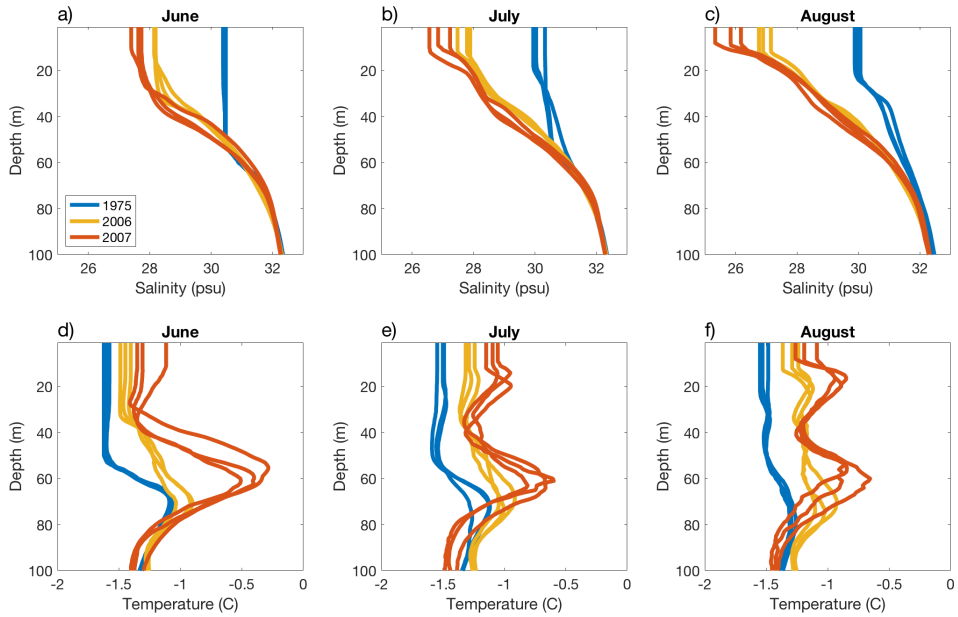

Figure 5.3: Observed 10-day mean salinity and temperature profiles for (a,d) June, (b,e) July, and (c,f) August during 1975 (blue), 2006 (yellow), and 2007 (red).

Consistent with this description, we find a clear seasonal cycle in sea ice concentration, mixed-layer temperature anomaly from freezing (where the freezing point is a function of the mixed-layer salinity), mixed layer salinity, and mixed layer depth during 1975, 2006, and 2007 (Figure 5.2). Low sea ice concentrations during the spring and summer months correspond to warmer, fresher, and shallower mixed layers, while high sea ice concentrations during the fall and winter correspond to cooler, saltier and deeper mixed layers. The differences between the three years in Figure 5.2b-d also reveal anecdotal evidence of the decadal trends toward warmer, fresher, and shallower mixed layers reported by Peralta-Ferriz & Woodgate (2015*b*).

As the mixed layer shoals and freshens, the seasonal halocline and the NSTM are formed (i.e., the structure below the mixed layer that is shallower than the winter mixed layer depth). To examine how differences in the mixed-layer evolution are reflected in the seasonal halocline and the NSTM, we examine the 10-day averaged salinity and temperature profiles during the summer months in 1975, 2006, and 2007

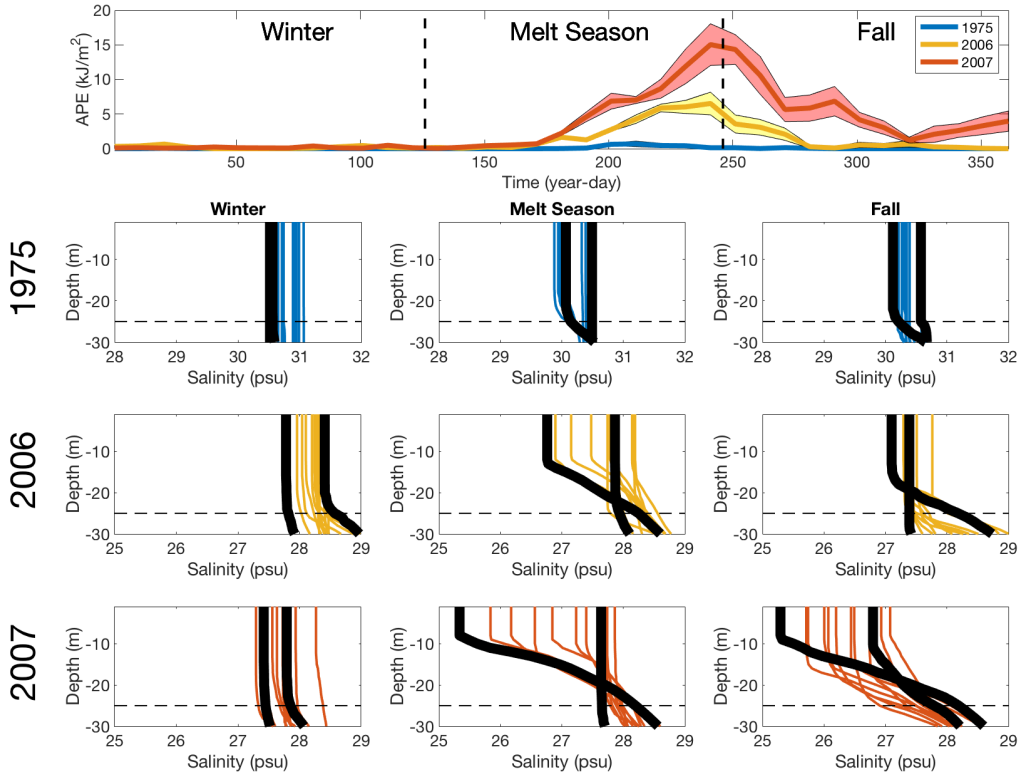

Figure 5.4: Observed change in potential energy to deepen the mixed layer to 25 meters (ΔPE) and associated haloclines in 1975 (blue), 2006 (yellow), and 2007 (red). Thick black lines indicate the first and last profile of each season, as defined in the top panel, corresponding to black astrisk marks. A horizontal black line is also indicated at the 25 meter mark, to illustrate the depth range over which the ΔPE is computed.

(Figure 5.3). We find that the NSTM is warmer and the seasonal halocline is more stratified in 2006 and 2007. This is consistent with previous observational studies that found longer-term trends toward a warmer NSTM and a more stratified seasonal halocline (Jackson *et al.*, 2010, 2011; Peralta-Ferriz & Woodgate, 2015*b*).

5.4 Influence of Seasonal Halocline Stratification

We estimate the extent to which the seasonal halocline stratification inhibits mixed-layer deepening and hence NSTM erosion during the year by computing the

change in potential energy that would occur if the mixed layer convectively deepened to 25 meters. That is, we compute

$$\Delta PE = \int_{25m} (\Delta\rho(z))gz \cdot dz, \tag{5.1}$$

where $\Delta\rho(z)$ is the observed potential density profile referenced to the surface, subtracted from the potential density profile that would occur if the mixed layer convected to 25 meters. We choose to compute ΔPE over the top 25 meters, because it is shallower than the winter mixed-layer depth and deeper than the summer mixed-layer depth in each of the three years (Figure 5.2). Therefore, choosing this depth allows us to exclude the influence of increased stratification below this depth, which is unlikely to inhibit mixed layer deepening and likely reflects decadal surface freshening rather than seasonal processes. Any year-to-year differences in ΔPE should, therefore, reflect the strength of the seasonal halocline in this depth range for each of the three years.

This convective mixed-layer deepening can occur as a result of either an increase in the surface density or an increase in the kinetic energy. We expect both factors to be important in the fall and winter, when sea ice formation adds density to the surface through brine rejection. IN CONTRAST, during the melt season, we expect that mixed layer deepening would mainly occur by added kinetic energy. Therefore, during the melt season, ΔPE represents the minimum kinetic energy required to convectively deepen the mixed layer to 25m (i.e. if dissipation were neglected and energy were conserved).

Figure 5.4 shows the 10-day averaged ΔPE and the corresponding 10-day average seasonal halocline throughout the year during 1975, 2006, and 2007. The mixed layer is approximately 25 meters or deeper during most of the year, causing the ΔPE to remain small ($< 1\text{kJ/m}^2$). The mixed layer shoals during the melt

season, and the seasonal pycnocline is established, causing the ΔPE to increase. Finally, roughly coinciding with the onset of freezing, the mixed layer deepens and erodes the seasonal pycnocline, causing the ΔPE to decrease.

We arrive at the same result if we assume that the profiles are held at freezing temperatures, implying that the seasonal pycnocline is only a function of salinity. This implies that the density in the upper 25m is mainly controlled by variations in salinity, and that the ΔPE is controlled by the evolution of the seasonal halocline and are not influenced by the NSTM (Figure D.1). Based on this, we focus the rest of our analysis on how the ΔPE evolves in response to the evolution of the seasonal halocline.

We consider differences in the ΔPE evolution in 1975, 2006, and 2007. First, we find that the maximum ΔPE differs substantially between the three years. The maximum ΔPE is nearly ten times larger in 2006 compared to 1975 (6.6 vs. 0.7 kJ/m^2), and the maximum ΔPE in 2007 is more than twice as large as in 2006 (15.1 vs. 6.6 kJ/m^2). Second, we find that years with a larger ΔPE have a seasonal halocline for a longer period of time (i.e., the ΔPE remains larger than 1 kJ/m^2). This is consistent with previous studies which found that the strengthened seasonal halocline appears to strongly impede entrainment during the melt season in recent years (Jackson *et al.*, 2010; Toole *et al.*, 2010). Moreover, this implies that years with a more stratified halocline also have an NSTM that survives for a more extended period of time, consistent with previous studies (Jackson *et al.*, 2010; Steele *et al.*, 2011). These results suggest that understanding differences in the ΔPE evolution during the melt season may help explain why, in recent years in the Canada Basin, the NSTM can survive well into the fall and winter (Jackson *et al.*, 2010; Steele *et al.*, 2011).

Lastly, we can roughly estimate the amount of energy necessary to erode the

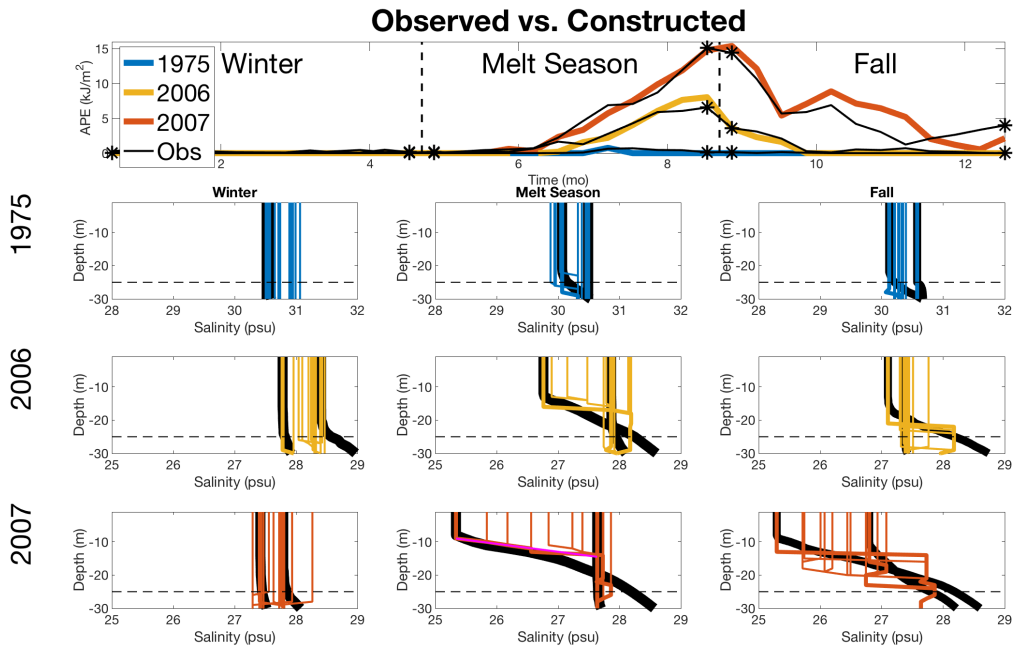

Figure 5.5: As in Figure 5.4, where thin black lines represent the observations and colored lines represent the constructed halocline and associated available potential energy.

halocline to 25m during the melt season by computing the time rate of change of the ΔPE (d(ΔPE)/dt) during seasonal halocline formation (i.e., when the ΔPE increases). We find that this value is between 10^{-5} and 10^{-4} W/m^2 throughout the melt season in 2006 and 2007, and 10^{-7} W/m^2 in 1975. For comparison, Lemke & Manley (1984) estimated that the kinetic energy input from the wind was on the order of 10^{-7} W/m^2 in 1975. This suggests that the kinetic energy input would have had to increase by 2-3 orders of magnitude from 1975 to cause entrainment.

5.4.1 Influence of surface processes on ΔPE

The mixed layer is relatively isolated from the influence of underlying water masses on seasonal timescales as a result of the strongly stratified permanent halocline (Toole *et al.*, 2010). We, therefore, expect seasonal mixed-layer evolution to be mainly influenced by surface processes. Further, the seasonal halocline is formed when the

mixed layer shoals, causing signatures of surface processes that occur during mixed layer shoaling to be imprinted onto the seasonal pycnocline (Kraus & Turner, 1967; Turner, 1967). That is, the seasonal halocline could be considered a structure made up of remnant mixed layers that become altered by various processes. Here, we examine the extent to which such one-dimensional processes forced by the surface alone could explain variations in the observed seasonal halocline and the associated ΔPE. Under such a scenario, the mixed-layer depth and mixed-layer salinity evolution would be directly related to the structure of the seasonal halocline. We, therefore, construct a seasonal halocline made entirely of remnant mixed layers and compare the resulting ΔPE to the observations.

Figures D.2-D.4 illustrate how this idealized one-dimensional pycnocline is constructed using the observed mixed-layer depth and mixed-layer salinity in 1975, 2006, and 2007. The first observations at the beginning of the year (blue dots) provide our initial conditions, characterized by a well-mixed layer with a depth and salinity that are consistent with the observations from that period (black line, Figures D.2-D.4c). Each subsequent observation of mixed-layer salinity and mixed-layer depth is then used to evolve the seasonal pycnocline by setting the properties of the next mixed layer at a fixed increment in time. If the mixed layer is shallower than the previous mixed layer, the mixed-layer properties that are deeper than the new mixed layer are preserved below the new mixed layer and become part of the seasonal pycnocline. If the mixed layer is deeper than the previous mixed layer than the memory of the previous mixed layers is effectively erased down to the new mixed-layer depth. This process continues until we have constructed a seasonal pycnocline that corresponds to the observations of each 10-day averaged mixed layer during the year.

The resulting 10-day mean, constructed, seasonal haloclines for 1975, 2006, and 2007 are shown in Figure 5.5. Using these constructed one-dimensional seasonal

haloclines, we examine the resulting ΔPE during the same time period compared to the observations (compare black and colored lines). We find that the constructed ΔPE agrees well with the observations, perhaps due to the extent to which the observed winter mixed layer is preserved at depth, consistent with our constructed seasonal pycnocline. Although, there are other possible mechanisms, these results suggest that surface forcing acting on a one-dimensional system is consistent with the observed patterns of seasonal halocline evolution.

5.5 Idealized Framework

The results above suggest that understanding differences in the mixed-layer depth and mixed-layer salinity evolution may explain differences in the ΔPE in 1975, 2006, and 2007. Motivated by this, we present an idealized framework aimed at examining factors controlling year-to-year variations in the mixed-layer depth and mixed-layer salinity evolution. Specifically, we examine how the freshwater flux and the kinetic energy input influence mixed-layer evolution by adopting a one-dimensional model of the seasonal thermocline in mid-latitudes (Kraus & Turner, 1967) to mixed-layer evolution and seasonal halocline formation in the Canada Basin

5.5.1 1D model of seasonal mixed-layer evolution

Kraus & Turner (1967) consider an idealized one-dimensional system driven by solar heating and wind. During the formation of the seasonal thermocline, they assume that the mixed layer mainly shoals or remains constant and that entrainment can, therefore, be neglected. That is, they neglect background stratification during the spring and summer, as its main function would be to inhibit entrainment. Additionally, they neglect dissipation and consider an energy balance between the kinetic

energy flux from the wind (W) and the potential energy input driven by the surface mass flux (Φ) from solar heating. Based on this, the governing equations of their model during seasonal pycnocline formation are:

$$D = \frac{2W}{g\Phi} \tag{5.2}$$

$$D\frac{d\rho}{dt} = \Phi, \tag{5.3}$$

where ρ is the mixed-layer density.

These equations can be adapted to describe how the mixed layer evolves in the Canada Basin below Arctic sea ice by assuming that the mixed-layer density is driven by salinity, which we find to be a good assumption in 1975, 2006, and 2007 (Fig. D.1). We therefore let $d\rho/dt = \beta dS/dt$ and let $\Phi = \beta\phi$, where ϕ is the surface freshwater flux and β is the haline contraction coefficient. Applying these assumptions to equations 5.2 and 5.3, we find:

$$D = \frac{2W}{g\beta\phi}, \tag{5.4}$$

$$D\frac{dS}{dt} = \phi. \tag{5.5}$$

5.5.2 Influence of mixed-layer evolution on the seasonal halocline

By combining equations 5.2 and 5.3 and taking the time derivative of D, Kraus & Turner (1967) arrive at a set of equations describing the relative evolution of the

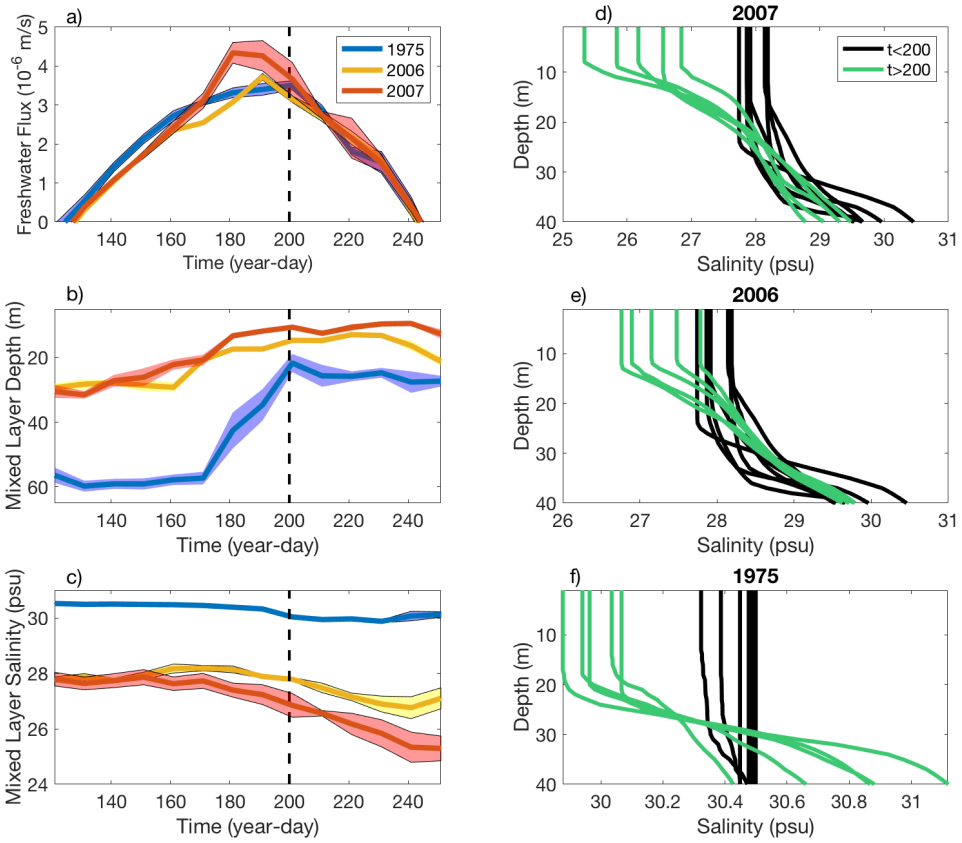

Figure 5.6: (a) Estimated freshwater flux, (b) observed mixed layer depth, (c) observed mixed layer salinity, and (d-f) observed salinity profiles in 1975, 2006, and 2007. (a-c) Shows the surface evolution using observations from 1975 (blue), 2006 (yellow), and 2007 (red). Solid lines represent 10-day means and shadings indicate the standard error, and the vertical dashed line indicates year-day 200 ($t = t_X$). (d-f) Show the associated 10-day averaged salinity profiles for these three years. Profiles that occur before year-day 200 are in black, and profiles that occur after year-day 200 are indicated in green. Note that (b-c) are the same as in Figure 5.2.

mixed-layer depth and the mixed-layer density:

$$\frac{dD}{dt} = D\left(\frac{dW/dt}{W} - \frac{d\Phi/dt}{\Phi}\right), \quad \frac{d\rho}{dt} = \frac{g\Phi^2}{2W}. \tag{5.6}$$

Assuming that $dW/dt/W \ll d\Phi/dt/\Phi$ on seasonal timescales, they suggest that these expressions imply that the mixed-layer depth should evolve in step with the solar heating (directly related to Φ), and therefore reach a minimum during the summer solstice. By contrast, the mixed-layer temperature (directly related to ρ) would be expected to continue increasing well after the summer solstice, as Φ would remain positive through the summer months.

In the case where $dW/dt/W \ll d\phi/dt/\phi$ on seasonal timescales, this would imply a similar relative evolution between mixed-layer salinity and mixed-layer depth in the polar regions. That is, this would imply that the mixed-layer depth will evolve in phase with the freshwater flux, and would, therefore, reach its shallowest value when the freshwater flux reaches a maximum. The mixed layer can continue freshening throughout the summer as the sea ice continues to melt. This would cause the seasonal halocline stratification to increase substantially after the freshwater flux reaches a maximum.

To test this possibility in the observations, we apply the framework developed in Chapter 4 to estimate the freshwater flux from sea ice melt using the observed mixed-layer temperature anomaly from freezing (δT_{obs}, Figure 5.2b) and the observed sea ice concentration (A_{obs}, Figure 5.2a):

$$\phi_{est} = \frac{\sigma A_{obs}}{\rho_i L}(F_{atm} + k\delta T_{obs}), \tag{5.7}$$

where $\sigma = 20$ psu is the difference between the mixed-layer salinity and the sea ice salinity, $\rho_i = 900\text{kgm}^{-3}$ is the density of sea ice, and $L = 3.3 \cdot 10^5$ J/kg is the latent

heat of fusion of sea ice. $F_{atm} = (1 - \alpha_i)F_0 \cos \omega t - F_{lw,t}$ is the heat flux to the surface of the sea ice, where $\alpha_i = 0.6$ is the sea ice albedo, $F_0 = 200\text{W/m}^2$ is the solar radiation, and $F_{lw,t} = 50\text{W/m}^2$ is a combination of the longwave and turbulent heat flux components. The ocean-driven heat flux is derived following Maykut & McPhee (1995), who set $k = \rho_w c_p c_h u_*$, where $\rho_w = 1026$ kg/m^3 is the density of water, $c_p = 3980$ J/kg is the uniform heat of fusion, $c_h = 0.006$ is the non-dimensional heat transfer coefficient, and $u_* = 0.005$m/s is the frictional velocity. See Chapter 4 for details.

We examine the relative evolution of the estimated freshwater flux (ϕ_{est}), the observed mixed-layer depth, and the observed mixed-layer salinity in 1975, 2006, and 2007 (Figure 5.6a). Qualitatively, we find that the mixed layer shoals mainly during the spring and early summer when the freshwater flux is increasing, and the mixed layer continues to freshen later into the summer, consistent with the scenario described above. We find that the mixed layer in each case has reached its minimum value by approximately year-day 200 (July 19), indicated by the dashed black line. This is slightly later than the estimated maximum freshwater flux, because the timing of halocline formation is expected to align with melt pond drainage rather than sea ice melt (Gallaher *et al.*, 2017).

In the simplified scenario described by the above equations, the seasonal halocline stratification would be driven almost entirely by the freshening that occurs after the mixed layer shoals and before it begins to deepen towards the end of the melt season. To investigate the extent to which this idea is consistent with the observations, we examine the 10-day averaged profiles that occur before $t = 200$ (black lines) compared to the profiles that occur after $t = 200$ (green lines) in 1975, 2006, and 2007. Indeed, Figure 5.6d-f indicates that the majority of the seasonal halocline stratification appears to increase after the mixed layers have shoaled. This effect can

also be seen in the observed ΔPE evolution, where we find that the ΔPE increases at a modest rate before year-day 200, and then more rapidly after this point.

5.5.3 Simplified Equations

This study aims to examine the relative influence of the kinetic energy input (W) and the freshwater flux (ϕ) on mixed-layer and ΔPE evolution. We, therefore, use a simplified representation of the freshwater flux, which in turn gives us a simplified framework that depends only on two parameters that represent the influence of these two factors. Specifically, we represent the freshwater flux evolution as an asymmetric sine wave given by:

$$\phi(t) = \begin{cases} \phi_0 \sin\left(\omega_1(t - t_0)\right), & t_0 \leq t \leq t_x \\ \phi_0 \sin\left(\omega_2(t - t_0 - C)\right), & t_x \leq t \leq t_f, \end{cases}$$

where ϕ_0 is the maximum freshwater flux, t_0 is the beginning of the melt season, t_f is the end of the melt season, t_x is the instant when the mixed-layer depth reaches its shallowest value, which occurs when $\phi = \phi_0$, $\omega_1 = \pi/2(t_x - t_0)^{-1}$, $\omega_2 = \pi/2(t_f - t_x)^{-1}$, and $C = 2t_x - t_f$. Note that this reduces to a regular sine wave in the case that the freshwater flux reaches a maximum halfway through the melt season (i.e. $t_x = (t_f - t_0)/2$).

Equation 5.4 describes the mixed-layer depth evolution as the freshwater flux is increasing (i.e. during $t_0 \leq t \leq t_x$). We make the simplifying assumption that the mixed-layer depth is held at this minimum value throughout the remainder of the melt season (i.e., entrainment is neglected). The resulting mixed-layer depth evolution is then given by:

$$D(t) = \begin{cases} \frac{2W}{g\beta\phi(t)}, & t_0 \leq t \leq t_x \\ \frac{2W}{g\beta\phi_0}, & t_x \leq t \leq t_f. \end{cases}$$

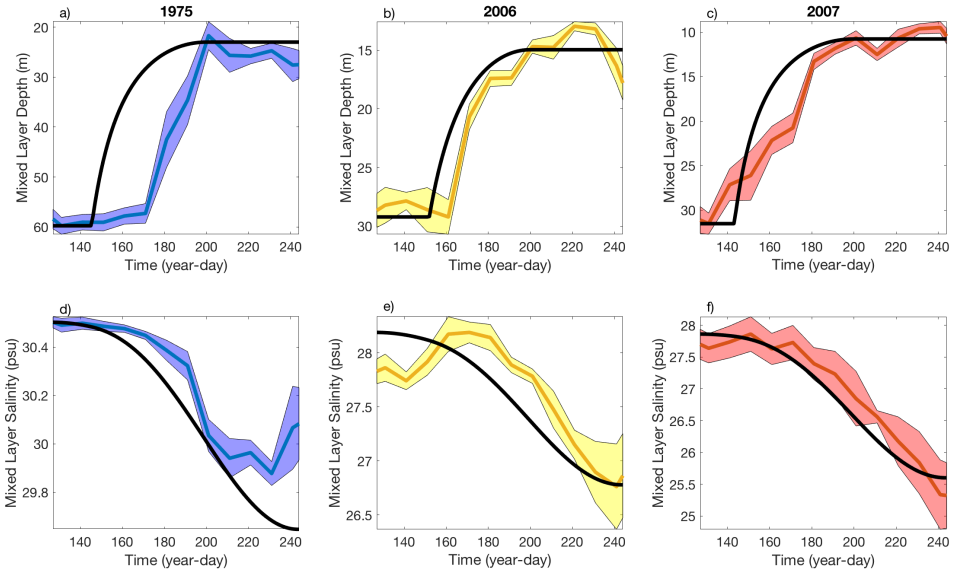

Figure 5.7: Observed (colored lines) and model estimated (black lines) mixed layer evolution. (a-c) Mixed-layer depth evolution and (d-f) mixed-layer salinity evolution during the melt season are shown for (a,d) 1975, (b,e) 2006, and (c,f) 2007. Solid colored lines indicated the observed 10-day average and shadings indicate the standard error.

The salinity evolution is given by integrating equation 5.5 ($S(t) = \int_{t_0}^{t_f} \frac{\phi(t)}{D(t)} \cdot dt + S(t_0)$). Combining this expression for $S(t)$ with the expressions for $\phi(t)$ and $D(t)$ above, we arrive at the following expression for the mixed-layer salinity evolution during the melt season:

$$S(t) = \begin{cases} S(t_0) - \frac{g\beta\phi_0^2}{2W}\left(\frac{t}{2} - \frac{\sin\left(2\omega_1(t-t_0)\right)}{4\omega_1}\right), & t_0 \leq t \leq t_x \\ S(t_0) - \frac{g\beta\phi_0^2}{2W}\left(\frac{t_x}{2} - \frac{\cos\left(\omega_2(t-t_0-C)\right)}{\omega_2}\right), & t_x \leq t \leq t_f. \end{cases}$$

5.6 Comparison with observations

5.6.1 Parameters

We examine the extent to which the mathematical framework above could explain differences in the observed mixed layer and ΔPE evolution in 1975, 2006,

and 2007 (Figures 5.2 and 5.4). To make this comparison, we set the constants to values that are motivated by a series of observations and previous studies.

The constants necessary to compute the freshwater flux (ϕ) are determined based on the estimated freshwater flux (ϕ_{est}, Figure 5.6a), which was shown to result in a seasonal mixed-layer salinity evolution that was consistent with the observations during these three years (see Ch. 4). First, we set the maximum value of the freshwater flux (ϕ_0) for each year to the maximum estimated freshwater flux. Second, we set the start and end of the melt season based on when the estimated freshwater flux reaches zero during these three years. That is, in year-days, we set $t_0 = 127$ (May 7) and $t_f = 244$ (Sept. 1). We set $t_x = 200$ (July 19), based on the earliest instance in which the seasonal halocline has formed (i.e., the mixed layer has shoaled) in all three years, roughly consistent with observations from in-situ data (Gallaher *et al.*, 2016).

The kinetic energy input (W) is tuned by assuming that the observed mixed layer depth at $t = t_X$ ($D_{obs}(t_X)$) and the maximum freshwater flux, ϕ_0, satisfies equation 5.4. That is, we assume that there is a balance of kinetic energy input from the wind and potential energy from the freshwater flux, such that the estimated mixed-layer depth at $t = t_X$ is consistent with the observations. Specifically, we assume that for each year, the relationship between the observed mixed-layer depth, kinetic energy input, and freshwater flux is given by

$$D_{obs}(t_X) = \frac{2W}{g\beta\phi_0}. \tag{5.8}$$

That is, for each year, we set $W = g\beta\phi_0 D_{obs}(t_x)/2$, following this method, we estimate that the kinetic energy input is 3.1, 2.2, and $1.8 \cdot 10^{-7}$ W/m^2 in 1975, 2006, and 2007, respectively. We note that this value for 1975 is consistent with an observational estimate that also used AIDJEX data (Lemke & Manley, 1984). To our

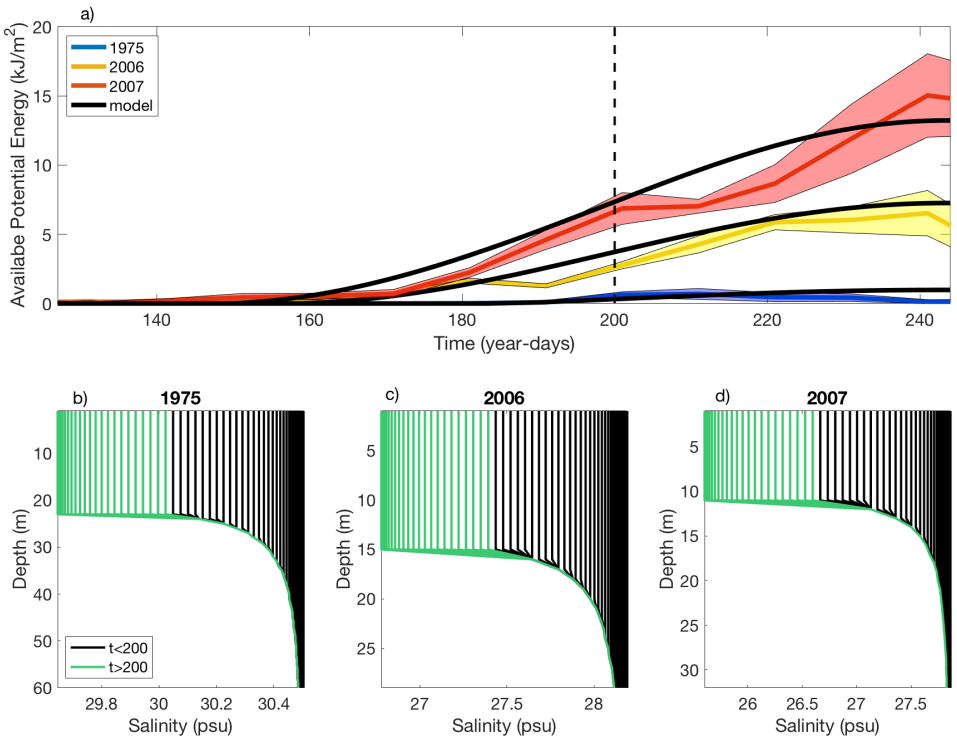

Figure 5.8: (a) Observed and modeled ΔPE evolution during the melt season and (b-d) corresponding modeled halocline profiles. The observed 10-day averaged ΔPE evolution is shown for 1975 (blue), 2006 (yellow), and 2007 (red), with the standard error indicated by colored shadings and the model estimated ΔPE evolution is shown in black. Corresponding salinity profiles for (a) 1975, (b) 2006, and (c) 2007 indicate the profiles that occur before year-day 200 (black) and after year-day 200 (green).

knowledge, there are no observational studies that estimate this bulk parameter for more recent years in this region. However, previous studies suggest that it is indeed reasonable to expect the kinetic energy input to decrease by approximately a factor of 2 (McPhee, 2012).

Lastly, we set the initial conditions for the mixed-layer salinity, and mixed-layer depth to the maximum observed values during the melt season for each year. That is, for each year, we set $D(t_0) = max(D_{obs})$ and $S(t_0) = max(S_{obs})$.

5.6.2 Model Estimates

Using the parameters described above together with the mathematical framework in Section 5.5.3, we estimate the mixed-layer salinity and mixed-layer depth evolution in 1975, 2006, and 2007 (Figure 5.7). Following the same procedure as Section 5.4.1, we use the mixed-layer evolution to construct a seasonal halocline made up of remnant mixed layers (Figure 5.8b-d). From these profiles, we can further estimate the ΔPE during the melt season for each of these years (Figure 5.8a).

Despite the model simplicity, we find that the estimated mixed-layer and ΔPE evolution are relatively consistent with the observations (Figure 5.7). In particular, in each year, the model estimates a ΔPE, and mixed-layer freshening is consistent with the observations when it reaches the maximum value. Though the observations indicate a significant amount of variation that is not captured by the model, this result suggests that this mathematical framework may be enough to explain leading order differences between 1975, 2006, and 2007. We suggest that this is related to the strong influence of the mixed-layer depth on seasonal mixed-layer freshening (Ch. 4), particularly at $t = t_x$ (Figure 5.6, which was used to tune the model).

There are, on the other hand, many processes not represented by the model, which may cause this framework to accurately simulate aspects of the seasonal halocline for the wrong reasons. First, comparing modeled seasonal salinity profiles (Figure 5.8b-d) to the observed salinity profiles (Figure 5.3), we find that there is significantly more mixing that causes the stratification near the surface to decrease and the stratification near the winter mixed-layer depth to increase. We also find that the observations indicate a more rapid shoaling of the mixed layer, coinciding with a more rapid change in the seasonal halocline stratification (compare black and green lines in Figures 5.8b-d) and 5.6). Finally, because seasonal mixed layer freshening is strongly influenced by the mixed-layer depth (Ch. 4), biases in the mixed-layer depth

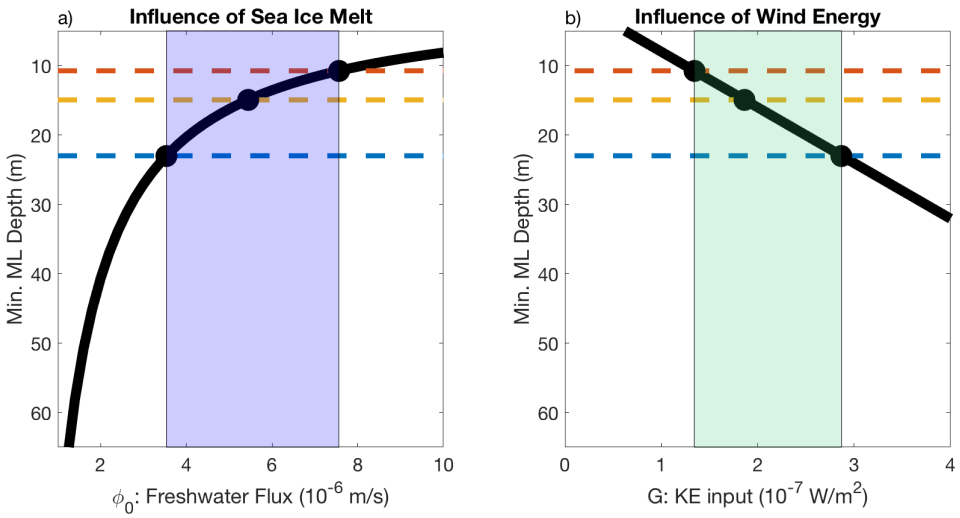

Figure 5.9: (a) The theoretical relationship between the mixed-layer depth and the freshwater flux in the scenario where the kinetic energy is held constant at its estimated 1975 value and (b) the theoretical relationship between the mixed-layer depth and kinetic energy input in the scenario where the freshwater flux is held constant at its 1975 value (black lines). The observed mixed-layer depths for 1975 (blue), 2006 (yellow), and 2007 (red) are indicated by dashed lines. The blue shading in (a) indicates the range of freshwater fluxes necessary to explain the change in mixed-layer depth if the kinetic energy were held fixed at its estimated 1975 value. The green shading in (b) indicates the range of kinetic energy inputs necessary to explain the change in mixed-layer depth if the freshwater flux were held fixed at its estimated 1975 value.

appear to be reflected in the mixed-layer salinity evolution. That is, biases toward shallower mixed layers cause biases toward fresher mixed layers and vice versa.

5.7 The role of freshwater vs wind energy

5.7.1 The influence of freshwater flux

Here, we consider a scenario in which the kinetic energy input is the same as estimated in 1975, and we examine how changes in the freshwater flux alone could influence mixed-layer and ΔPE evolution. As in Section 5.6, we assume that there is an energy balance between the estimated freshwater flux and the kinetic energy input such that the model accurately estimates the mixed-layer depth at $t = t_X$ by satisfying equation 5.4. That is, we assume that in this scenario, the maximum

freshwater flux (ϕ_0) is given by

$$\phi_0 = \frac{2W_{1975}}{g\beta D_{obs}}, \tag{5.9}$$

where W_{1975} is the estimated kinetic energy input in 1975 (see Section 5.6).

Figure 5.9a shows this relationship between ϕ_0 and the mixed-layer depth (black lines), the observed mixed-layer depths at $t = t_X$ during the three years (horizontal dashed lines), and resulting value of ϕ_0 (x-coordinate of the black dots). This relationship demonstrates that for shallower mixed layers, changes in the freshwater flux have a weaker influence on the mixed-layer depth. As a result, we estimate that a 50% increase in ϕ_0 is necessary to explain both the $\sim$16m difference between the mixed-layer depths in 1975 and 2006 and the $\sim$4m difference between the mixed-layer depths in 2006 and 2007.

To put these changes into context, we consider how these numbers fit in with the reported estimate that indicated that the summer mixed layer depth is shoaling at a rate of 3.3 m/dec in the Canada Basin (Peralta-Ferriz & Woodgate, 2015*a*). Starting in 1975, this would result in a summer mixed layer of 13m in 2005. This is a significantly larger increase in freshwater flux than the observational estimate from Yamamoto-Kawai *et al.* (2009), who estimated that surface freshening increased by approximately 1.35 meters per unit area in the same region. In our framework, this would result in ϕ_0 increasing by approximately only 40% over 30 years. Moreover, this may be an overestimate since the majority of this change was attributed to a decrease in sea ice formation rather than an increase in sea ice melt (Yamamoto-Kawai *et al.*, 2009).

Figures 5.10-5.11 show the resulting freshwater flux, mixed layer depth evolution, mixed-layer salinity evolution and ΔPE evolution in 2006 and 2007 (blue lines). We compare this model estimate to the observations (colored lines) and the model es-

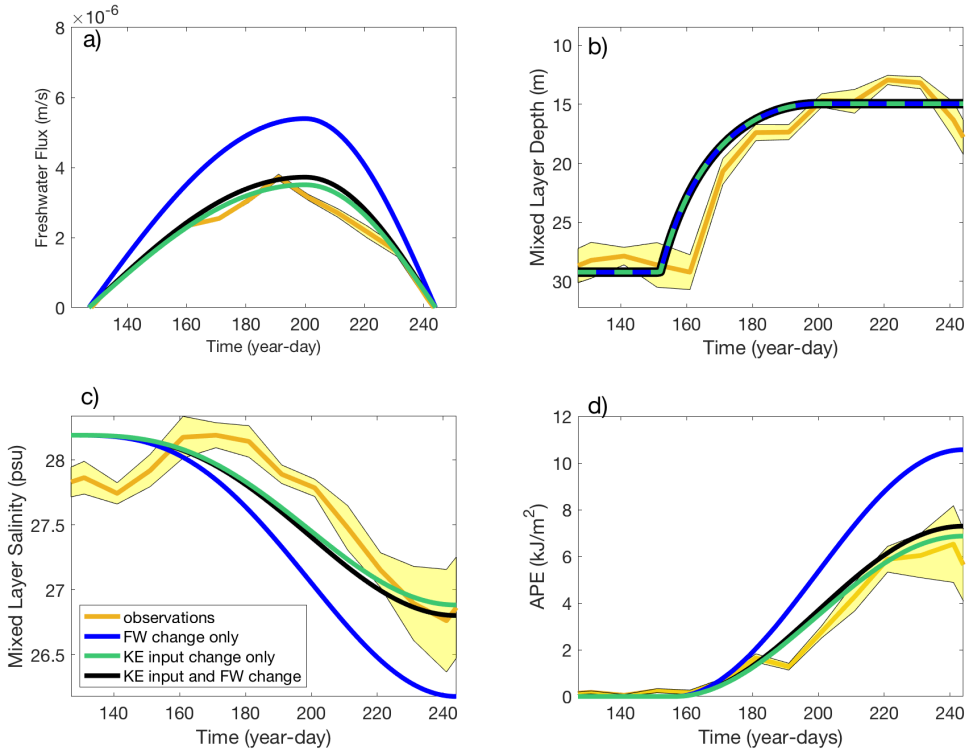

Figure 5.10: Observed and modeled (a) freshwater flux, (b) mixed-layer depth, (c) mixed-layer salinity, and (d) ΔPE evolution in 2006. Yellow and black lines are the same as in Figures 5.7 and 5.8. Blue lines represent the model estimated scenario in which the kinetic energy input remains at its 1975 value and only freshwater flux changes. Green lines represent the model estimated scenario in which the freshwater flux remains at its 1975 value and only kinetic energy input changes.

timate presented in Section 5.6 (black lines). The maximum freshwater flux increases by 45% in 2006 and by 73% in 2007 compared to the estimates in Section 5.6 (compare blue and black lines). The ratio between ϕ_0 and W is the same in each model estimate through the conditions set by equations 5.8 and 5.9, causing the mixed-layer depth evolution to be the same for both estimates. Next, we find that the model estimate for the mixed-layer salinity and ΔPE evolution is not consistent with the observations. Instead, this version of the model overestimates the amount of freshening and ΔPE, in contrast with our results in Section 5.6. This result indicates that the amount of freshwater flux necessary to explain recent mixed-layer depths could not explain changes in the mixed-layer freshening and resulting halocline stratification.

5.7.2 The influence of kinetic energy

Next, we consider the reverse scenario in which the freshwater flux is the same as estimated in 1975, and we examine how changes in the kinetic energy input alone could influence mixed-layer and ΔPE evolution. As above, we assume that the freshwater flux and kinetic energy input cause an observed mixed-layer depth that is consistent with the observations at $t = t_X$. Under this condition, the kinetic energy input in 2006 and 2007 is given by

$$W = \frac{g\beta\phi_{0,1975}D_{obs}}{2}, \tag{5.10}$$

where $\phi_{0,1975}$ is the estimated maximum freshwater flux in 1975 (Figure 5.6a). Figure 5.9a shows the relationship between the kinetic energy input and the mixed-layer depth at $t = t_X$ (black lines), the observed mixed-layer depths at $t = t_X$ during each of the three years (horizontal dashed lines), and the resulting estimated value of W (x-coordinate of black dots).

We find that the kinetic energy input would have to decrease by roughly a factor of 2 to explain changes between 1975 and 2007 mixed-layer depths if the freshwater flux remained constant. The kinetic energy input to the mixed layer is roughly expected to be given by the product of the ocean surface stress and the frictional velocity. To our knowledge, there is no observational estimate for the change in the kinetic energy input into the Canada Basin over the past several decades. However, there have been several observational studies on the frictional velocity (Cole *et al.*, 2017; Gallaher *et al.*, 2017; Maykut & McPhee, 1995) and one model study on decadal changes to the ocean surface stress. Interestingly, each of these studies finds that decreasing sea ice roughness could be causing the kinetic energy input into the upper ocean to be decreasing. Specifically, Martin *et al.* (2016) demonstrate that when

changes to sea ice roughness are included in their model study, the ocean surface stress reduces by approximately 3.1% per decade. Further, Cole *et al.* (2017) show estimated values of frictional velocity that are generally between 1-3 cm/s in 2014. They note that this is approximately a factor of 2 smaller than the 1975 estimates reported by Maykut & McPhee (1995). Based on this, we suggest that the estimated decrease in kinetic energy input from 1975 to 2006-2007 could plausibly be consistent with the observations.

Next, we examine how changes in the kinetic energy input since 1975 alone could influence the mixed layer and ΔPE evolution (green lines, Figures 5.10-5.11). As before, our tuning parameters ensure that the mixed-layer depth evolution is the same for each model estimate, but the mixed-layer salinity and ΔPE evolution are expected to vary. In both 2006 and 2007, we find that the decrease in kinetic energy input causes less mixed-layer freshening and less ΔPE than in original model (compare black and green lines), though the differences are modest. In 2006, we find that in spite of this decrease, the model estimate still agrees well with the observations at the end of the melt season. In 2007, the estimate is relatively consistent with the observations for much of the melt season but underestimates the total mixed-layer freshening and maximum ΔPE. Together, these results suggest that a very modest decrease in the kinetic energy input is enough to explain significant differences in the mixed layer and ΔPE evolution between 2006-2007 and 1975.

5.8 Discussion

This study is focused on examining the extent to which changes in the kinetic energy versus changes in the freshwater flux might explain how the seasonal halocline stratification has increased in recent years (Peralta-Ferriz & Woodgate, 2015*a*), by examining mixed layer and ΔPE evolution in 1975, 2006, and 2007. Our results

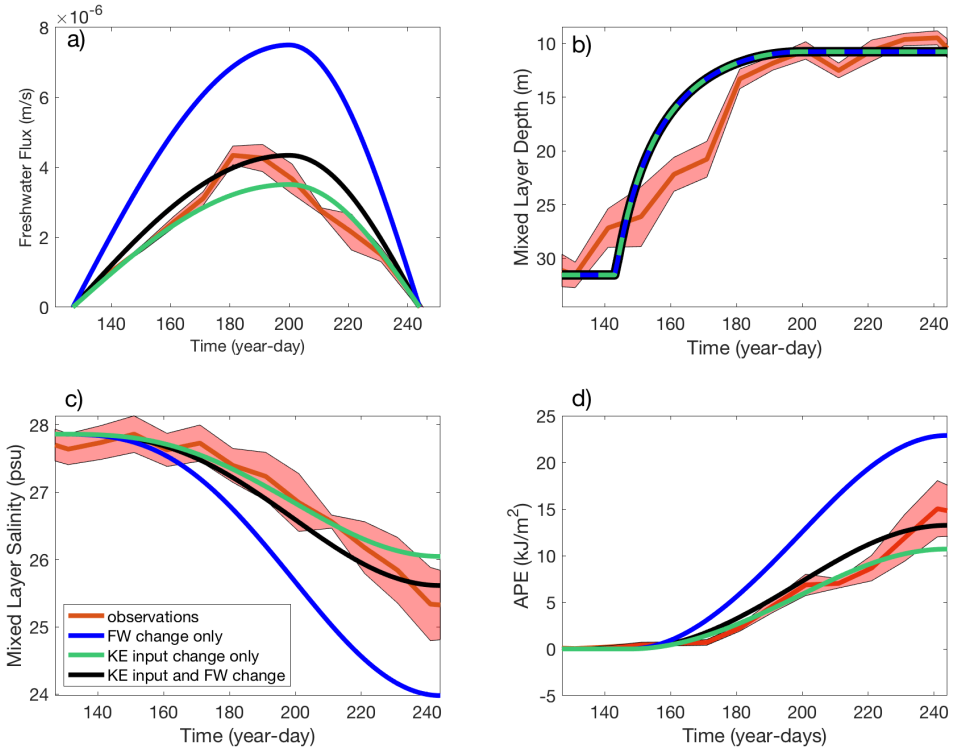

Figure 5.11: As in Figure 5.10, but for 2007.

suggest that the amount of buoyancy required to explain the shallower mixed layers in 2006 and 2007 would cause significantly more surface freshening than observed. This suggests that reductions in the momentum transfer could play an important role in causing the mixed layer to shoal, which in turn increases the seasonal halocline stratification.

This idea is consistent with studies that suggest that (1) the freshwater flux in the spring controls mixed-layer shoaling (Gallaher *et al.*, 2017), (2) the freshwater flux in the spring is dominated by top melt (Steele *et al.* (2010), Chapter 4), (3) sea ice top melt has remained relatively constant over the past several decades in this region (Perovich & Richter-Menge, 2015), (4) surface momentum transfer is expected to decrease in areas that are transitioning from multi-year to first-year ice cover (McPhee, 2012). This would suggest that the influence of the freshwater flux on the mixed-layer depth has not changed dramatically over the past decades, while the kinetic energy input may have decreased enough to cause shallower summer mixed layers. The shallower summer mixed layers then concentrate similar amounts of freshwater over a smaller volume, leading to more seasonal mixed-layer freshening (see Ch. 4) and hence a stronger seasonal halocline.

Several factors limit this analysis. First, the ITP instrument system is likely to have mixed-layer depths that are biased too deep in the summer (Toole *et al.*, 2010) and may incorrectly indicate that mixed-layer shoaling occurs as much as two weeks later than in reality (Gallaher *et al.*, 2017). Second, this idealized representation of the mixed-layer salinity evolution does not include entrainment, which appears to be an important component controlling mixed-layer salinity and ΔPE evolution, particularly in 1975. Third, we have only examined three years of observations taken in different locations in the Canada Basin. It is therefore likely that other factors such as regional and inter-annual variability play an important role in explaining

the differences between these three years. Fourth, we have neglected potentially important temporal and spatial variations in the kinetic energy input (Cole *et al.*, 2017).

5.9 Summary

The seasonal halocline stratification has increased in recent years, suppressing convective mixed-layer deepening and isolating the NSTM from the surface (Jackson *et al.*, 2010, 2011; Steele *et al.*, 2011; Carmack *et al.*, 2015; Gallaher *et al.*, 2017, 2016). Here, we examine factors controlling the strength of this stratification in 1975, 2006, and 2007. First, we quantify differences in the seasonal halocline during each of the three years by examining the change in potential energy required to convectively deepen the mixed layer to 25 meters (ΔPE). We find that there are significant differences between each of the three years (Figure 5.4) and that these differences can largely be explained by differences in the seasonal mixed layer evolution (Figure 5.5). Second, we present an idealized framework to estimate seasonal mixed-layer evolution during the melt season (Section 5.5). The model uses the observed mixed-layer depth when the seasonal halocline is formed in each of the years to estimate the kinetic energy input for each year. We find that this leads to estimates of a mixed-layer depth, a mixed-layer salinity, and ΔPE evolution that are consistent with the observations during the three years (Figure 5.7-5.8). This suggests that the framework may, therefore, capture the underlying processes that explain the differences in the three years.

Motivated by this, we next estimate the possibility that variations to the freshwater flux alone could explain differences in the seasonal halocline stratification, as suggested by previous studies (Jackson *et al.*, 2010, 2011; Steele *et al.*, 2011; Carmack *et al.*, 2015). Our estimate suggests that the amount of freshwater flux required to

shoal the mixed layer to the values in 2006 and 2007 would cause the mixed layer to freshen significantly more than observed and hence produce a seasonal halocline that is more stratified than observed. Further, it would require a freshwater flux that is considerably larger than current observational estimates. On the other hand, we find that modest variations to the kinetic energy alone could plausibly explain much of the difference between the strength of the seasonal halocline stratification during the three years. These results, therefore, suggest that variations in the momentum transfer under different sea ice conditions can have a significant impact on seasonal halocline stratification and hence upper ocean heat storage.

Acknowledgements

This work was supported a National Science Foundation Graduate Research Fellowship and a Chateaubriand Research Fellowship.

Chapter Five, in part, is currently being prepared for submission for publication of the material. Rosenblum, E., Gille, S., Lique, C. The dissertation author was the primary investigator and author of this paper.

Appendix A

Chapter 2 Supporting Figures

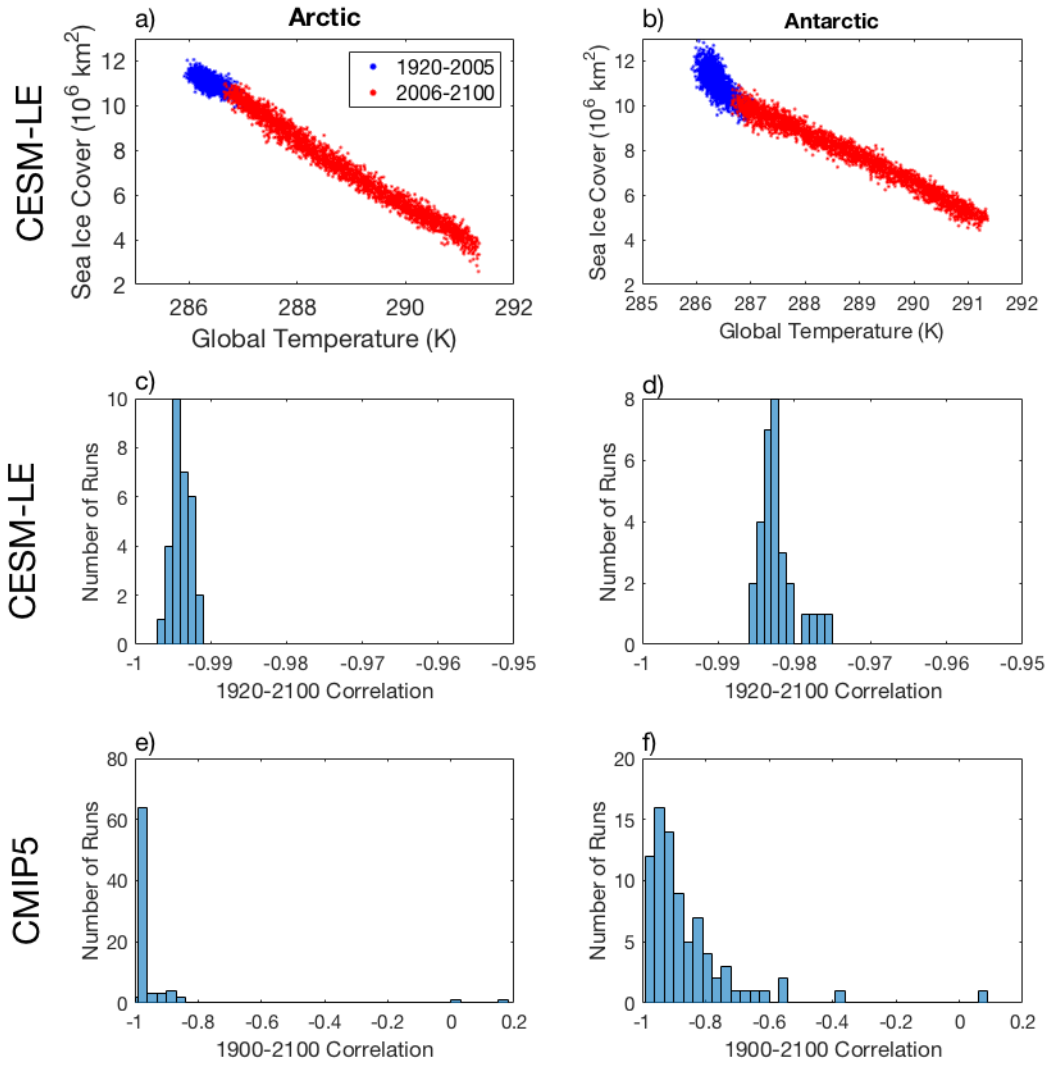

Figure A.1: Annual (a) Arctic and (b) Antarctic sea ice extent versus global-mean surface air temperature using 30 CESM-LE simulations of 1920-2100. Years associated with 1920-2005 (blue) and 2006-2100 (red) are indicated. (c-f) Histograms of the correlations between (c,e) Arctic sea ice extent and (d,f) Antarctic sea ice extent with the global-mean surface air temperature from each (c,d) CESM-LE simulation of 1920-2100 and (e,f) CMIP5 simulation of 1900-2100.

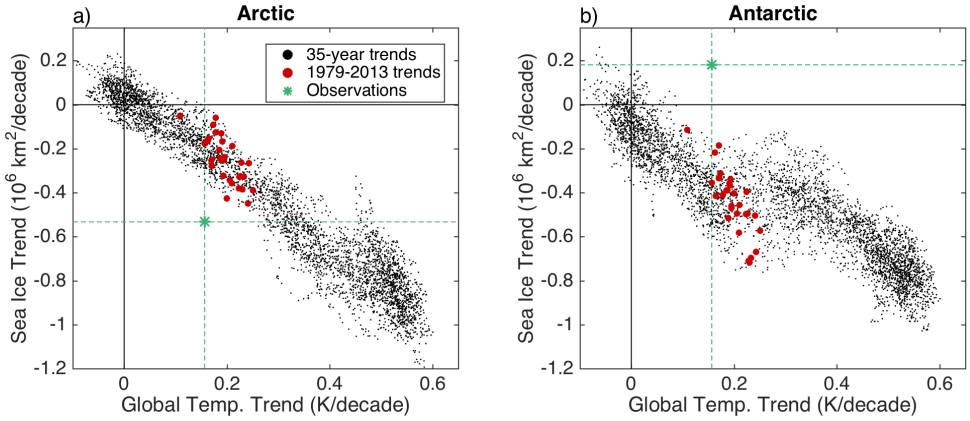

Figure A.2: As in Figs. 4a,b but for the 30 CESM-LE simulations of 1920-2100 (4 410 points in total).

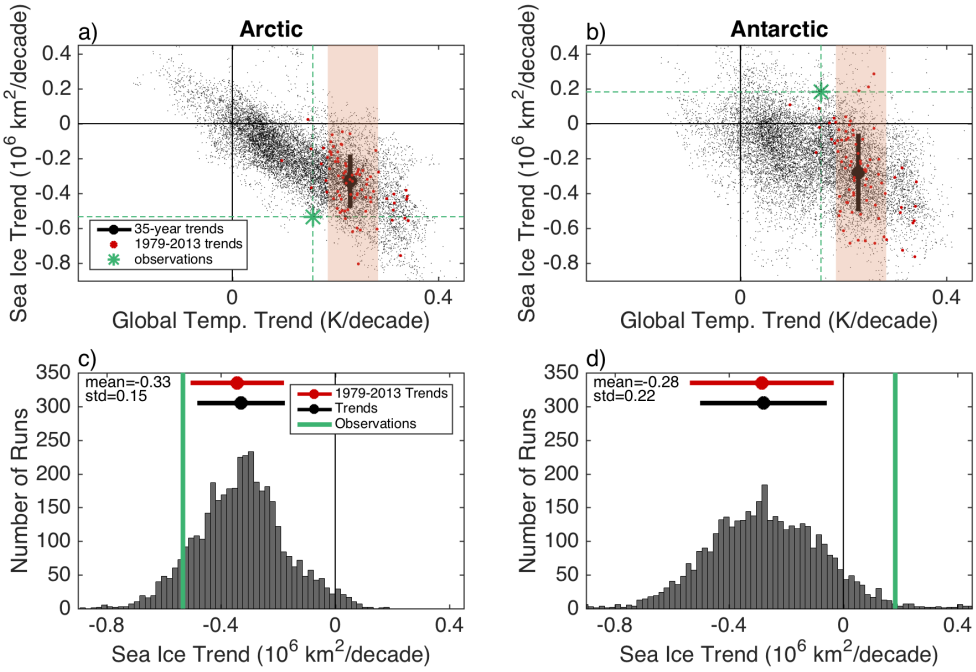

Figure A.3: (a-b) As in Figs. 4a,b, but here the red highlighted region indicates all 35-year global-mean surface air temperature trends that are within one standard deviation of the 1979-2013 CMIP5 ensemble mean (Fig. 1d). Sea ice trends for the periods that fall within the highlighted regions are shown in the histograms below (c,d), with the observed trend indicated by a thick green line. Standard deviations of these distributions (black error bars) and the distribution of 1979-2013 sea ice trends (red error bars) are also shown. The mean and standard deviation of the trends that fall within the highlighted regions are repeated for comparison in the top panel (black vertical error bars).

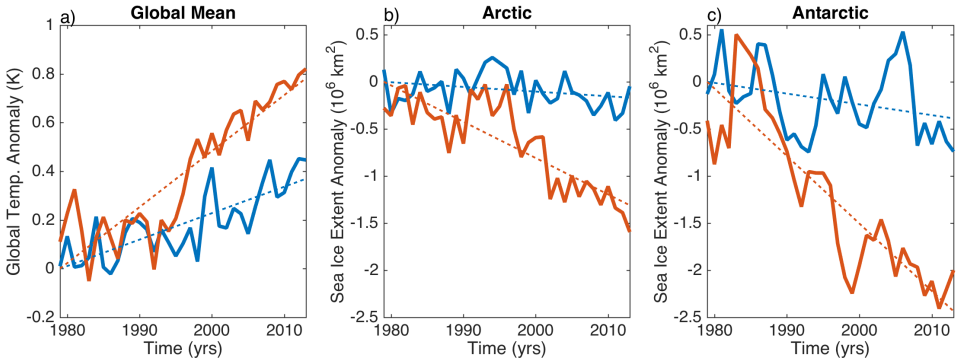

Figure A.4: Time series of annual-mean (a) global-mean surface air temperature, (b) Arctic sea ice extent, and (c) Antarctic sea ice extent from two CESM-LE simulations. Linear trends are indicated by dashed lines. The simulation with a large level of global warming (red) has more sea ice loss in both hemispheres than the simulation with a small level of global warming (blue).

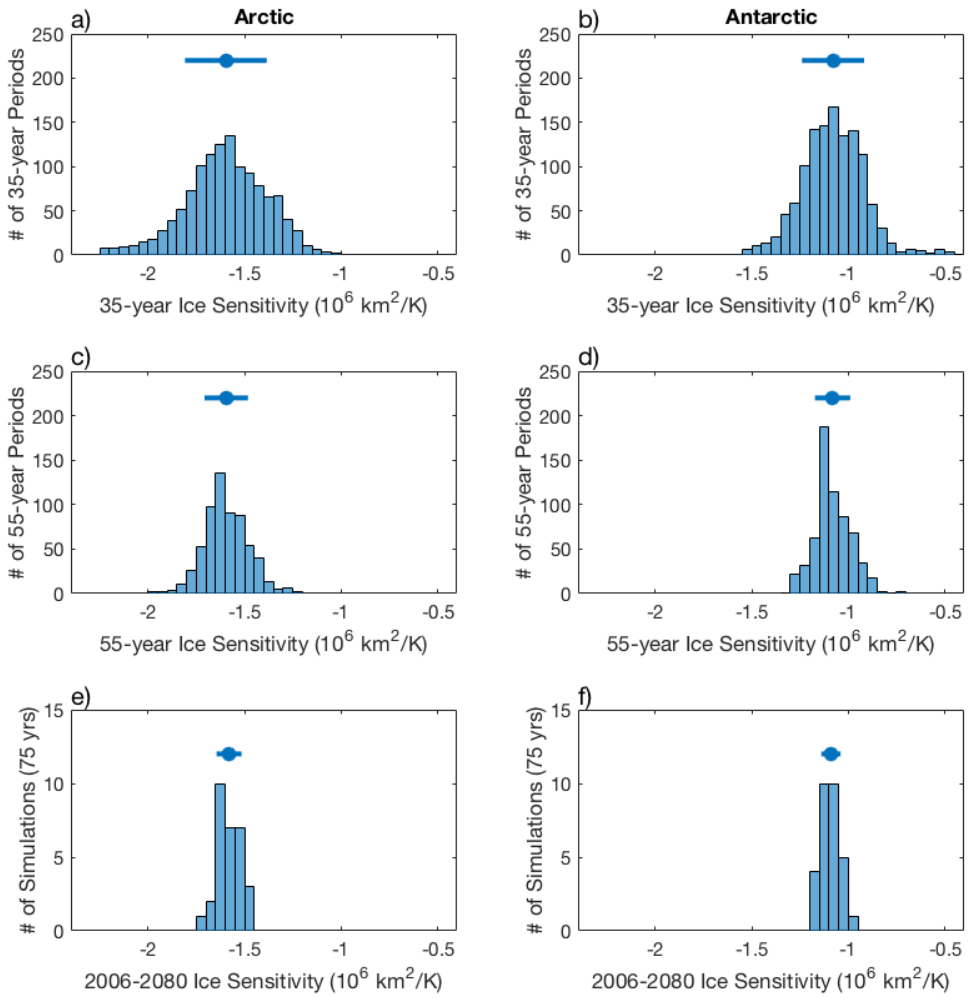

Figure A.5: Distributions of annual (a,c,e) Arctic and (b,d,f) Antarctic sea ice trends divided by the annual global-mean surface temperature trends, which gives an estimate of the sea ice sensitivity, using 30 CESM-LE simulations of 2006-2080. The distribution of the ratio of these trends is shown for each of the 30 simulations (e,f), as well as for each (c,d) 55-year and (a,b) 35-year period within each simulation. The mean and standard deviation of each distribution is also indicated (error bars). The widening of the distributions illustrates the influence of internal variability, which increases for shorter time scales and makes the relationship between sea ice retreat and global warming more variable.

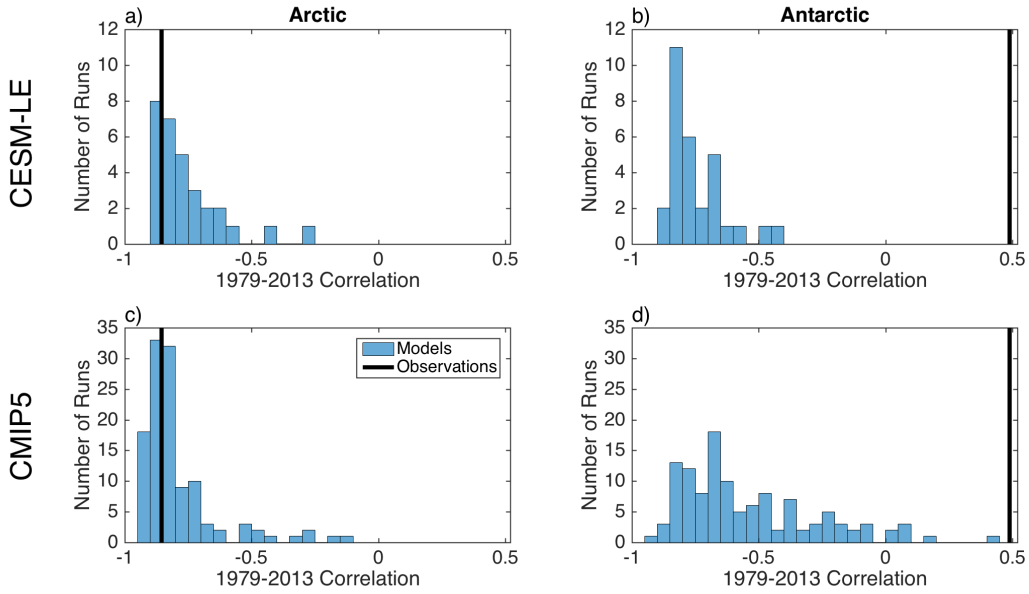

Figure A.6: Histograms of the correlations between (a,c) Arctic sea ice extent and (b,d) Antarctic sea ice extent with the global-mean surface air temperature from each (a,b) CESM-LE simulation and (c,d) CMIP5 simulation of 1979-2013. Observed correlations between Arctic sea ice extent and global-mean surface temperature are indicated in black.

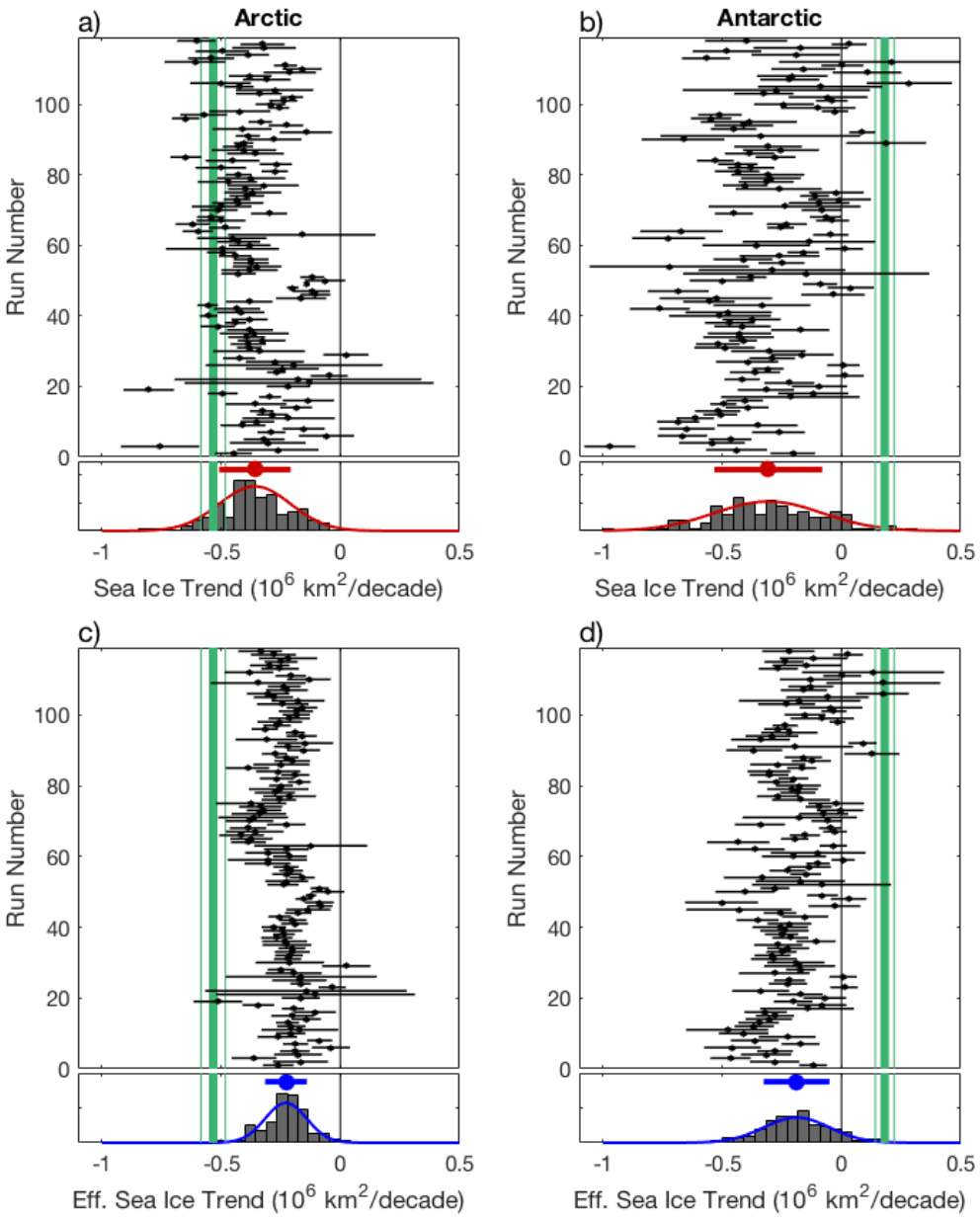

Figure A.7: Distribution of 118 CMIP5 simulated 1979-2013 (a,c) Arctic and (b,d) Antarctic (a,b) sea ice trends and (c,d) effective sea ice trends, as in Figs. 1e,f and 3c,d. The trends and 68% regression confidence intervals for all simulated 35-year trends are indicated as error bars above the histograms (see Appendix B for details). The observed trend is indicated by a thick green vertical line, with thin green vertical lines indicating the 68% regression confidence interval.

Appendix B

Chapter 3 Supporting Figures

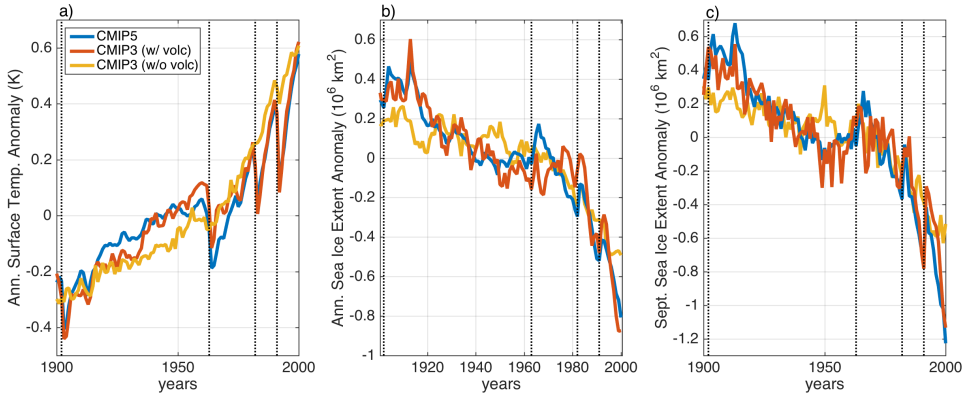

Figure B.1: As in Figure 2, but showing the simulations only and looking at an extended time period that includes the additional volcanic eruptions of Santa Maria (1901) and Agung (1963).

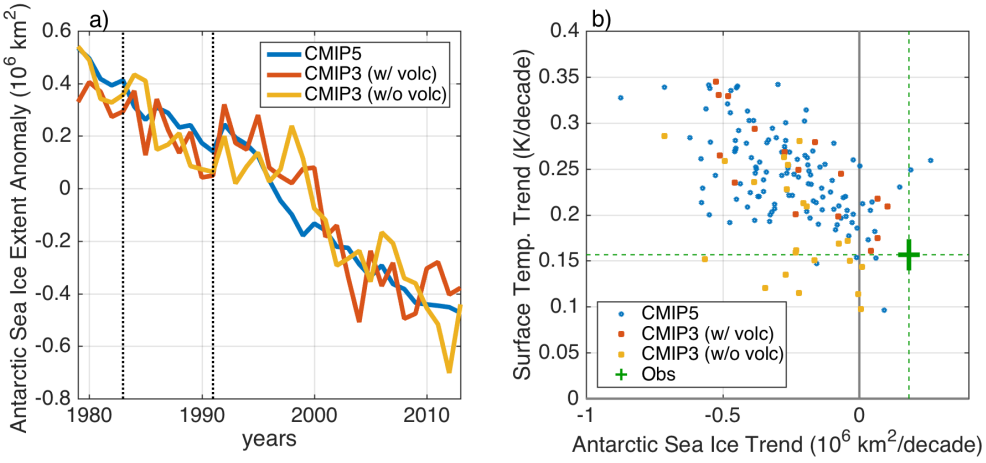

Figure B.2: As in (a) Figure 2b and (b) Figure 3a, but for annual-mean Antarctic sea ice trends.

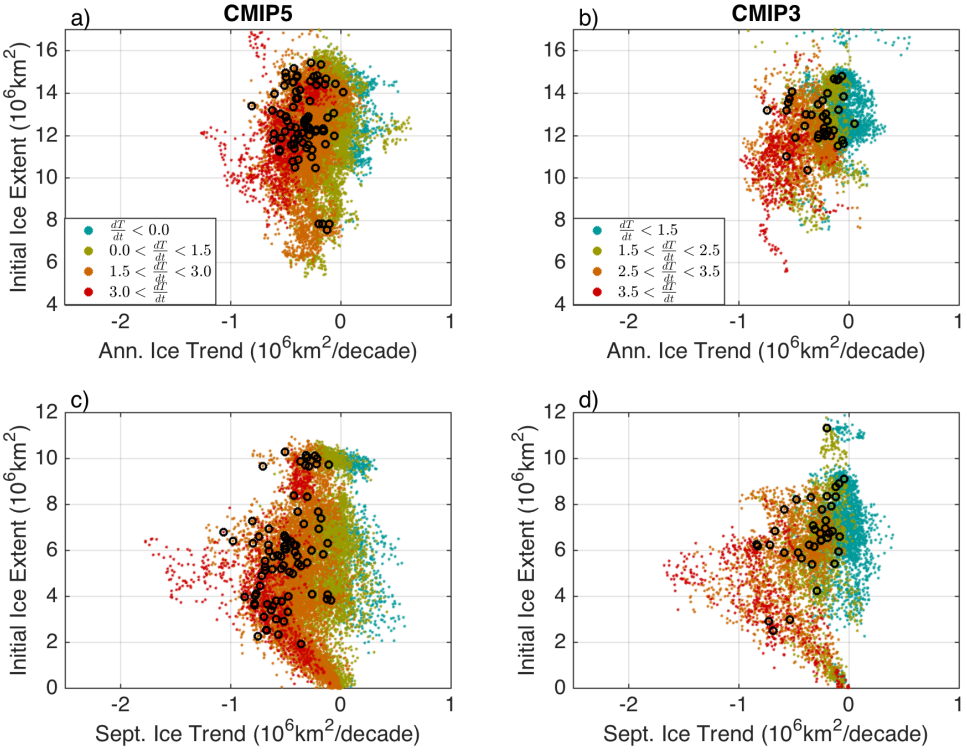

Figure B.3: As in Figure 4 but using initial Arctic sea ice extent on the horizontal axis rather than global surface temperature trends. Additionally, the level of warming is indicated by the colors. 1979-2013 trends are indicated in black.

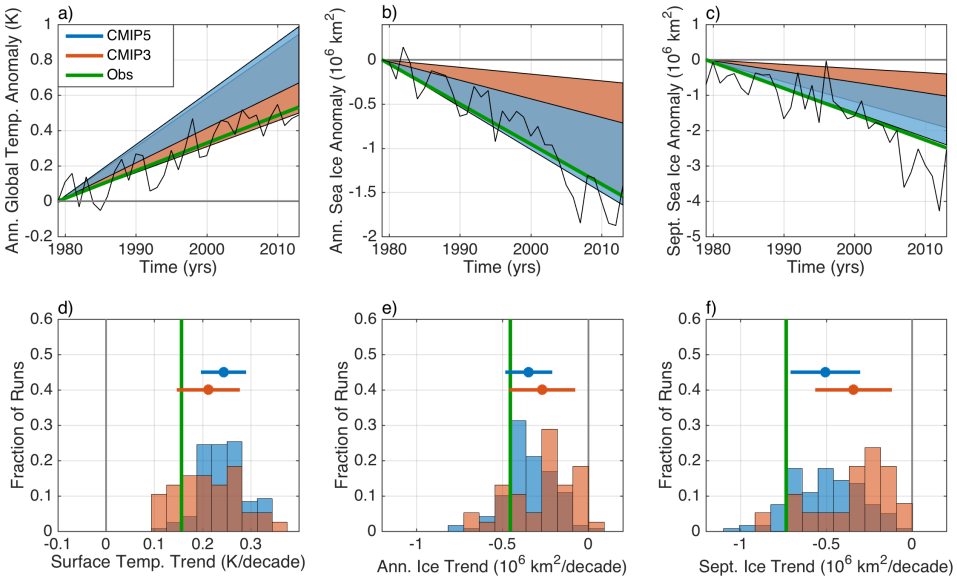

Figure B.4: As in Figure 1, but using sea ice area rather than extent.

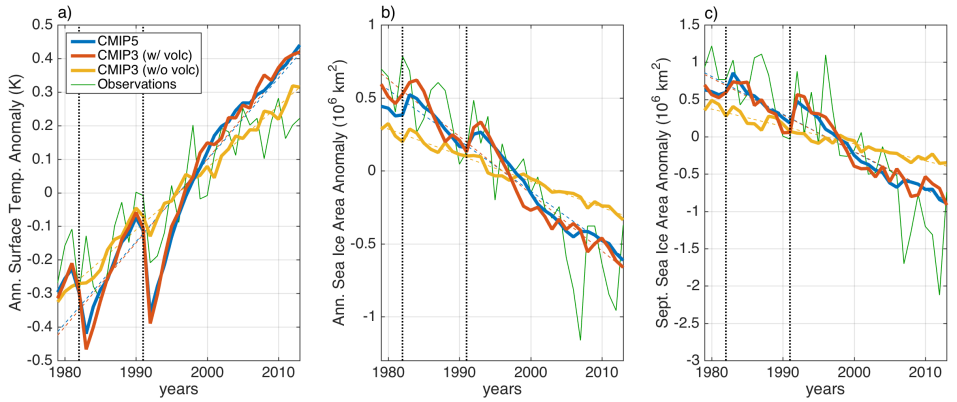

Figure B.5: As in Figure 2, but using sea ice area rather than extent.

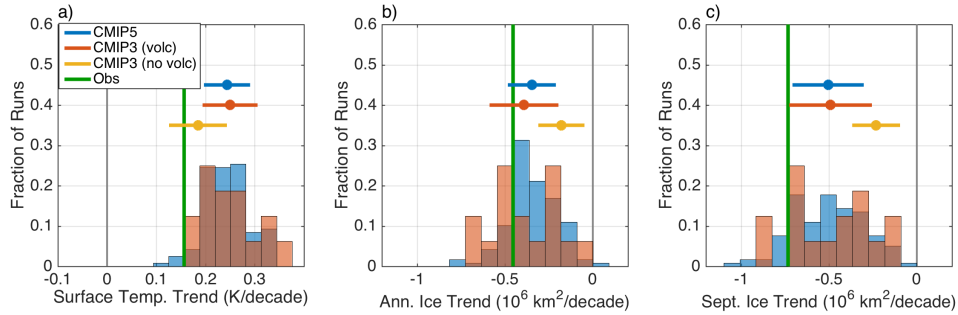

Figure B.6: As in Figure 3, but using sea ice area rather than extent.

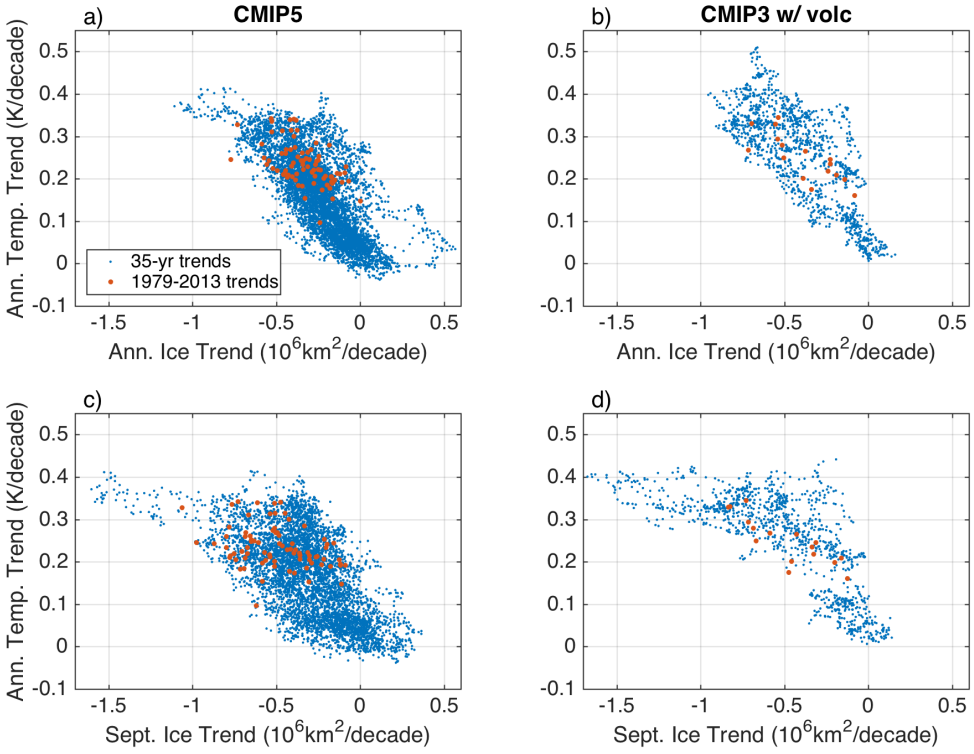

Figure B.7: As in Figure 4, but using sea ice area rather than extent.

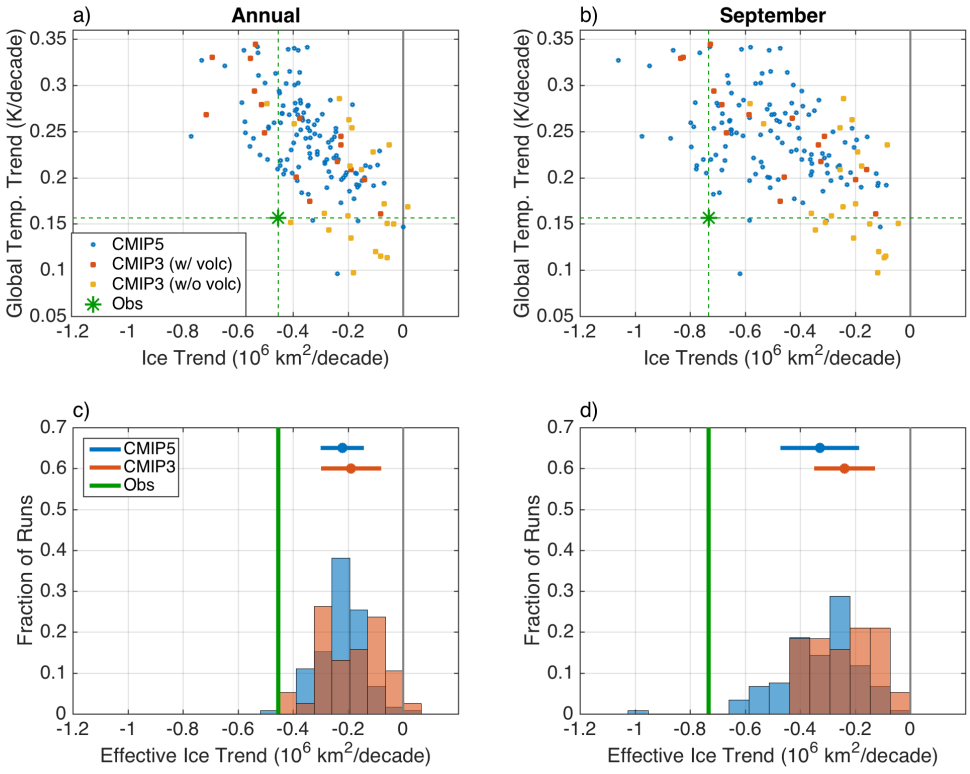

Figure B.8: As in Figure 5, but using sea ice area rather than extent.

Appendix C

Chapter 4 Supporting Figures

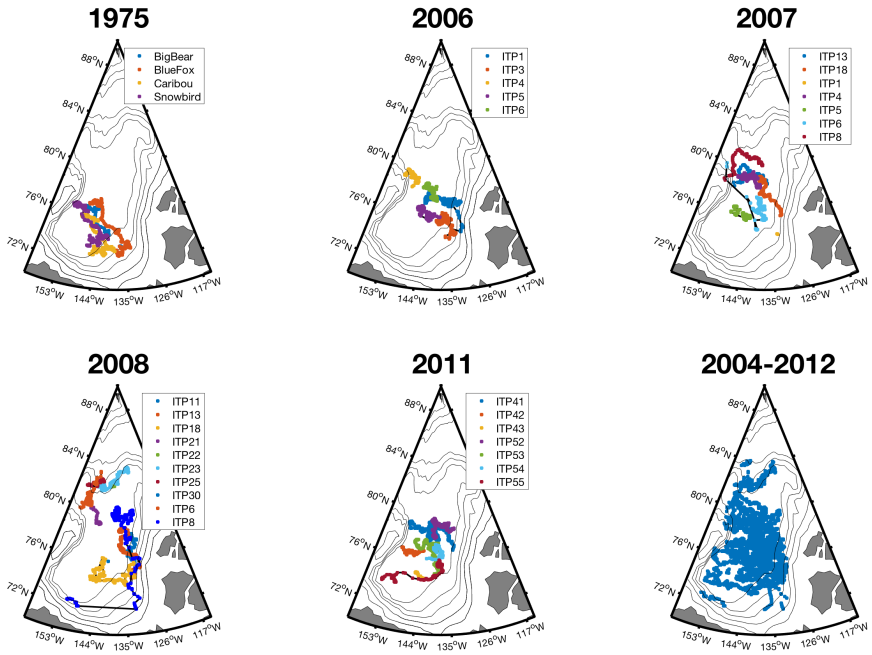

Figure C.1: Location of observations in 1975, 2006, 2007, 2008, 2011, and 2004-2012. Different colors indicate that the observations come from different ITPs or AIDJEX ice camps.

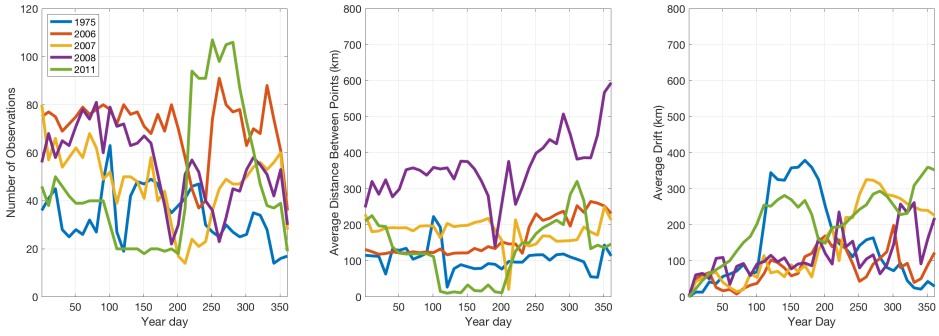

Figure C.2: Temporal evolution of (a) the number of observations, (b) the average distance between points, and (c) the average drift of the observations from the beginning of the year for all available ITP data in 1975, 2006, 2007, 2008, and 2011.

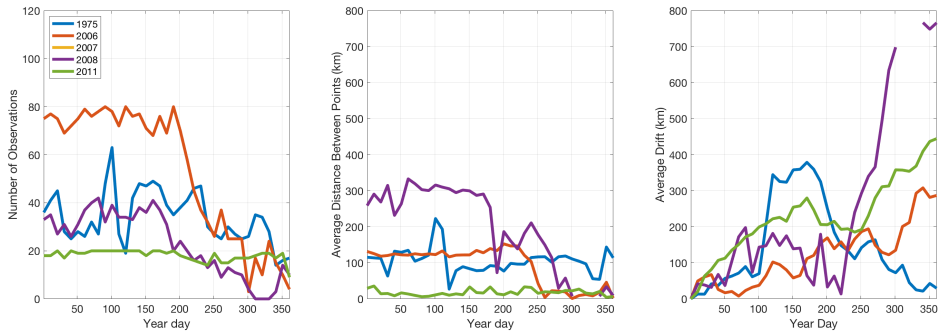

Figure C.3: As in Figure S2, but using only observations from ITPs that collect data throughout the melt season.

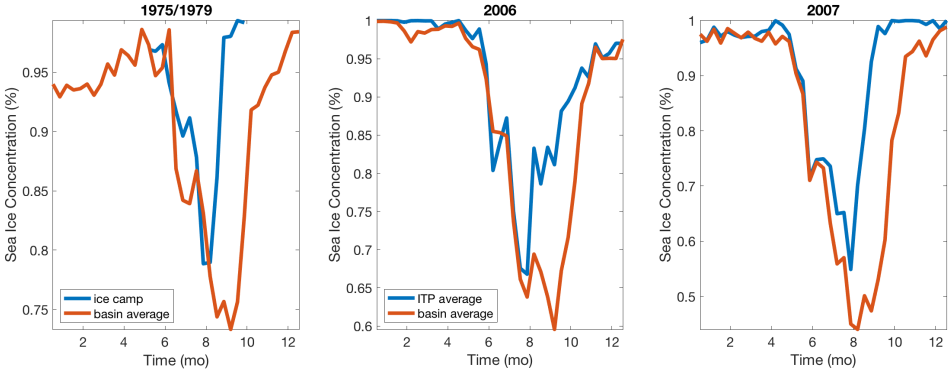

Figure C.4: Observed sea ice concentration using two different methods in 1975/1979, 2006, and 2007. The blue line indicates the average over the Canada Basin in 1979, 2006, and 2007. The red line indicates the estimated sea ice concentration in 1975 (Maykut and McPhee 1995) and the estimate sea ice concentration by locating the sea ice grid point closest to each individual ITP and then taking the average.

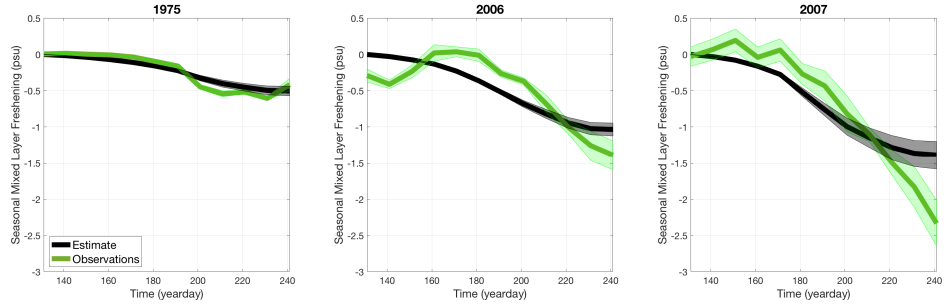

Figure C.5: As in Figure 4, but using a different method to compute the observed sea ice concentration (red lines in Figure S12).

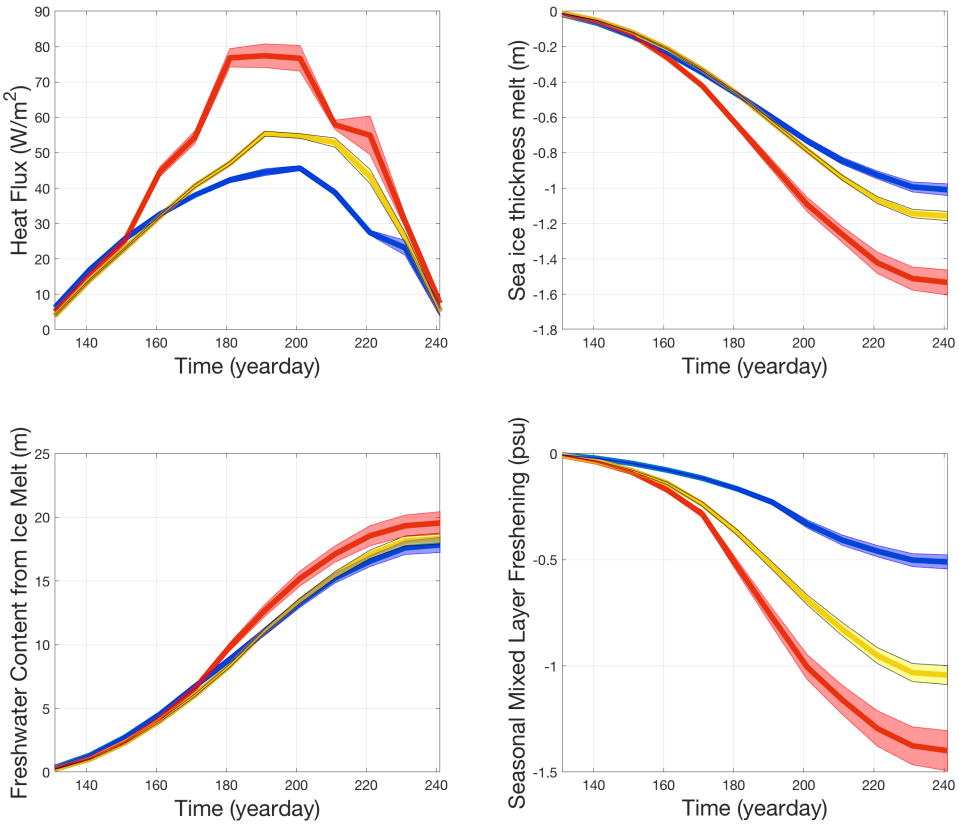

Figure C.6: As in Figure 5c, 6c, 7c, and 8c, but using a different method to compute the observed sea ice concentration (red lines in Figure S12).

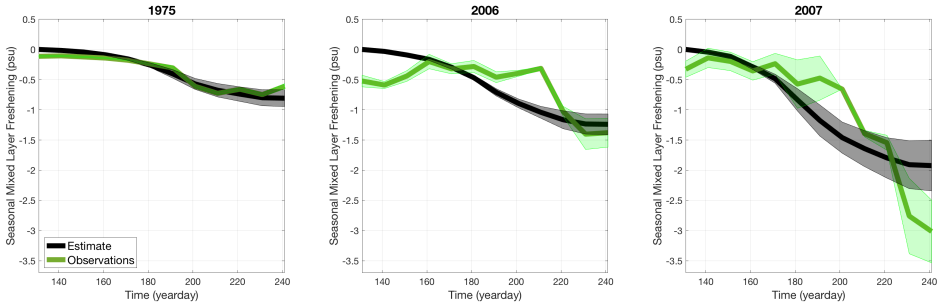

Figure C.7: As in Figure 4, but using a different method to compute the observed mixed layer depth.

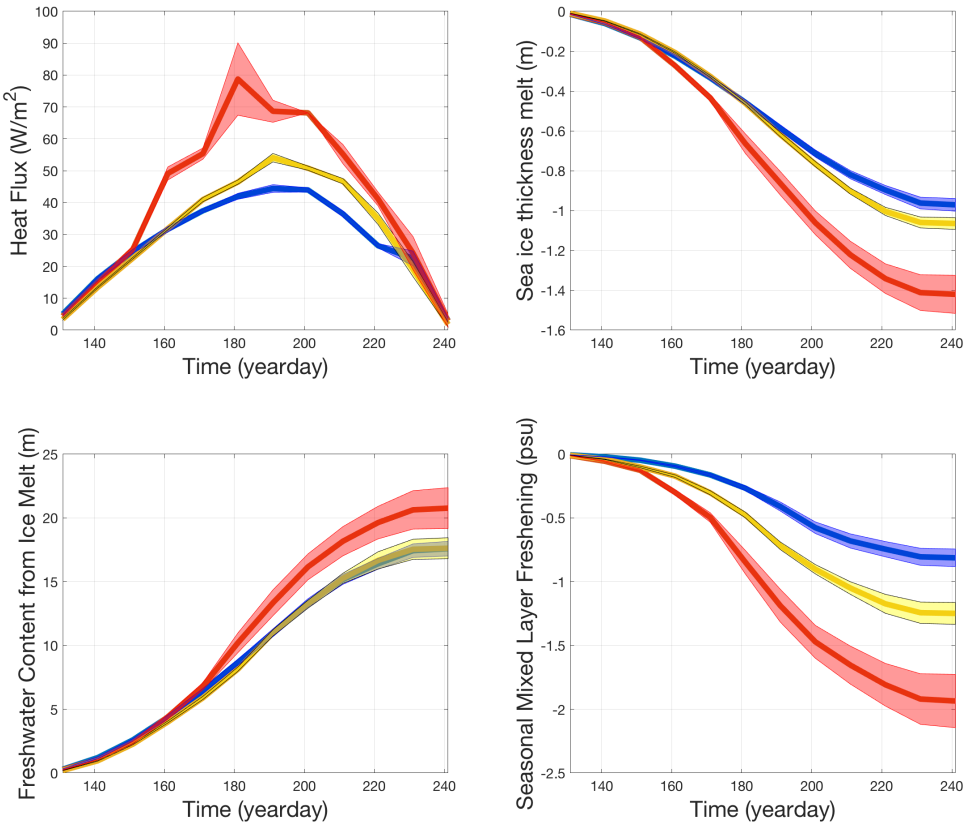

Figure C.8: As in Figure S5, but using a different method to compute the observed mixed layer depth.

Table C.1: Average and standard deviation of the number of observations, the average distance between observations, and the average drift from initial location during the 1975, 2006-2008, and 2011 melt season. Top 5 rows are computed using all available data points during the melt season, bottom 3 rows are computed using only ITPs that collect data throughout the course of the melt season.

Year	Number of Obs.	Distance between Obs.	Drift (km)
1975	38 ± 10	96 ± 34	257 ± 99
2006	68 ± 15	147 ± 35	103 ± 40
2007	36 ± 13	173 ± 48	140 ± 85
2008	50 ± 17	329 ± 68	116 ± 41
2011	45 ± 36	65 ± 68	231 ± 40
2006	61 ± 19	117 ± 39	125 ± 45
2008	26 ± 10	227 ± 75	147 ± 92
2011	18 ± 2	19 ± 9	221 ± 27

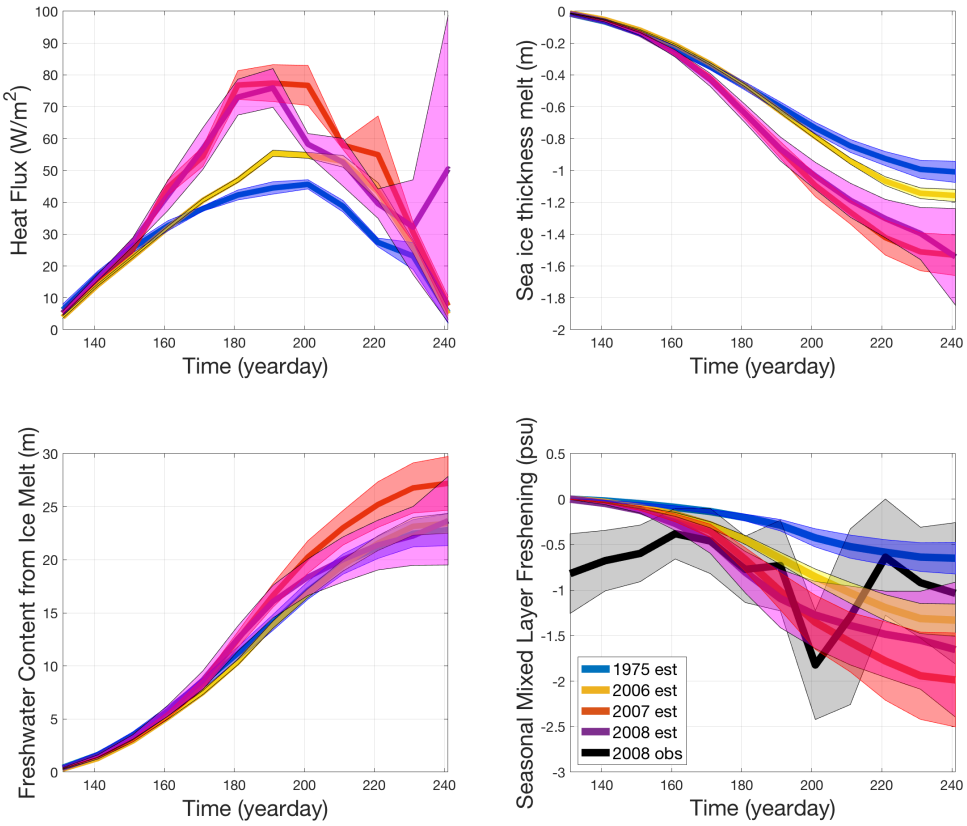

Figure C.9: As in Figure 10, but for 2008 instead of 2004-2012.

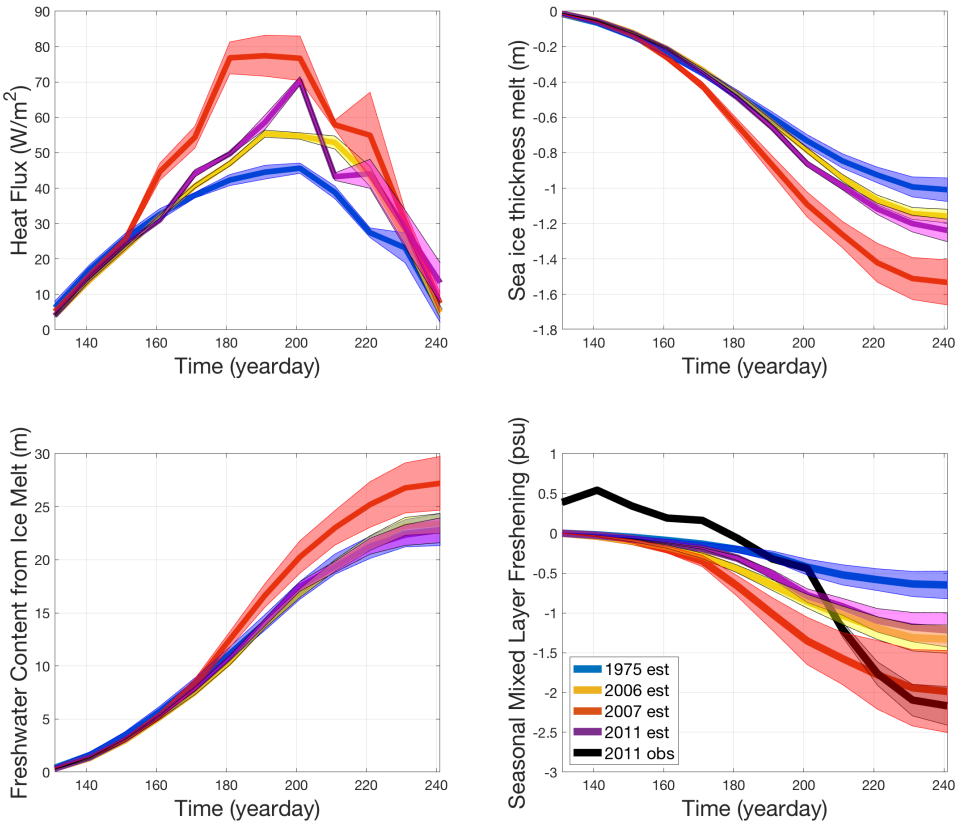

Figure C.10: As in Figure 10, but for 2011 instead of 2004-2012.

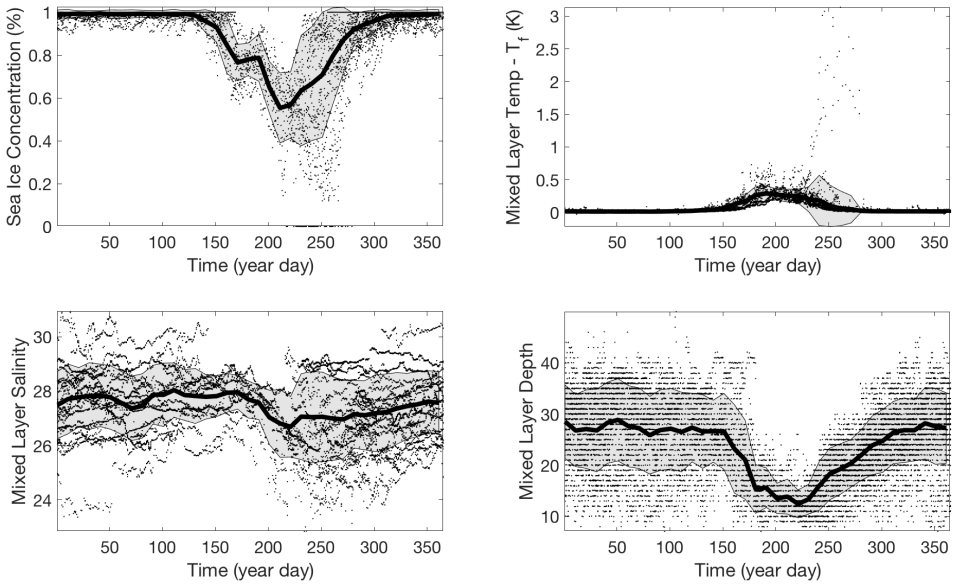

Figure C.11: Observed sea ice concentration, mixed layer temperature anomaly from freezing, mixed layer salinity, and mixed layer depth for all available, level 3 processed ITP data between 2004-2012 (black dots). Solid lines indicate the mean grey shading indicates one standard deviation.

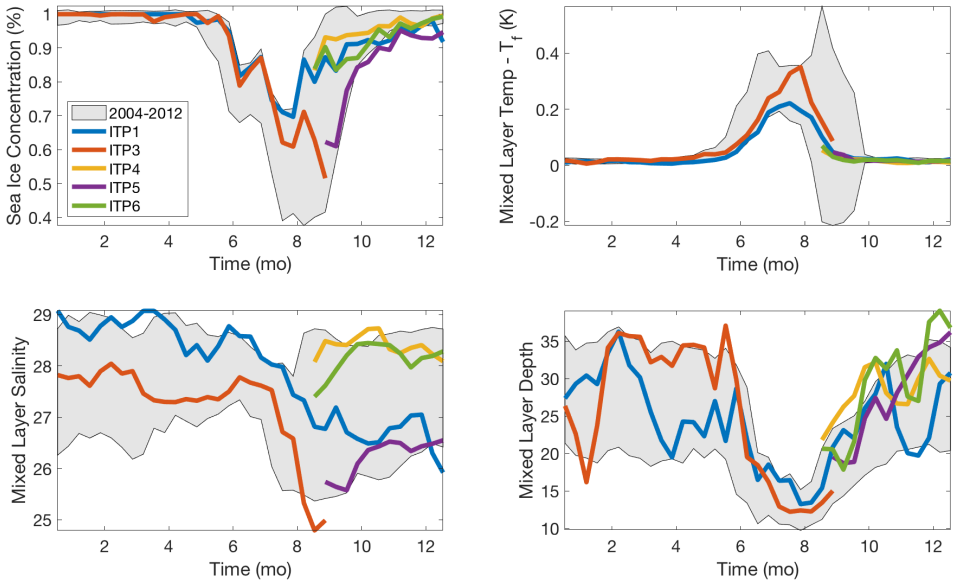

Figure C.12: As in Figure S11, but with colored solid lines indicating the mean of observations taken from different ITPs in 2006.

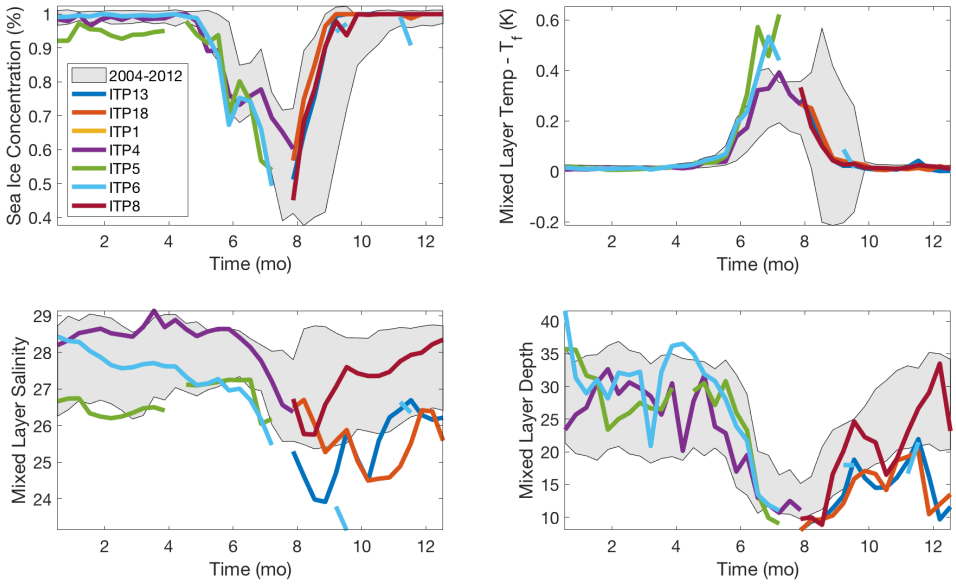

Figure C.13: As in Figure S12, but for 2007.

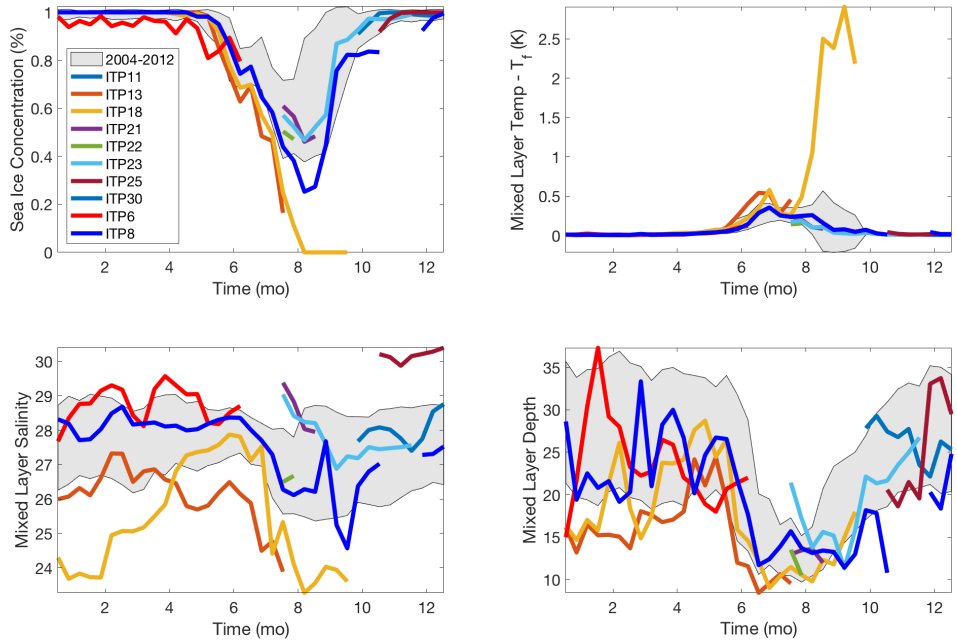

Figure C.14: As in Figure S12, but for 2008.

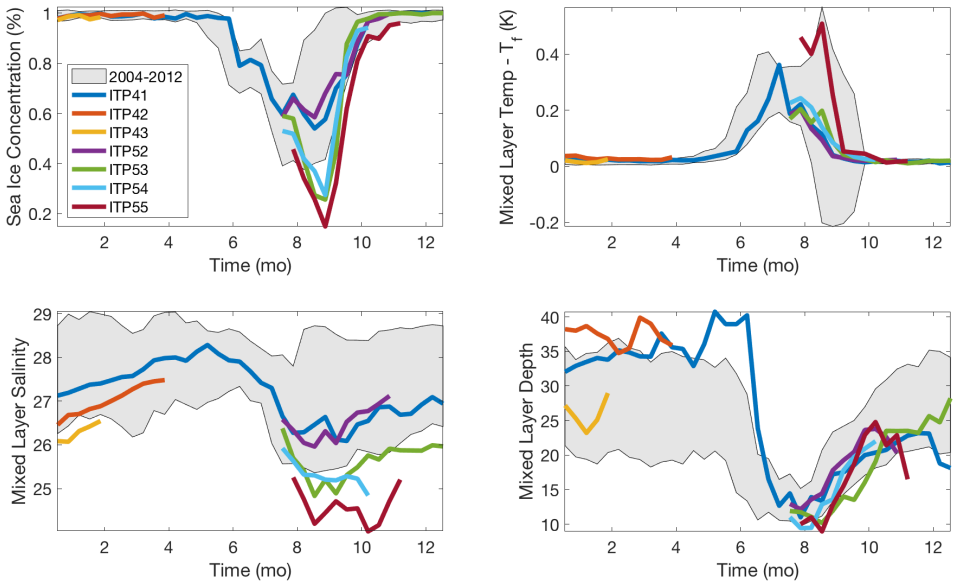

Figure C.15: As in Figure S12, but for 2011.

Appendix D

Chapter 5 Supporting Figures

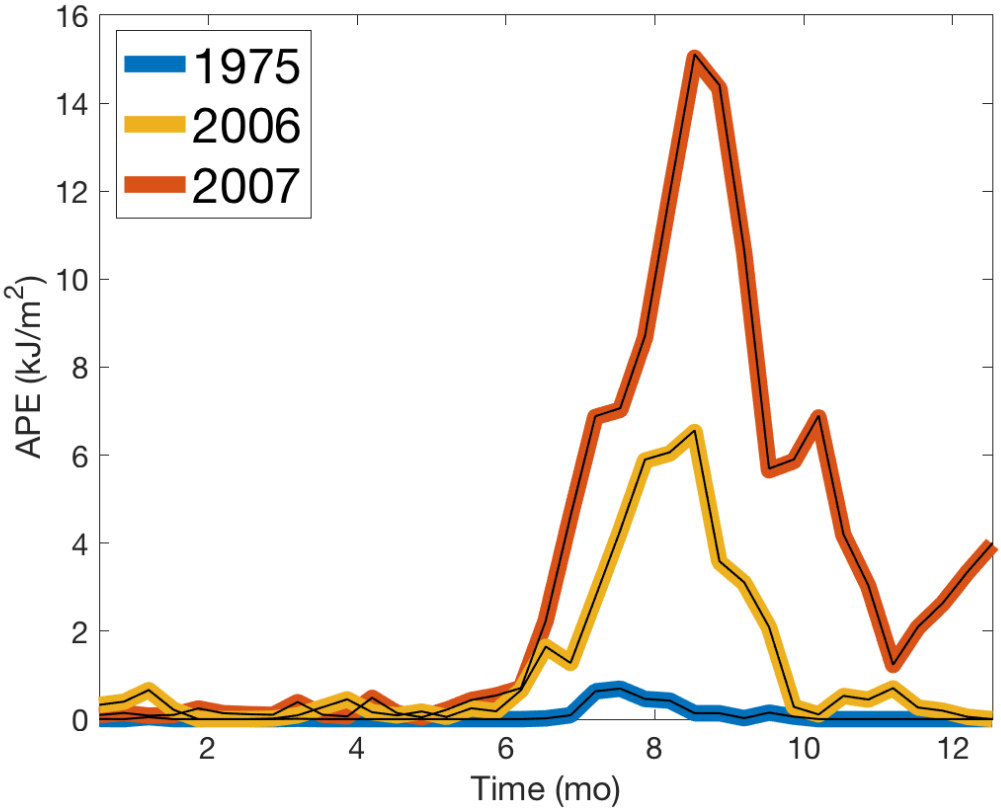

Figure D.1: Observed change in potential energy required to deepen the mixed layer to 25 meters (ΔPE) in 1975 (blue), 2006 (yellow), and 2007 (red). Red lines indicate observed ΔPE, as in Figure 4 in main text, thin black lines represent observed ΔPE that is computed assuming the temperature is fixed at the freezing point. This figure illustrates that the ΔPE is controlled by the evolution of the seasonal halocline.

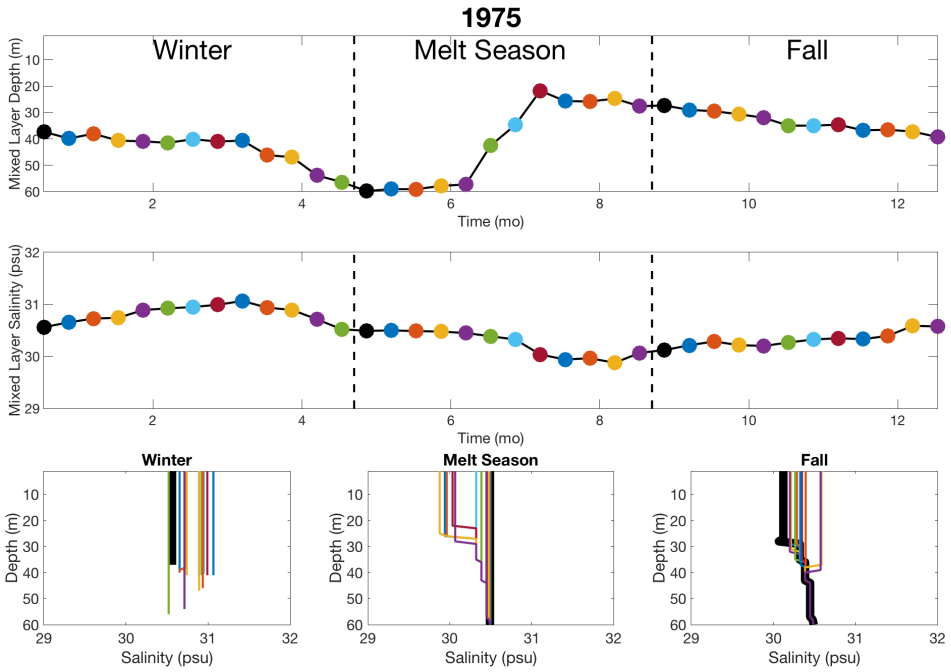

Figure D.2: The 1975 observed evolution of (top) the mixed layer depth and (center) mixed layer salinity. The bottom three panels show the resulted constructed seasonal pycnocline (see text for details). Colored dots in top panels correspond to colored lines the three bottom panels.

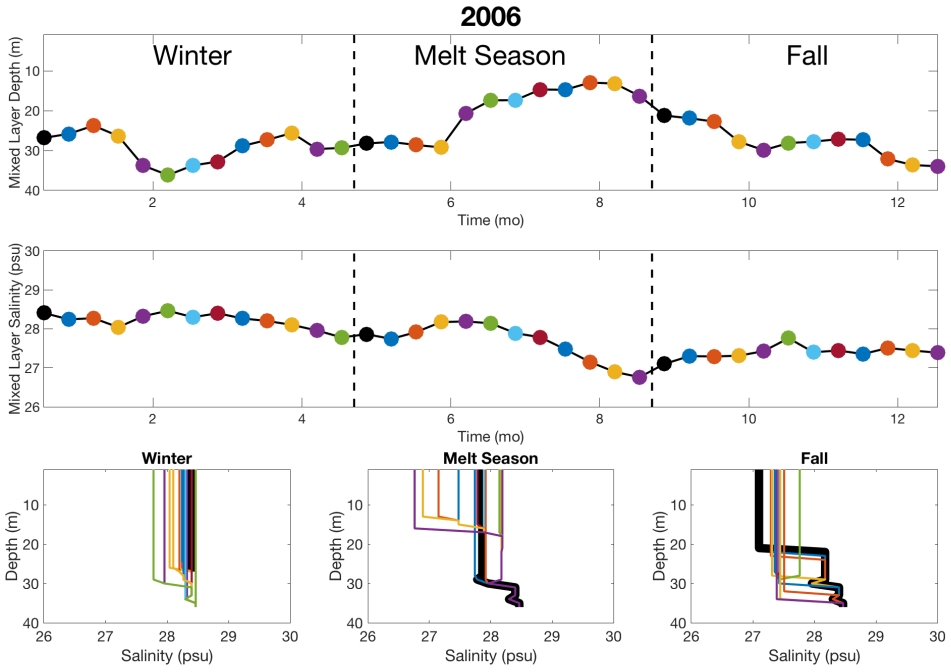

Figure D.3: As in Figure S2, but for 2006 instead of 1975.

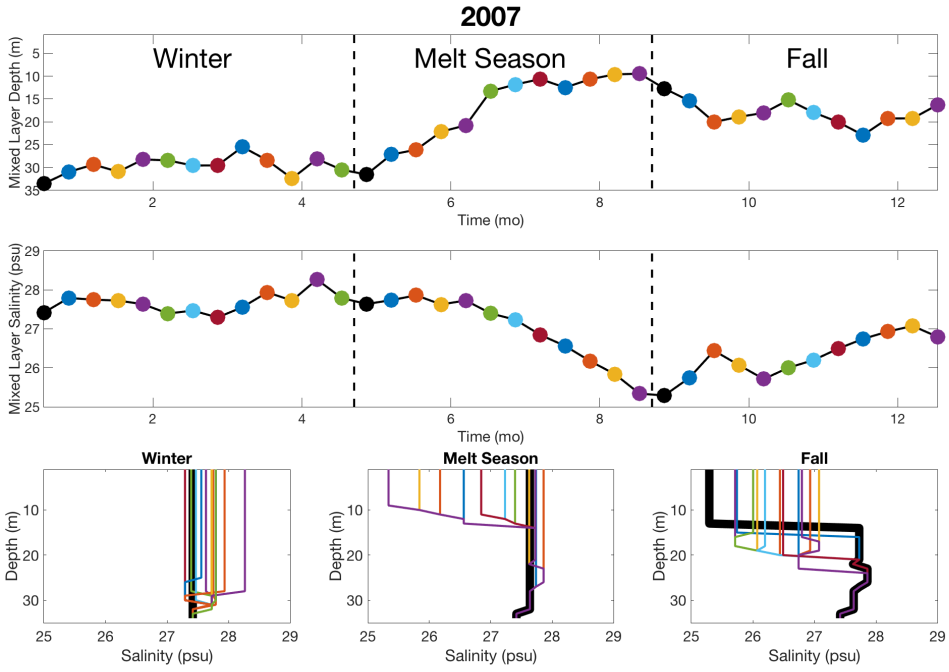

Figure D.4: As in Figure S2, but for 2007 instead of 1975.

Bibliography

Arfeuille, F., Weisenstein, D., Mack, H., Rozanov, E., Peter, T. & Brönnimann, S. 2014 Volcanic forcing for climate modeling: A new microphysics-based data set covering years 1600-present. *Climate of the Past* **10** (1), 359–375.

Armour, K. C., Eisenman, I., Blanchard-Wrigglesworth, E., McCusker, K. E. & Bitz, C. M. 2011 The reversibility of sea ice loss in a state-of-the-art climate model. *Geophysical Research Letters* **38**.

Bintanja, R., van Oldenborgh, G. J., Drijfhout, S. S., Wouters, B. & Katsman, C. A. 2013 Important role for ocean warming and increased ice-shelf melt in Antarctic sea-ice expansion. *Nature Geoscience* **6**, 376–379.

Björk, Göran 2002 Dependence of the Arctic Ocean ice thickness distribution on the poleward energy flux in the atmosphere. *Journal of Geophysical Research* **107** (C10).

Carmack, E., Polyakov, I., Padman, L., Fer, I., Hunke, E., Hutchings, J., Jackson, J., Kelley, D., Kwok, R., Layton, C., Melling, H., Perovich, D., Persson, O., Ruddick, B., Timmermans, M.-L., Toole, J., Ross, T., Vavrus, S. & Winsor, P. 2015 Towards Quantifying the Increasing Role of Oceanic Heat in Sea Ice Loss in the New Arctic. *Bulletin of the American Meteorological Society* p. 150203142711003.

Cole, S. T., Toole, J., Lele, R., Timmermans, M.-L., Gallaher, S. G., Stanton, T. P., Shaw, W. J., Hwang, B., Maksym, T., Wilkinson, J. P., Ortiz, M., Graber, H., Rainville, L., Petty, A. A., Farrel, S. L., Richter- Menge, J. A. & Haas, C. 2017 Ice and ocean velocity in the Arctic marginal ice zone: Ice roughness and momentum transfer. *Elementa: Science of the Anthropocene, in press* .

Comiso, Josefino C. & Nishio, Fumihiko 2008 Trends in the sea ice cover using enhanced and compatible AMSR-E, SSM/I, and SMMR data. *Journal of Geophysical Research* **113**, C02S07.

Cowtan, Kevin & Way, Robert G. 2014 Coverage bias in the HadCRUT4 temperature series and its impact on recent temperature trends. *Quarterly Journal of the Royal Meteorological Society* **140**, 1935–1944.

Eisenman, Ian 2010 Geographic muting of changes in the Arctic sea ice cover. *Geophysical Research Letters* **37** (16).

Eisenman, I., Meier, W. N. & Norris, J. R. 2014 A spurious jump in the satellite record: has Antarctic sea ice expansion been overestimated? *The Cryosphere* **8**, 1289–1296.

Eisenman, Ian, Schneider, Tapio, Battisti, David S. & Bitz, Cecilia M. 2011 Consistent Changes in the Sea Ice Seasonal Cycle in Response to Global Warming. *Journal of Climate* **24**, 5325–5335.

Fan, Tingting, Deser, Clara & Schneider, David P. 2014 Recent Antarctic sea ice trends in the context of Southern Ocean surface climate variations since 1950. *Geophysical Research Letters* **41**, 2419–2426.

Fetterer, F., Knowles, K., Meier, W. & Savoie, M. 2002 Sea ice index. *Natl. Snow and Ice Data Cent., Boulder, Colo.* (Updated 2012.) http://nsidc.org/data/g02135.html.

Flato, G., Marotzke, J., Abiodun, B., Braconnot, P., Chou, S.C., Collins, W., Cox, P., Driouech, F., Emori, S., Eyring, V., Forest, C., Gleckler, P., Guilyardi, E., Jakob, C., Kattsov, V., Reason, C. & Rummukainen, M. 2013 Evaluation of Climate Models. *In Climate Change 2013: The Physical Science Basis. Contribution of Working Group I to the Fifth Assessment Report of the Intergovernmental Panel on Climate Change* pp. 741–866.

Fyfe, John C. 2006 Southern Ocean warming due to human influence. *Geophysical Research Letters* **33**, 1–4.

Fyfe, John C, Gillett, Nathan P & Zwiers, Francis W 2013 Overestimated global warming over the past 20 years. *Nature Climate Change* **3** (9), 767–769.

Gagné, M.-È., Gillett, N P & Fyfe, J C 2015 Observed and simulated changes in Antarctic sea ice extent over the past 50 years. *Geophysical Research Letters* **41**, 90–95.

Gallaher, S.G., Stanton, T.P., Shaw, W.J., Kang, S.-H., Kim, J.-H. & Cho, K.-H. 2017 Field observations and results of a 1-D boundary layer model for developing near-surface temperature maxima in the Western Arctic. *Elementa* **5**, 1–21.

Gallaher, Shawn G., Stanton, Timothy P., Shaw, William J., Cole, Sylvia T., Toole, John M., Wilkinson, Jeremy P, Maksym, Ted & Hwang, Byongjun 2016 Evolution of a Canada Basin ice-ocean boundary layer and mixed layer across a developing thermodynamically forced marginal ice zone. *Journal of Geophysical Research: Oceans* **121** (8), 6223–6250.

Goosse, H. & Zunz, V. 2014 Decadal trends in the Antarctic sea ice extent ultimately controlled by iceocean feedback. *The Cryosphere* **8**, 453–470.

Gregory, Jonathan M, Stott, P. A., Cresswell, D. J., Rayner, N. A., Gordon, C. & Sexton, D. M. H. 2002 Recent and future changes in Arctic sea ice simulated by the HadCM3 AOGCM. *Geophysical Research Letters* **29**, 2175.

Hansen, J, Ruedy, R, Sato, M & Lo, K 2010 Global surface temperature change. *Reviews of Geophysics* **48**, RG4004.

Haumann, F Alexander, Notz, Dirk & Schmidt, Hauke 2014 Anthropogenic influence on recent circulation-driven Antarctic sea ice changes. *Geophysical Research Letters* **41**, 8429–8437.

Holland, Marika M., Bitz, Cecilia M., Tremblay, L.-Bruno & Bailey, David A. 2008 The Role of Natural Versus Forced Change in Future Rapid Summer Arctic Ice Loss. In *Arctic Sea Ice Decline: Observations, Projections, Mechanisms, and Implications*. Washington, D. C.: American Geophysical Union.

IPCC 2007 *Climate Change 2007: The Physical Science Basis. Contribution of Working Group I to the Fourth Assessment Report of the Intergovernmental Panel on Climate Change*. Cambridge University Press, Cambridge, UK.

IPCC 2013 *Climate Change 2013: The Physical Science Basis. Contribution of Working Group I to the Fifth Assessment Report of the Intergovernmental Panel on Climate Change*. Cambridge University Press, Cambridge, UK.

Jackson, J. M., Allen, S. E., McLaughlin, F. a., Woodgate, R. a. & Carmack, E. C. 2011 Changes to the near-surface waters in the Canada Basin, Arctic Ocean from 1993-2009: A basin in transition. *Journal of Geophysical Research: Oceans* **116** (10), 1–21.

Jackson, J. M., Carmack, E. C., McLaughlin, F. A., Allen, S. E. & Ingram, R. G. 2010 Identification, characterization, and change of the near-surface temperature maximum in the Canada Basin, 1993-2008. *Journal of Geophysical Research: Oceans* **115** (5), 1–16.

Jahn, Alexandra, Sterling, Kara, Holland, Marika M., Kay, Jennifer E., Maslanik, James A., Bitz, Cecilia M., Bailey, David A., Stroeve, Julienne, Hunke, Elizabeth C., Lipscomb, William H. & Pollak, Daniel A. 2012 Late-twentieth-century simulation of arctic sea ice and ocean properties in the CCSM4. *Journal of Climate* **25**, 1431–1452.

Jones, Julie M., Gille, Sarah T., Goosse, Hugues, Abram, Nerilie J., Canziani, Pablo O., Charman, Dan J., Clem, Kyle R., Crosta, Xavier, de Lavergne, Casimir, Eisenman, Ian, England, Matthew H., Fogt,

Ryan L., Frankcombe, Leela M., Marshall, Gareth J., Masson-Delmotte, Valérie, Morrison, Adele K., Orsi, Anaïs J., Raphael, Marilyn N., Renwick, James A., Schneider, David P., Simpkins, Graham R., Steig, Eric J., Stenni, Barbara, Swingedouw, Didier & Vance, Tessa R. 2016 Assessing recent trends in high-latitude Southern Hemisphere surface climate. *Nature Climate Change* **6**, 917–926.

Karl, Thomas R, Arguez, Anthony, Huang, Boyin, Lawrimore, J. H., McMahon, J. R., Menne, Matthew J, Peterson, T. C., Vose, Russell S & Zhang, H.-M. 2015 Possible artifacts of data biases in the recent global surface warming hiatus. *Science* **348**, 1469–1472.

Kay, J. E., Deser, C., Phillips, A., Mai, A., Hannay, C., Strand, G., Arblaster, J. M., Bates, S. C., Danabasoglu, G., Edwards, J., Holland, M., Kushner, P., Lamarque, J. F., Lawrence, D., Lindsay, K., Middleton, A., Munoz, E., Neale, R., Oleson, K., Polvani, L. & Vertenstein, M. 2015 The community earth system model (CESM) large ensemble project : A community resource for studying climate change in the presence of internal climate variability. *Bulletin of the American Meteorological Society* **96**, 1333–1349.

Kay, Jennifer E., Holland, Marika M. & Jahn, Alexandra 2011 Inter-annual to multi-decadal Arctic sea ice extent trends in a warming world. *Geophysical Research Letters* **38**.

Knutson, Thomas R., Zeng, Fanrong & Wittenberg, Andrew T. 2013 Multimodel assessment of regional surface temperature trends: CMIP3 and CMIP5 twentieth-century simulations. *Journal of Climate* **26** (22), 8709–8743.

Knutti, Reto & Sedláček, Jan 2012 Robustness and uncertainties in the new CMIP5 climate model projections. *Nature Climate Change* **3** (4), 369–373.

Kosaka, Yu & Xie, Shang-Ping 2013 Recent global-warming hiatus tied to equatorial Pacific surface cooling. *Nature* **501**, 403–407.

Kraus, E B & Turner, J S 1967 A one-dimensional model of the seasonal thermocline II. The general theory and its consequences. *Tellus* **19** (1), 98–106.

Krishfield, Richard, Toole, J., Proshutinsky, A. & Timmermans, M. L. 2008 Automated ice-tethered profilers for seawater observations under pack ice in all seasons. *Journal of Atmospheric and Oceanic Technology* **25** (11), 2091–2105.

Lemke, Peter 1987 A coupled one-dimensional sea ice-ocean model **92**, 164–172.

Lemke, P. & Manley, T. O. 1984 The seasonal variation of the mixed layer and the pycnocline under polar sea ice. *Journal of Geophysical Research* **89** (C4), 6494.

Mahlstein, Irina, Gent, Peter R. & Solomon, Susan 2013 Historical Antarctic mean sea ice area, sea ice trends, and winds in CMIP5 simulations. *Journal of Geophysical Research: Atmospheres* **118**, 5105–5110.

Mahlstein, Irina & Knutti, Reto 2012 September Arctic sea ice predicted to disappear near 2C global warming above present. *Journal of Geophysical Research* **117**, D06104.

Marotzke, Jochem & Forster, Piers M 2015 Forcing, feedback and internal variability in global temperature trends. *Nature* **517** (7536), 565–570.

Martin, Torge, Tsamados, Michel, Schroeder, David & Feltham, David 2016 The impact of variable sea ice roughness on changes in Arctic Ocean surface stress: A model study. *Journal of Geophysical Research: Oceans* pp. 1–22.

Martinson, Douglas G. 1990 Evolution of the southern ocean winter mixed layer and sea ice: Open ocean deepwater formation and ventilation. *Journal of Geophysical Research* **95** (C7), 11641.

Massonnet, F., Fichefet, T., Goosse, H., Bitz, C. M., Philippon-Berthier, G., Holland, M. M. & Barriat, P.-Y. 2012 Constraining projections of summer Arctic sea ice. *The Cryosphere* **6** (6), 1383–1394.

Maykut, G. A. & McPhee, Miles G. 1995 Solar heating of the Arctic mixed layer. *Journal of Geophysical Research* **100** (C12), 24691.

McLaughlin, F., Carmack, E., Proshutinsky, A., Krishfield, R.A., Guay, C., Yamamoto-Kawai, M., Jackson, J.M. & Williams, B. 2011 The Rapid Response of the Canada Basin to Climate Forcing. *Oceanography* **24** (3), 136–145.

McPhee, Miles G 2012 Advances in understanding ice ocean stress during and since AIDJEX. *Cold Regions Science and Technology* **76-77**, 24–36.

McPhee, Miles G. & Smith, J. Dungan 1976 Measurements of the turbulent boundary layer under pack ice.

McPhee, Miles G., Stanton, Timothy P., Morison, James H. & Martinson, Douglas G. 1998 Freshening of the upper ocean in the Arctic: Is perennial sea ice disappearing? *Geophysical Research Letters* **25** (10), 1729.

Meehl, Gerald A., Arblaster, Julie M., Bitz, Cecilia M., Chung, Christine T. Y. & Teng, Haiyan 2016 Antarctic sea-ice expansion between 2000 and 2014 driven by tropical Pacific decadal climate variability. *Nature Geoscience* **9**, 590–595.

Meehl, Gerald A., Covey, Curt, Taylor, Karl E., Delworth, Thomas, Stouffer, Ronald J., Latif, Mojib, McAvaney, Bryant & Mitchell, John F B 2007 THE WCRP CMIP3 Multimodel Dataset: A New Era in Climate Change Research. *Bulletin of the American Meteorological Society* **88**, 1383–1394.

Morice, Colin P., Kennedy, John J., Rayner, Nick A. & Jones, Phil D. 2012 Quantifying uncertainties in global and regional temperature change using an ensemble of observational estimates: The HadCRUT4 data set. *Journal of Geophysical Research: Atmospheres* **117** (D08101), 1–22.

Morison, James & Smith, J Dungan 1981 Seasonal variations in the upper Arctic Ocean as observed at T3. *Geophysical Research Letters* **8** (7), 753–756.

Notz, D. 2014 Sea-ice extent and its trend provide limited metrics of model performance. *The Cryosphere* **8**, 229–243.

Notz, Dirk & Stroeve, Julienne 2016 Observed Arctic sea-ice loss directly follows anthropogenic CO 2 emission. *Science* **354**, 747–750.

Peralta-Ferriz, Cecilia & Woodgate, Rebecca A. 2015*a* Seasonal and interannual variability of pan-Arctic surface mixed layer properties from 1979 to 2012 from hydrographic data, and the dominance of stratification for multiyear mixed layer depth shoaling. *Progress in Oceanography* **134**, 19–53.

Peralta-Ferriz, Cecilia & Woodgate, Rebecca A. 2015*b* Seasonal and interannual variability of pan-Arctic surface mixed layer properties from 1979 to 2012 from hydrographic data, and the dominance of stratification for multiyear mixed layer depth shoaling. *Progress in Oceanography* **134**, 19–53.

Perovich, D., Richter-Menge, J., Elder, B., Arbetter, T., Claffey, K. & Polashenski, C. 2017 Observing and understanding climate change: Monitoring the mass balance, motion, and thickness of Arctic sea ice. *http://imb-crrel-dartmouth.org* .

Perovich, D. K., Jones, K. F., Light, B., Eicken, H., Markus, T., Stroeve, J. & Lindsay, R. 2011 Solar partitioning in a changing Arctic sea-ice cover. *Annals of Glaciology* **52** (57 PART 2), 192–196.

Perovich, Donald K., Richeter-Menge, Jacqueline A., Jones, Kathleen F. & Light, Bonnie 2008 Sunlight, water, and ice: Extreme Arctic sea ice melt during the summer of 2007. *Geophysical Research Letters* **35** (11), 2–5.

Perovich, Donald K & Richter-Menge, Jacqueline A 2015 Regional variability in sea ice melt in a changing Arctic. *Phil.Trans.R.Soc.A 373:* **373**, 20140165.

Petty, Alek A., Feltham, Daniel L. & Holland, Paul R. 2013 Impact of atmospheric forcing on Antarctic continental shelf water masses. *Journal of Physical Oceanography* **43** (5), 920–940.

Polvani, Lorenzo M. & Smith, Karen L. 2013 Can natural variability explain observed Antarctic sea ice trends? New modeling evidence from CMIP5. *Geophysical Research Letters* **40**, 3195–3199.

Proshutinsky, Andrey, Krishfield, Richard, Timmermans, Mary-Louise, Toole, John, Carmack, Eddy, McLaughlin, Fiona, Williams, William J., Zimmermann, Sarah, Itoh, Motoyo & Shimada, Koji 2009 Beaufort Gyre freshwater reservoir: State and variability from observations. *Journal of Geophysical Research* **114**, C00A10.

Purich, Ariaan, Cai, Wenju, England, Matthew H. & Cowan, Tim 2016 Evidence for link between modelled trends in Antarctic sea ice and underestimated westerly wind changes. *Nature Communications* **7**, 10409.

Rampal, P., Weiss, J., Dubois, C. & Campin, J.-M. 2011 IPCC climate models do not capture Arctic sea ice drift acceleration: Consequences in terms of projected sea ice thinning and decline. *Journal of Geophysical Research* **116**, C00D07.

Ramudu, Eshwan, Gelderloos, Renske, Yang, Di, Meneveau, Charles & Gnanadesikan, Anand 2018 Large Eddy Simulation of Heat Entrainment Under Arctic Sea Ice. *Journal of Geophysical Research: Oceans* pp. 287–304.

Rayner, N. A., Parker, D.E., Horton, E.B., Folland, C.K., Alexander, L.V., Rowell, D.P., Kent, E.C. & Kaplan, A. 2003 Global analyses of sea surface temperature, sea ice, and night marine air temperature since the late nineteenth century. *Journal of Geophysical Research* **108** (D14), 4407.

Richardson, Mark, Cowtan, Kevin, Hawkins, Ed & Stolpe, Martin B. 2016 Reconciled climate response estimates from climate models and the energy budget of Earth. *Nature Climate Change* **6**, 931–935.

Rosenblum, Erica & Eisenman, Ian 2016 Faster Arctic Sea Ice Retreat in CMIP5 than in CMIP3 due to Volcanoes. *Journal of Climate* **29**, 9179–9188.

Santer, Benjamin D, Bonfils, Céline, Painter, Je F, Zelinka, Mark D, Mears, Carl, Solomon, Susan, Schmidt, Gavin a, Fyfe, John C, Cole, Jason N S, Nazarenko, Larissa, Taylor, Karl E & Wentz, Frank J 2014 Volcanic contribution to decadal changes in tropospheric temperature. *Nature Geoscience* **7** (3), 185–189.

Santer, B. D., Thorne, P. W., Haimberger, L., Taylor, K. E., Wigley, T. M. L., Lanzante, J. R., Solomon, S., Free, M., Gleckler, P. J., Jones, P. D., Karl, T. R., Klein, S. A., Mears, C., Nychka, D., Schmidt, G. A., Sherwood, S. C. & Wentz, F. J. 2008 Consistency of modelled and observed temperature trends in the tropical troposphere. *International Journal of Climatology* **28**, 1703–1722.

Schmidt, Gavin A., Shindell, Drew T. & Tsigaridis, Kostas 2014 Reconciling warming trends. *Nature Geoscience* **7** (3), 158–160.

Screen, James A. & Francis, Jennifer A. 2016 Contribution of sea-ice loss to Arctic amplification is regulated by Pacific Ocean decadal variability. *Nature Climate Change* **6**, 856–860.

Screen, James A., Simmonds, Ian & Keay, Kevin 2011 Dramatic interannual changes of perennial Arctic sea ice linked to abnormal summer storm activity. *Journal of Geophysical Research* **116**, D15105.

Segschneider, J, Beitsch, A, Timmreck, C, Brovkin, V, Ilyina, T, Jungclaus, J, Lorenz, S J, Six, K D & Zanchettin, D 2013 Impact of an extremely large magnitude volcanic eruption on the global climate and carbon cycle estimated from ensemble Earth System Model simulations. *Biogeosciences* **10**, 669–687.

Serreze, Mark C., Barrett, Andrew P., Slater, Andrew G., Steele, Michael, Zhang, Jinlun & Trenberth, Kevin E. 2007 The large-scale energy budget of the Arctic. *Journal of Geophysical Research Atmospheres* **112** (11), 1–17.

Sillmann, J., Kharin, V. V., Zhang, X., Zwiers, F. W. & Bronaugh, D. 2013 Climate extremes indices in the CMIP5 multimodel ensemble: Part 1. Model evaluation in the present climate. *Journal of Geophysical Research: Atmospheres* **118** (4), 1716–1733.

Steele, Michael 1992 Sea ice melting and floe geometry in a simple ice-ocean model. *Journal of Geophysical Research Oceans* **97** (C), 17729.

Steele, Michael, Ermold, Wendy & Zhang, Jinlun 2011 Modeling the formation and fate of the near-surface temperature maximum in the Canadian Basin of the Arctic Ocean. *Journal of Geophysical Research* **116** (C11), C11015.

Steele, Michael, Zhang, Jinlun & Ermold, Wendy 2010 Mechanisms of summertime upper Arctic Ocean warming and the effect on sea ice melt. *Journal of Geophysical Research: Oceans* **115** (11), 1–12.

Stenchikov, Georgiy, Delworth, Thomas L., Ramaswamy, V., Stouffer, Ronald J., Wittenberg, Andrew & Zeng, Fanrong 2009 Volcanic signals in oceans. *Journal of Geophysical Research: Atmospheres* **114** (16), 1–13.

Stroeve, Julienne, Holland, Marika M., Meier, Walt, Scambos, Ted & Serreze, Mark 2007 Arctic sea ice decline: Faster than forecast. *Geophysical Research Letters* **34**, L09501.

Stroeve, Julienne & Notz, Dirk 2015 Insights on past and future sea-ice evolution from combining observations and models. *Global and Planetary Change* **135**, 119–132.

Stroeve, Julienne & Notz, Dirk 2016 Corrigendum to insights on past and future sea-ice evolution from combining observations and models [Glob. Planet. Change (2015) 119132]. *Global and Planetary Change* **144**, 270.

Stroeve, Julienne C., Kattsov, Vladimir, Barrett, Andrew, Serreze, Mark, Pavlova, Tatiana, Holland, Marika & Meier, Walter N. 2012 Trends in Arctic sea ice extent from CMIP5, CMIP3 and observations. *Geophysical Research Letters* **39**, L16502.

Swart, N. C. & Fyfe, J. C. 2013 The influence of recent Antarctic ice sheet retreat on simulated sea ice area trends. *Geophysical Research Letters* **40**, 4328–4332.

Swart, Neil C, Fyfe, John C, Hawkins, Ed, Kay, Jennifer E & Jahn, Alexandra 2015 Influence of internal variability on Arctic sea-ice trends. *Nature Climate Change* **5**, 86–89.

Taylor, Karl E., Stouffer, Ronald J. & Meehl, Gerald A. 2012 An overview of CMIP5 and the experiment design. *Bulletin of the American Meteorological Society* **93**, 485–498.

Timmermans, M. L. 2015 The impact of stored solar heat on Arctic sea ice growth. *Geophysical Research Letters* **42** (15), 6399–6406.

Timmermans, M.-L., Toole, J., Krishfield, R. & Winsor, P. 2008 Ice-Tethered Profiler observations of the double-diffusive staircase in the Canada Basin thermocline. *Journal of Geophysical Research* **113**, C00A02.

Toole, J. M., Timmermans, M. L., Perovich, D. K., Krishfield, R. a., Proshutinsky, a. & Richter-Menge, J. a. 2010 Influences of the ocean surface mixed layer and thermohaline stratification on Arctic Sea ice in the central Canada Basin. *Journal of Geophysical Research: Oceans* **115**, 1–14.

Turner, J.S. 1967 A onedimensional model of the seasonal thermocline I. A laboratory experiment and its interpretation. *Tellus* **19** (1), 88–97.

Turner, John, Bracegirdle, Thomas J., Phillips, Tony, Marshall, Gareth J. & Hosking, J. Scott 2013 An Initial Assessment of Antarctic Sea Ice Extent in the CMIP5 Models. *Journal of Climate* **26**, 1473–1484.

Turner, John, Hosking, J Scott, Bracegirdle, Thomas J, Marshall, Gareth J & Phillips, Tony 2015 Recent changes in Antarctic Sea Ice. *Philosophical Transactions of the Royal Society A* **373**, 1 – 13.

Uotila, P., Holland, P. R., Vihma, T., Marsland, S. J. & Kimura, N. 2014 Is realistic Antarctic sea-ice extent in climate models the result of excessive ice drift? *Ocean Modelling* **79**, 33–42.

Wagner, Till J.W. & Eisenman, Ian 2015 How Climate Model Complexity Influences Sea Ice Stability. *Journal of Climate* p. 150310071401001.

Watanabe, Masahiro, Kamae, Youichi, Yoshimori, Masakazu, Oka, Akira, Sato, Makiko, Ishii, Masayoshi, Mochizuki, Takashi & Kimoto, Masahide 2013 Strengthening of ocean heat uptake efficiency associated with the recent climate hiatus. *Geophysical Research Letters* **40** (12), 3175–3179.

Winton, Michael 2011 Do Climate Models Underestimate the Sensitivity of Northern Hemisphere Sea Ice Cover? *Journal of Climate* **24**, 3924–3934.

Xie, Shang-Ping, Kosaka, Yu & Okumura, Yuko M. 2016 Distinct energy budgets for anthropogenic and natural changes during global warming hiatus. *Nature Geoscience* **9**, 29–33.

Yamamoto-Kawai, M., McLaughlin, F. A., Carmack, E. C., Nishino, S., Shimada, K. & Kurita, N. 2009 Surface freshening of the Canada Basin, 2003-2007: River runoff versus sea ice meltwater. *Journal of Geophysical Research: Oceans* **114** (4), 2003–2007.

Zanchettin, Davide, Bothe, Oliver, Graf, Hans F., Lorenz, Stephan J., Luterbacher, Juerg, Timmreck, Claudia & Jungclaus, Johann H. 2013 Background conditions influence the decadal climate response to strong volcanic eruptions. *Journal of Geophysical Research: Atmospheres* **118** (10), 4090–4106.

Zanchettin, D., Bothe, O., Timmreck, C., Bader, J., Beitsch, A., Graf, H.-F., Notz, D. & Jungclaus, J. H. 2014 Inter-hemispheric asymmetry in the sea-ice response to volcanic forcing simulated by MPI-ESM (COSMOS-Mill). *Earth System Dynamics* **5** (1), 223–242.

Zanchettin, D., Timmreck, C., Graf, H.-F., Rubino, A., Lorenz, S., Lohmann, K., Krüger, K. & Jungclaus, J. H. 2012 Bi-decadal variability excited in the coupled oceanatmosphere system by strong tropical volcanic eruptions. *Climate Dynamics* **39** (1-2), 419–444.

Zhong, Y., Miller, G. H., Otto-Bliesner, B. L., Holland, M. M., Bailey, D. A., Schneider, D. P. & Geirsdottir, A. 2011 Centennial-scale climate change from decadally-paced explosive volcanism: a coupled sea ice-ocean mechanism. *Climate Dynamics* **37** (11-12), 2373–2387.

Zunz, V., Goosse, H. & Massonnet, F. 2013 How does internal variability influence the ability of CMIP5 models to reproduce the recent trend in Southern Ocean sea ice extent? *The Cryosphere* **7**, 451–468.